TOR VERGATA
UNIVERSITÀ
DEGLI STUDI
DI ROMA

UNIVERSITY OF ROME "TOR VERGATA"

PhD in INDUSTRIAL ENGINEERING
XXXIV CYCLE

A.A 2021/2022

Infrared imaging techniques for the stratigraphic analysis of Cultural Heritage

Tutor: Prof. Fulvio Mercuri

Candidate: Sofia Ceccarelli

Coordinator: Prof. Marco Marinelli

Table of content

Acknowledgments

The PhD programme was an extraordinary experience, making me grow both as a person and as a researcher, especially thanks to who supported and accompanied me on this journey.

My first and sincere thanks is for my supervisor Prof. Fulvio Mercuri, to whom I am grateful for his patience and inspiring spirit during these years.

A special thanks to my team members: Dr. Noemi Orazi, Prof. Ugo Zammit, Prof. Stefano Paoloni, Dr. Cristina Cicero for their support, the precious teachings and the funny lunches!

Thanks to Prof. Roberto Montanari and Prof. Marco Marinelli as coordinators of the PhD program.

I also want to warmly thank the researchers with whom I collaborated for the laboratory and in situ measurements: Dr. Giovanni Caruso from ITABC CNR Montelibretti, Dr. Anna Candida Felici from LANDA laboratory of "La Sapienza" University, Dr. Paola Calicchia and Dr. Sara De Simone from the LARCH laboratory of CNR Tor Vergata and (once again!) Dr. Massimiliano Guarneri and Dr. Massimo Francucci from the DIM laboratory of ENEA Frascati.

I would to thank the Museo delle Civiltà in Rome, especially Dr. Serena Francone and Mrs. Maria Francesca Quarato of the Laboratory of Restoration, Dr. Loretta Paderni, Director of the Asian Department at Museum "Luigi Pigorini", Dr. Gabriella Pace, head of the Laboratory of Restoration of Istituto Nazionale della Grafica, Dr. Giacomo Fiocco and Dr. Michela Albano from the ARVEDI Laboratory of Cremona, for their availability in the study of the artworks preserved in their institutions and their contribution and collaborations for the publications.

A special thanks also to Dr. Francesco Petrucci, director of Palazzo Chigi of Ariccia who warmly hosted me and my colleagues in his institution during the measurement campaigns and contributed to my interest in the local history of my hometown area.

Another very special thanks go to my precious and dearest friends Irene, Virna, Gloria, Silvia, Michele, Lizeth, Claudia, Mohamad, Greta&Fabrizio, Gianmarco and Carlo who listened, supported and encouraged me when I needed it most with tips, laughs and love.

Last but not least, the most special, deepest and beloved thanks is for my family who have never stopped believing in me and helping in any circumstance: my mother, the strongest woman I know, and my dad, the precious dispenser of advice on research (and life); my sister and my brother who have always been there for me with their curiosity and unconditional love, even from far away.

And finally, as I started the acknowledgement of my master's degree, I'll finish the PhD ones by thanking and dedicating this work to my little-not-so-little wonderful daughter Greta, who inspires me to do my best every day.

Acronyms

3D: three-dimensional
AM: amplitude modulation
CCD: charged coupled device
CH: cultural heritage
CIE: commission international de l´eclairage
CIS: cold image subtraction
CS: conservation science
DL: digital level
FEM: finite element model
FIR: far infrared
FORS: fiber optics reflectance spectroscopy
FTIR: fourier-transform infrared spectroscopy
IR: infrared
IR-ITR: infrared imaging topological radar
IRR: infrared reflectography
IRT: infrared thermography
LDV: laser doppler vibrometry
LWIR: long-wave infrared
MIR: middle-wave infrared reflectography
MS: mass spectrometry
MWIR: middle-wave infrared
NDT: non-destructive testing
NETD: noise equivalent temperature difference
NIR: near infrared/near infrared reflectography
PIXE: particle induced x-ray emission
PT: pulsed thermography
RLP: raking light photography
RX: X-ray radiography
SEM: scanning electron microscope
SWIR: short-wave infrared
TEM: transmission electron microscopy
UV: ultraviolet
UVF: ultraviolet fluorescence
UVR: ultraviolet reflectography
VIS: visible
XRD: X-ray diffraction
XRF: X-ray fluorescence

Abstract

This thesis provides an overview on the infrared imaging techniques focusing on the ones working in the middle-wave infrared range, namely pulsed thermography and reflectography, for the study of layered Cultural Heritage items. In the framework of non-destructive methods, middle-wave techniques, especially the thermography, are commonly used singularly for the stratigraphic analysis of artefacts. In this thesis, the two techniques were used together in a combined approach for the characterisation of subsurface features not visible at naked eye in several multi-layered structures, as painted artefacts on different supports and bookbinding of library heritage, simulated in laboratory samples. Among other advantages, the non-destructive nature and the use of the same device as detector that ensures the pixel-by-pixel correspondence of thermographic and reflectographic images make this approach suitable as diagnostic survey in many application, without compromising the artefact and aimed to assess its preservation state. A theoretical modelling was also proposed for the characterisation of the blurring in thermographic images and the quantitative evaluation the edges distortion in the detection of hidden text buried inside the bookbinding. The confirm of the capabilities of the proposed techniques and approach was achieved by their application on the study of original artefacts coming from several museums and institutions with different structures and conservative issues, comparing, in many cases, the thermographic and reflectographic results with the ones obtained with other imaging techniques for a more complete characterisation of the layered structure of a particular kinds of artefacts.

Introduction

The geopolitical and environmental events of the last decades led to a greater consideration of the cultural heritage (CH) and to a growing awareness of the connection between the culture and the history of a community and its artistic expression. In this context, the application of advanced technologies in many disciplines, as well as the birth of new ones, including conservation science (CS), was possible due to an important scientific progress. CS is an internationally well-known discipline, it deals with the application of scientific methods to the study of every kind of works of art, from archaeological sites to small artifacts and librarian heritage, with the final purpose of analysing their state of conservation and preserving it. Indeed, scientific measurements are powerful tools for the characterization of an artwork, in terms of both the materials and the artistic/historic/geographic provenance, providing very different results and information according to the approach used. Among the scientific methods, several distinctions can be done referring to the many aspects involved, such as for example the analytical approach or the application fields. In CH analysis, the main aspect to keep in mind is the preservation of the artwork, avoiding as much as possible its damage. In order to maintain the integrity of the studied object, especially in those cases where the conservation conditions of the artwork are very unstable or where the sampling is impossible, non-destructive testing (NDT) have to be preferred during the diagnostic analyses, thanks to the capability of such an approach able to perform investigations without causing damage [1]. Examples of diagnostic techniques are reported in Table I. I, distinguishing them between destructive and non-destructive methods.

Table I. I- Examples of techniques applied in Conservation Science.

Method	***Technique***
Destructive	Microscopies (SEM, TEM)
	Chemical mapping with sampling (XRD, MS, PIXE)
	Dating techniques (Dendrochronology, C^{14})
Non- Destructive	Imaging techniques, 3D modelling
	Spectroscopies (Raman, XRF, FTIR)
	Colorimetry

The possibility of employing NDT is fundamental in CH studies, especially in those cases where the conservation conditions of the artwork are very unstable and fragile or where the sampling is forbidden or impossible. Further distinction can be done considering the examination areas: imaging methods provide information on extended areas by giving results in format of images, while spectroscopies allow obtaining punctual data on very small areas, typically on the molecular/elemental structure of the materials. Nowadays, imaging techniques are widely used for contactless investigation of structures, materials and hidden features of CH, being the most suitable methods for stratigraphic studies of an artwork without the need of sampling. Such kind of techniques is generally grouped in several classes differentiated by the spectral range of the specific perturbation and detection, as summarised in Table I. II.

Table I. II - Distinction of imaging techniques by the spectral range investigated.

Spectral range	***Imaging technique***
X-rays (10nm ÷ 0.01 nm)	Radiography (RX)
Ultraviolet (UV: 400 nm ÷ 10 nm)	Reflectography (UVR), Fluorescence (UVF)
Visible (VIS: 400 ÷ 700nm)	Photography, Raking Light Photography (RLP)
Infrared (IR: 700 nm ÷ 10^6 nm)	Reflectography (IRR), Infrared Thermography (IRT)

Thus, the layered structure of an artwork can be investigated without sampling or inducing any damage, using the different interactions between the artwork's materials and the chosen wavelengths which probe different layers. Indeed, for investigation of the support structure, it is usually employed X-ray radiography [2], [3], while IR reflectography can provide information on the preparatory level where often underdrawings are present [4], [5] and IRT is a technique used for its capability to reveal surface and subsurface features within the analysed artefacts [6], [7]. Finally, VIS techniques are able to examine the pictorial layer obtaining data on the surface conditions and on the artistic technique [8], while UV fluorescence is a useful method for studying superficial varnishes [9], [10]. A schematic graphical representation of the different penetration depths of the mentioned techniques within a typical layering in paintings is represented Figure I.I [11].

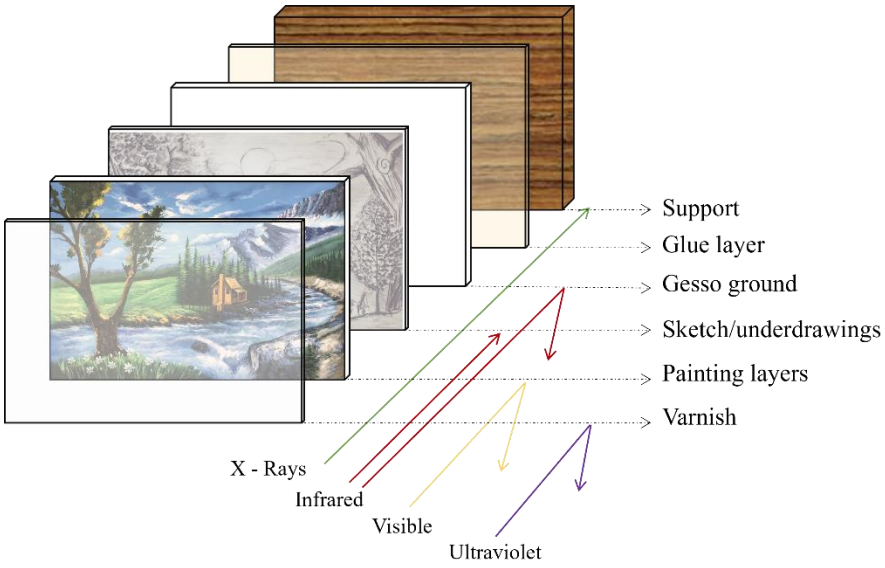

Figure I.I - Schematic representation of the typical layered structure of paintings with the main imaging methods [11].

Among the cited NDT methods, the ones employed in this thesis are based on the use of imaging techniques in the IR range for the study of the surface and subsurface features within the multi-layered structures of artefacts. The techniques discussed in the next chapters perform the analyses in the working ranges from the near to the mid-wave IR. Among the classification methods available for distinguishing the bands of the IR region [12], [13], the used one in the discussion of this thesis is reported in Table I. III, as the most commonly applied in the imaging techniques context.

Table I. III. scheme of the IR ranges classification employed in this thesis [14].

IR classification scheme
Near-IR (NIR): 0.75 μm ÷ 1.4 μm
Short-wavelength IR (SWIR): 1.4 μm ÷ 3 μm
Mid-wavelength IR (MWIR): 3 μm ÷ 5 μm
Long-wavelength IR (LWIR): 8 μm ÷ 15 μm
Far- IR (FIR): 5 μm ÷ 1000 μm

In this thesis, a combined approach of MWIR non-destructive imaging techniques is applied to the study of multilayer structure of CH items. In particular, reflectographic and thermographic methods were used in a novel methodology for non-destructive investigation of painted artefacts and books, both in laboratory samples and original artefacts, with the final aim to characterize the in-depth capability of such methods to explore subsurface features beneath materials like paint and paper. The

following radiations were employed for the analyses in this thesis: NIR (near IR: 0.9-1 μm), SWIR (short-wave IR: 1.55 μm) and MWIR (mid-wave IR: 3-5 μm) using two reflectographic systems (a standard NIR camera and a prototypal laser scanner), MWIR reflectography and pulsed thermography, respectively. The techniques were compared in several applications by investigating original artefacts where the complementary approach was needed to achieve information about the multilayer structures.

In this thesis, an overview of the typical layering of CH items is presented, by describing the materials, the manufacturing processes and the defects.

In particular, in Chapter 1, the layering of the two categories of CH investigated in this thesis will be illustrated, by introducing the different kind of each layer in painted artefacts and historical books, corresponding to supports, pictorial/graphical elements and features hidden under paper and parchment leaves. IR imaging techniques are able to investigate under the superficial layer, allowing the detection of structural defects and graphical features. Each IR band can provide different information about the artefact, so that a different approach has to be endorsed in diagnostic surveys according to the layer to be investigated.

In Chapter 2, an overview of the imaging techniques in the IR range employed in this thesis will be provide, focusing on MWIR techniques. In particular, pulsed thermography and MWIR reflectography are proved to be an efficient combined tool for the detection of subsurface elements in opaque and semi-transparent materials, such as paintings and paper-based artefacts. In order to better explore the generation and the behaviour of the signal coming from thermographic measures, two laboratory samples were properly designed and elaborated, such as a wooden painted panel and an inked paper sheet, replicating the two categories of CH items investigated in this thesis.

In Chapter 3 the laboratory tests performed for this thesis will be presented as well as the making phases of both the samples. The results obtained on the wooden sample are presented by showing the capability of the different techniques of identified features beneath the superficial visible layer, also by comparing them with other imaging techniques, such as NIR reflectography. Moreover, the results achieved on the study of the paper-based sample will show the capability of the PT technique in the detection of hidden features in fibrous semi-transparent materials such as paper or parchment, such as buried texts in historical books, exploiting the different contrast generation phenomena of the involved materials with the respect to VIS range stimulation and MWIR range detection.

Applications of the developed method on case studies are presented in Chapter 4, by showing non-destructive investigations on original artefacts with several conservative issues. In order to study the behaviour of the detection on different materials of MWIR techniques, *in situ* examinations were

performed on different kinds of artefacts, among which panel and canvas paintings, wall drawings, decorated handscroll and papier-mâché puppets.

As a conclusion, the great advantage of integrating more techniques, both commercial and prototypal, will be discussed, by citing the most relevant results obtained during this thesis and demonstrating the efficient capability of the MWIR approach to qualitatively and quantitatively characterising multi-layered CH items.

1 The layered structures of Cultural Heritage

Cultural Heritage can be complex items composed by several materials and features overlapped and assembled in multi-layered structures. The ancient recipes handed down over the centuries by the workshops masters often allow to historically reconstruct part of the materials and the manufacturing procedures of an artwork, however, these do not give information about the *modus operandi* of the single artist. Conservation Science allows the scientific characterisation of the materials and their layering, also providing the analysis of hidden features which can often reveal precious details about the creative process of the artist.

These hidden elements can be founded at different depths, thus being difficult to detect, i.e., the preparatory sketch of a painting under the pictorial layer or a reused paper leave in a historical book. The aim of this thesis is indeed the analysis of such hidden features and the study of the capability of IR imaging techniques to investigate under several levels of materials without compromising the artefact integrity. To better understand the complexity of such approach, an overview of the structure of the two categories of ancient artefact studied in this thesis will be described: paintings and manuscripts. In general, the layered structures of both categories can be summarised in three main elements, as reported in Figure 1.1: front medium, i.e. the surface layer (for example pigments + medium in painted artworks, written paper leaves in manuscripts) under which is buried the graphical or pictorial element (underdrawings or hidden texts) and finally the support.

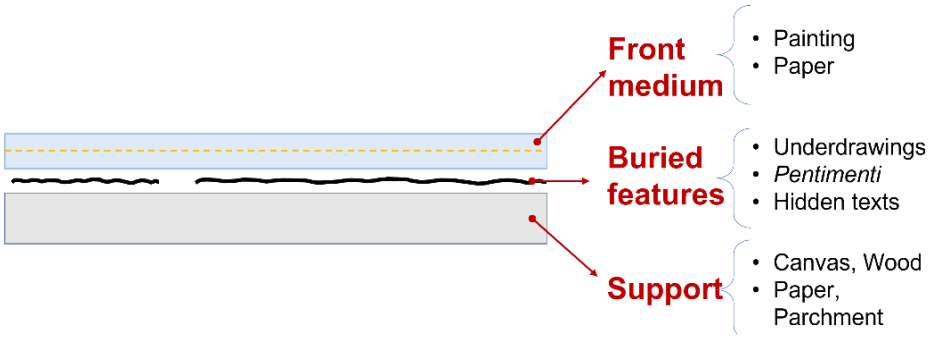

Figure 1.1 - Sketch of the typical multi-layering of CH items with the three main elements: support, buried features and front medium.

Using MWIR techniques combined with NIR ones, an in-depth investigation of the sample is possible, providing the detection and characterisation of most of the hidden features buried under several surface and sub-surface layers.

1.1 Painted artefacts

Painting is an art old as humankind who has always pursued, developed and improved materials and techniques that enable the best artistic expression and durability. The great multitude of works of art in the world and the historical sources have transmitted these elements for millennia, not always very defined in the eyes of those who look at them today. One of the main historical references about the recipes and practices for the creation of an artwork is Cennino Cennini, who explains in his *Libro dell'arte* every phase of the realisation of a painting up to the 15th century [15]. The tradition described by Cennino was maintained for centuries as a reference by ancient and modern artists, especially for what concerns the preparation of a painted artwork.

Indeed, before the application of surface layer of a painting, the entire structure has to be prepared to embed the mixture of dyes (whether natural or synthetic) and media. In general, a painted artwork can be considered as composed by three main layers and the related commonly used materials, as summarised in Table 1.1.

Table 1.1- The main layer categories of a painted artefact and the most commonly used materials.

Layer	***Materials***
Pictorial	Mineral Pigments, Acrylic, Dyes (and more) + medium + varnishes
Preparatory	Rabbit glue, Gypsum, White lead
Support	Wood, Canvas, Paper, Combination of materials

Each layer is interconnected with the next, creating an active structure that can change and deteriorate over time due to several causes such as physical (stress, atmospheric agents), chemicals (pigment interaction, pollution) and biological (attack of bacteria/insects). Thus, an artwork is not just the expression of the human creativity skill and emotions but also a complicate and delicate system where the artist overlaps several elements made by varied materials which interact with the surrounding environmental. A painting executed on a wooden panel is a complex composite structure consisting not only of a number of layers of different materials with different physical and chemical properties, but often also a number of three-dimensional structural elements with differing mechanical properties.

1.1.1 Support

In the case of paintings, the term "support" refers to any material onto which paint is applied. The choice of the kinds of the support depends on several factors such as: purpose of the object (votive, functional, ornamental), its conservation/exposition environmental (internal, external), costs and material availability. Sometimes the support is an integral part of the painting itself, for example in wooden statues or papier-mâché puppets, others it is simply a flat surface for a decorative application.

The supports studied and characterised in this thesis belongs to the category of movable objects, such as paintings, handscrolls, puppets, made by organic materials of plant origin as wood, canvas, paper and miscellaneous materials. The support has the important function of maintaining the body of the entire artwork itself and supporting the movements of the entire structure in solidarity with the other layers. Indeed, the choice of the proper raw materials and their preparation is crucial for the durability of the final artwork.

Wood

Because of the large variety of vegetal species and their characteristics, the type of the wood for the support is the first crucial choice made by an artist for the realisation of a painted artefact. The criteria followed for such a selection should be based on several factors, including geographical availability, physical and mechanical characteristics and financial dispositions. Further distinctions for the choice of the wooden species are made according to the type of artefact: for the supports of the paintings on wood, the species must be characterized by an excellent dimensional stability to the variations of the surrounding thermo-hygrometric conditions, while for the sculptures, fundamental are the easy workability and the aesthetic aspect. The main species employed in historical CH are summarised in Table 1.2, which also describes the main mechanical/physical features, the principal use and their geographic areas [16], [17].

Table 1.2– Main vegetal species in CH with specifications of their features, main use and geographical areas.

Species	***Features***	***Main use***	***Geographic areas***
Poplar	Widely diffused, low volumetric mass, reduced dimensional variations	Paintings	Italy
Lime tree	Easy availability, carving ability, fine texture	Sculptures	Germany and Italy

Walnut	Tenacious, resistant to the split	Paintings	South of France, Spain
Oak	High humidity resistance, natural durability of duramen to biological attacks	Paintings	Netherlands, Germany
Pear tree	Heavy and hard, tendency to crack	Inlaid objects, musical instrument	Europe (calcareous ground)

The most significant characteristic in the conservation of panel paintings is the hygromechanical behaviour of wood. Since wood is hygroscopic material, it will absorb and release moisture from the environmental in order to remain in equilibrium with its surroundings, swelling as the moisture content increases and shrinking as it decreases. Shrinking and swelling differ depending on direction in wood. For example, shrinkage is least in the longitudinal (fibre) direction, and greatest in the tangential direction. Dimensional movement in the longitudinal direction can usually be neglected, but the large difference between radial and tangential shrinkage leads to warping and changes in shape, as can be seen from Figure 1.2 [18]. Due to these effects, the second fundamental factor on the use of wood as support is the position of the cut with the respect to fibres. Transverse cuts run at right angles to the trunk axis, across the fibres, which means that cells complexes running parallel to the axis are severed. The most used cut is the tangential one, which run parallel to the trunk axis and tangential to the growth rings, giving a U-shaped pattern. While radial cuts run parallel to the trunk axis and the medullar rays. Woods that form clear growth rings, such as oak, show a stripy pattern when they are cut radially [18]. A further consideration has to be made in the study of wooden supports. Veining and knots are intrinsic characteristics of wood, while joint lines and shrinkage cracks further elements typically present in wooden boards used as supports for works of art. Thus, the detection of these elements can be very useful as indication in the identification of the wood species and especially in the characterisation of the state of preservation.

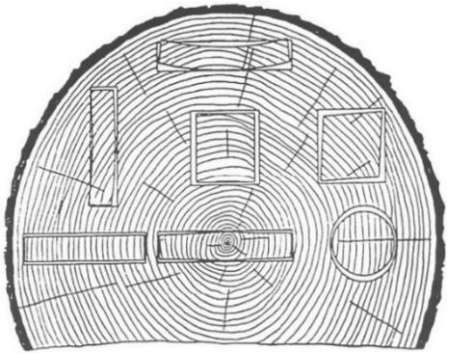

Figure 1.2 - Effects of variously shaped wood members according to their location in the cross section [19].

Canvas

Different types of fabrics belong to this category of support which includes flexible material stretched over a wooden frame to keep it plane and give it stability. The main fabric used for easel painting in western art is made by cotton, flax, hemp or silk. Cotton textile derives from the fibre and flower of cotton shrub; flax and hemp are obtained from the fibre that form part of the stems of the respective plants, while silk is secreted material from the cocoons of the silkworm. The fabric obtained are woven materials with a final quality and behaviour that is influenced by the manufacturing and the quality of raw sources. Among the materials, cotton and flax are the most employed in European art, thanks to several factors such as the great elasticity of cotton fibres, the strength of flax and their great availability in the continent. Cotton and linen canvas were the main support for religious artefacts from the Middle Ages, while silk is mostly employed as material in east, mainly as precious fabric for cloths [20].

In the past, the reduced dimensions of the weaving looms led to the limitation on the fabric width, problem overcame by the common practice of sewing canvases together, as can be seen in many paintings between the 15^{th} and 19^{th} centuries. An integral part of the support is the frame used for tensioning the canvas, called stretcher, also useful for facilitating the transport of the work itself. The stretcher is composed by fours wooden members with adjustable corner joints and it can be referred as an auxiliary support, often holding evidence about the history of the painting such as labels or inscription about its provenance or exhibition details. The method of attachment of the canvas to the stretcher can provide information about the painting itself, from the creation to the technology employed and its conservation conditions.

Also in this case, preparatory layers are applied on the support, comprehending sizing and ground in different thickness and numbers depending on the period, the type of painting (oil or *tempera*), the atelier and the artist technique. The sizing should be composed mainly of glue spread on the canvas by brush and it has the aim of laying down the fibres, filling the interstices and protect the fabric from the binder. The ground is a mixture of glue and fine gypsum to which are sometimes mixed small amounts of pigment to give a homogeneous coloured ground layer to the painting.

Several alterations can occur on fibres, providing different effects on their structure depending on the types of ageing cause. An ageing reaction may alter the molecular weight, crystallinity, or orientation of fibres, as well as their size or shape. In physical ageing, strictly physical structural changes occur over time, and no additional energy needs to be supplied for physical ageing to occur. Photochemical degradation is due to the absorption of electromagnetic radiation, such as visible or ultraviolet light. Thermal degradation occurs when structural changes result from the

absorption of heat. Chemical attack may be due to external chemical species, such as when oxidation occurs from peroxide bleach, which could alter the chemical composition of fibres, such as by altering the chemical structure of the polymer or by the addition of soil. Finally, ageing may occur through mechanical stress, such as when the gross shape of textiles changes as a result of sagging during display or storage. Finally, Natural ageing, on the other hand, results from complex mixtures of many or all of these types of ageing [21].

Paper

The term *paper* refers to a hygroscopic support consisting of vegetable fibres to which are added other substances such as adhesives, pigments and fillers with the aims of increasing their strength and opacity or changing their colouring, respectively. The concept of paper as a support made from wood is essentially modern and it has replaced the historic production from cotton and flax.

The invention of paper can be traced back to the 1st-2nd A.D. in China, where it was produced mainly from the fibres of mulberry and bamboo, replacing the supports in silk, particularly expensive. From China, the production of paper expanded to the Arab countries, which, in the absence of mulberry, used fibres from linen, hemp or cotton, coming mainly from fabric waste materials. Paper came to Europe nearly a thousand years after it was invented in China and then came in Italy around in the 10th century AD, becoming a competitor of the parchment, the most widely used writing support until the late Middle Ages. Although the paper was cheaper than parchment, such material had problems to be used for various reasons such as the low cultural level and the widespread illiteracy, but also the Arab and Eastern origin was often viewed with great suspicion in Christian countries. Between the 12th and the 13th centuries thanks to numerous technological innovations, the production of paper becomes a real industry, replacing the fibres of hemp, flax and cotton with those derived from wood. With the invention of 15th century movable-type printing, paper definitively replaced parchment as a writing support. By the 18th century, also North America started to produce its own paper [22]–[24].

The methods of papermaking have changed over the centuries as a result of various factors, such as availability of raw materials, geographical location and, above all, technological progress. Nevertheless, in general, the main phases of the process of creation of paper can be considered common, as follows:

- maceration of raw materials in water for the separation of fibres
- purification of raw materials and crushing in a slurry

- addition of adhesives (sizing) for enhancing the quality of the surface, its resistance to water and inks, and appearance, such as brightness and opaqueness
- sheet formation using frames
- drying and surface finishing.

Over the centuries, a series of new products have been further introduced in papermaking process, often worsening the quality such as acidic substances for sizing or whitening. Furthermore, modern machine processes produce different quality of papers with the respect to hand production: long fibres are undamaged in hand processing while short fibres indicate machine production. The quality of the fibres has a direct impact on paper longevity as they are less susceptible to mechanical breaking, or chemical and microbiological attack.

Concerning the paper degradation, it is characterized by various types of damage, among which:

• Mechanical or physical alterations, including tears, losses, abrasions and gouges due to physical impact, may occur during handling, incorrect framing, or lack of support during relocation of an object.

• Chemical changes at the molecular level include photochemical, caused by a wrong exposition to the light and acidity, due to possible content acidic media (e.g., iron gall ink) and contact with acidic materials (sizing).

• Microbiological damage due to activity of fungi and bacteria, which provide further physical and chemical alterations of paper. Among the most common alterations, foxing is a common type of small, brown-rusty stain scattered on paper, attributed to fungal activity, metal inclusion in paper and its composition.

Specific paper-based supports: the papier-mâché

Among the heterogeneous materials that can compose a painting support, an interesting one is the papier-mâché, used for the creation of several kind of 3D CH items, such as 3D-effect paintings or bas relieves, statues, globes and masks or puppets [23], [25]. The raw material of papier-mâché is paper, to which are mixed other components such as plaster, additives and colouring substances, typically pigments or laques, providing a solid and rigid consistence suitable for different shapes. Since in ancient times paper was made of textile fibres, ancient papier-mâché artefacts were mainly made of linen and cotton fibres. From the Renaissance and the invention of wood-based paper, the main components of such miscellaneous support were wooden fibres. In the process of making papier-mâché artefacts, waste materials were preferred, not only for economic issues but mainly

because the addition of other substances, already present in the paper component, was reduced to minimum. Among the elements added during the maceration of rags or paper, glues, fillers and other fibres, such as straw or gypsum, were added to the slurry in order to strengthen the final material. After the maceration, the drying phase was made using moulds, typically made of chalk or clay, and finally the object was extracted and finished before surface decoration. The latter was carried out using materials very similar to a painting on canvas such as with pigments spread on a preparatory layer made of plaster and animal glue then smoothed finely and painted. In conclusion, papier-mâché artefacts born from poor and waste raw materials but then they are embellished by the decoration, made mainly by a pictorial layer to which are sometimes added gold and silver finishes. One of the main papier-mâché object categories is associated with religious and public commissions, for the creation of statues of the patron saints led in processions. The lightness and the cheapness of the papier-mâché favoured its use in religious events, in substitution to heavier manufactured products made of wood, gypsum or bronze. During the 18th century, the papier-mâché began to replace the *stucco* for the wall decorations and it was the main material for the production of toys. The main toys produced in papier-mâché were the heads for dolls, made by pressing the dough inside moulds. It was also used for the creation of the faces and the arts of some puppets used within the theatrical world, such as *pupi*, marionette and puppets, very popular especially in southern Italy [11]–[13].

Intonaco

Another support commonly used for being painted and decorated is the plaster (*intonaco*), which is well-known as the support for the frescoes. This is composed by laying at least three layers of mortar: the first, generally referred to as *rinzaffo* (or rustic plaster), is a thick and rough mortar with the function of anchoring to the wall; the second, with the function of levelling, is the *arriccio*, less irregular but still rough to allow a good grip of the last finishing layer, the *intonachino*, characterised by a uniform and finest-grained smooth surface. On this most superficial layer is then applied the painting part while still not completely dry, giving life to the frescoes (because the painting takes place on plaster that is still fresh not completely dry) [15], [29]. The plaster in contact with the pigments reacts to give rise to what is known as carbonation, i.e. a precipitation reaction of the calcium carbonate of the lime that makes up the plaster. This reaction creates a bond between the two elements, strongly incorporating pigments that form the pictorial layer of a fresco so that the painting becomes an integral part of the wall. The timing and end result of this process depend on the composition of the mortar, the ambient and climatic conditions such as the humidity and the water content of the mixture, which can also cause variations in the durability of

the colour layers and degradation effects, such as efflorescence phenomena [30]. In addition to fresco painting, there are other types of painting and drawing on plaster, including half-fresco and *secco* painting, in which the pictorial-decorative part is applied on a partially or completely dried plaster, respectively [29]. In the case of *secco* painting, the *sinopia* red is the most commonly material used to create the drawings directly on the *arriccio*, often as preparation for the final fresco painting [31]. This last case was considered in a case study reported in section 4.2.2.

1.1.2 Preparatory layer

Before the application of decorative apparatus, the support has to be prepared in order to obtain the best surface possible for the best chromatic appearance of the artefact. The preparation includes several steps for every kind of support that can be summarised as follows:

- finishing of the surface,
- sizing
- application of preparatory layer.

For wooden and canvas supports the steps are quite similar, being distinguished mainly by thickness: the preparatory layer of wooden supports has to be more consistent than that for the canvases.

The finishing is performed by using tools to obtain a homogeneously smooth surface. The sizing of the support consists in the application on the surface of the size, which is a diluted glue, typically made from animal skins, such as the rabbit glue, spread directly on the support surface with the aim of coating and preventing the binder in the subsequent layers from being absorbed into the support itself. A preparatory layer, also called ground, is then applied on the size as preparation for the pictorial layer. The ground has a twofold goal: on one hand it isolates the support itself from the pictorial materials and it makes the surface tighter, less absorbent, and more luminous, avoiding the absorption of the binder and the colours between the fibres, on the other it provides a white and opaque surface for the paint layer. Characteristics such as layer thickness, texture, the degree of absorption of the ground, and ground colour are all related to painting technique (watercolour, tempera, oil). For canvas and wooden supports, such preparation consists of powdered chalk or gypsum mixed with an adhesive, typically an animal glue, spread in the surface in different number of layers depending on the support. The ground typically used in medieval Mediterranean paintings on wood consisted of several applications of *gesso grosso* (thick gypsum with great grain), followed by multiple smoothing and applications of *gesso sottile* (fine gypsum

with small grain), bound in animal glue [32]. While, for painting on canvas the preparation is usually very thin because it is made of few layers consisting of the simple glue sizing and the fine gypsum preparation, sometimes mixed with white lead in order to provide a more compact ground [33].

For what concerns paper sheets, the preparation consists in the paper ingredients themselves such as the adhesives as binder for the fibres, do not requiring a further level before the decorative and graphical apparatus.

1.1.3 Pictorial level

The painting layer is an intricate mixture of components made by two types of materials: the colours and the binder. There are many factors for colour classification but the very first division is between mineral and artificial. In this thesis, we focus the attention to the mineral pigments used in the pre-contemporary art before the intense chemical production of artificial colours that began in the mid-19th century [34]. Thus, the considered pigments come from natural origins, obtained from minerals, plants or animal remains. The main pigments used in painting up to the pre-contemporary age are summarised in Table 1.3 by colour distinction.

Table 1.3- The main pigments used in pre-contemporary painting [34].

Colour	***Pigment***
Black	Carbon Black, Bone Black, Lamp Black, Vine Black
Blue	Prussian Blue, Egyptian Blue, Azurite, Lapis Lazuli,
Green	Green Earth, Malachite, Chrysocolla
Red	Red Ochre, Cinnabar, Read Lead, Cadmium Red
Yellow	Yellow Ochre, Orpiment, Naples Yellow
White	San Giovanni White, Lead White

For the application over the ground layer, such pigments need to be mixed with a binder, also called medium, which is an adhesive substance that produces cohesion between pigment powder granules and the adhesion on the ground layer. Among the most used binders in the pre-modern art there are eggs, drying oils and casein, producing tempera and oil paintings, respectively.

The word *tempera* comes from the Latin verb "*temperare*" which means mixing in the right measure. This is the oldest painting technique used from the classical era and in the Medieval period and Early Renaissance, until the diffusion of the oil technique. This is based on the dispersion of pigments in a greasy binder that is miscible with water. Although the term is typically associated with egg yolk as the binder, it is also applied to paints made with casein, gum or animal collagen. The lipid and protein components of the binder provide the tempera paintings to dry to a hardened and durable paint film. The characteristic short drying time required utmost control from the painter and specific skills of applying the pictorial elements [15], [32], [35]–[37].

Oil paint is a slow-drying paint consisting of pigment particles suspended in a drying oil, extracted from various vegetable seeds. The most commonly used is the linseed oil, which, as the other drying oil, tends to reduce the opacity of colours and facilitate their drying. The viscosity of the paint may be modified by the addition of a solvent, such as turpentine, and varnish may be added to increase the glossiness of the dried pictorial film. Other additives may also be used either to accelerate or retard drying (various oils and resins), as well as to alter the transparency of the paint [15], [20], [37].

Hidden features

The main features that can be found hidden beneath the several layers of a painted artefact can be distinguished in two classes: structural and graphical. Belong to the first category the intrinsic characteristics of the materials, such as veining and knot in wood, the pattern in canvas or paper and any traces of plastering. Moreover, damage of the support is considered, such as voids in the structures, detachments between the layers, traces of biological attack (i.e., woodworm galleries in wooden supports). Such elements can be dangerous for the conservation of the pictorial apparatus and, in general, for the artwork itself, so their identification and characterisation are crucial for preservation purposes.

Regarding the decorative hidden features, underdrawings and *pentimenti* are the main elements that are buried under the superficial level. In particular, the underdrawings can be defined as the drawing made by the artist on the ground of a panel or canvas as the basis for a painting before the application of colours, so this is a sort of guideline for the painting [38]. This can be made by black materials such as charcoal or graphite or even with red ones, such as *sanguigna* (sanguine). Although both the black materials are carbon-based, they have differences in manufacturing provenance and chemical structure, showing different optical and thermal response to light stimulation. Charcoal is made from burning wood, while graphite is a mineral, an allotrope of the

element carbon, which occurs naturally in various types of rocks. Charcoal is considered a popular material for drawing since the Renaissance, when it was used for preparatory purposes such as to develop initial ideas, preliminary outlines and areas of shadow. In the 19th century, artists used charcoal to make highly detailed drawings thanks to its ability to produce an interplay between light and shadow known as chiaroscuro [39]. Graphite was employed for drawing in central Europe during the 16th century, but its use became more widespread in the late 18th century thanks to its massive fabrication [40].

The term *pentimenti* indicates the change of mind of the artist on the painting level then covered by further pictorial material in the final aspect of the artwork. Painters may make numerous revisions of the image, as the painting develops, thus such element is fundamental for the description of the creative process of a painting, reflecting on the artist's *modus operandi.*

1.2 Historical books and manuscripts

Before the invention of printing, all kinds of document were written by hand, originally in the form of scrolls and then as books. Manuscripts are worldwide considered CH because of their ancient tradition and complexity in realisation. Indeed, such artworks are elaborate multi-layered objects composed of many structural and decorative elements. Since the invention of mobile stamp and the worldwide spread of literacy, the creation of written texts was carried out by a very small number of artisans, thus producing a limited number of manuscripts. This limitation was also due to the long and complex process of books manufacturing, requiring expert skills in materials preparation, decoration and writing [41], [42].

1.2.1 Parchment support and structure

The first important step in books manufacturing was the preparation of the supports, historically made of parchment but later on of paper. The preparation of parchment writing support requires many phases, different depending on the historical period and geographical area. The main steps common for every case can be considered as following:

• Skin peeling

• Calcium hydroxide washes and baths,

• Hair removal

• Tensioning on frames to give the leaves rigid and flat shape

• Drying and sanding.

Since the preparation of the writing supports required long and complicates processes, in addition to expensive raw materials and manufacturing skills, they were often scarce in quantity. For such reasons, books considered no longer necessary or of minor importance were often reused in the composition of new books. The practice of reusing writing supports was very common in Middle Age and it consisted in disassemble older books for the recycling of parts to reinforce the structure or to replace parts difficult to obtain in new conditions. The reused papers, also called 'binding waste', inserted within the bookbinding as reinforcement was often hidden in the covering or in the sewing guards (Figure 1.3). Such practice has brought to the creation of unique documents as complex overlapping structures not detectable by naked eye, coming from different contexts and historical periods.

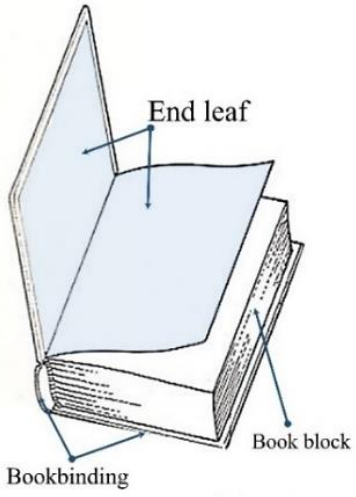

Figure 1.3 - Scheme of a typical bookbinding structure of an historical book.

1.2.2 Writing and decoration media

As the complex procedures for the preparation of the writing support, also the writing media required particular raw materials prepared with ancient recipes. The texts on historical book were usually written with black inks while the decorative parts, such as illumination or decorations on the pages, were made with pigments, often enriched with golden background. The earliest inks used on papyrus were principally simple suspensions of carbon in gum media. With the introduction of parchment as writing support, the change to iron-gall inks became essential, since carbon-gum ones would not adhere over the time to greasy parchment. From the 11th century, with the great use of parchment and paper as writing support, iron-gall inks began to be the main materials in books creation. Nevertheless, carbon-containing inks continued to be used for documents and very often small amounts of carbon pigment were used to make the iron-gall inks more legible immediately after writing [15], [43].

Regarding the illuminations, the presence or absence of decoration depends on the type of text and on its use, as well as on the commission. Undoubtedly, the holy books were of such value that it had to receive special attentions in terms of aesthetics and decorations. For such category of embellishment, a distinction must be made between the following elements:

- illumination, which is a figurative decoration, like pictorial scenes of various contents (naturalistic, figural, portrait, etc.) of small or large dimensions;
- ornamentation that has non-figurative role but rather aesthetic and beautification [41].

Despite their aims, these elements are complex structures, being made of many materials typical of paintings, such as underdrawings, golden leaves background, pigments mixed on binding media and, in some cases, also superficial varnishes as protection.

1.2.3 Hidden features and waste materials in bookbinding

Among the components of a historical book, several hidden features can be detected, mainly linked to two elements:

- bookbindings → reused sheets (waste materials)
- decorative elements → *pentimenti*, underdrawings.

The possibility of discovering hidden texts by means of non-destructive techniques is crucial for conservators and books researchers, since it allows to reveal the layering of the artefact and its features under the surface without dismantling the structure of the book.

As mentioned in section.1.2.1., the practice of reusing parts of older books was very common in the past for the construction of a new *codex*. The reused book fragments are commonly referred to the term 'binging waste' because the low consideration of the importance of the mentioned reused material. Nevertheless, such elements provide precious information, being documentary material about the evolution of writing and reading practices but also the literary preferences. Thus, the discovery of reused papers within the bookbinding structure can be really important for several factors: temporal reconstruction of the artefact through textual analysis of the hidden features, codicological evidence but also for the achievement of information about the manufacturing process itself. Hence, the importance of being able not only to identify hidden elements but, above all, to read them clearly. Indeed, the detection of such features without the capacity of reading them is useless for the achievement of a better understanding of the book history and manufacturing. Furthermore, the readability of hidden texts is crucial for palaeographic purposes,

aimed to the total characterisation of historical books and the documentation of the writing traditions.

For what concern the illuminations, as in the case of paintings, also in this kind of decoration can be found underdrawings or the *pentimenti*. Furthermore, it was a very common practice to censor nudity even in this type of decorative context, so in many cases, graphical or pictorial elements were superimposed on the original design. The possibility of investigating under such features is interesting for both artistic and historical motivations, being cable to recover the original appearance of the decoration.

2 Non-destructive IR imaging techniques

Infrared imaging is widely used as non-destructive diagnostics of painted artworks to reveal underlying features. Indeed, the operating principle of imaging techniques in the CH field is based on the analysis, in the form of images, of the interaction processes between the incident light and the matter that composes the artefact itself. The incident radiation can be reflected, absorbed and transmitted by the investigated object, depending on the combination of properties of the radiation and object (Figure 2.1). Therefore, the depth of the sample layer to be analysed addresses the choice of imaging technique, depending on the penetration capacity of the incident beam employed which, in turn, depends on its specific wavelength.

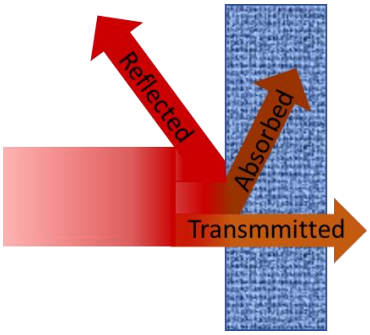

Figure 2.1 – Behaviours of an electromagnetic wave when incidence on a material: it can be reflected, absorbed or transmitted.

The work in this thesis is focused on the use of techniques operating in the middle wave-IR range, namely pulsed thermography and reflectography, being compared and completed with near-IR techniques (standard and laser reflectographies), allowing a deeper characterisation of the investigated sample.

With regard to the main technique, i.e. thermography, the investigated radiation is that emitted by the sample in the MWIR range, due to the absorption of the incident (VIS) light, as will be discussed in section 2.1. In the case of MWIR reflectography, on the other hand, the recorded radiations correspond to the MWIR ones reflected and backscattered by the sample, as illustrated in section 2.2.

In section 2.3, complementary techniques will be presented, describing NIR imaging techniques, colorimetry and vibro-acoustic method used in the study of laboratory samples and of original artefacts.

2.1 Pulsed Thermography

The MWIR spectral range is mainly exploited by thermographic techniques, being only recently adopted for reflectographic survey in particular cases. Among the different IRT active configurations [44], [45], such as for examples pulsed and lock-in ones, pulsed thermography (PT)

is a photothermal method widely used for the study of inhomogeneities in CH items based on the locally-resolved recording of the emitted IR radiation from the sample after an induced heating within its volume. One of the aims of this thesis is to study the types of the information achievable by the combined use of the two MWIR techniques in CH analysis by employing the same device. Moreover, the MWIR reflectography results provide a spectral extension of the ones obtained in the NIR range by different reflectographic methods and configurations.

2.1.1 Heat transfer principles and thermographic signal

The thermographic method used in this thesis investigates the different thermal response of the studied objects to the illumination with a visible light source. In particular, the thermographic signal evolution depends on the heat transfer processes activated in the sample by light absorption. Therefore, in this section, some main aspects of heat transfer processes are shortly discussed to provide a description of the MWIR techniques working principles.

The heat transfer processes generally occur by a combination of three different mechanisms, such as convection, irradiation and conduction [46].

The convective mechanism is the result of the movement of fluids carrying thermal energy in their motion. The equation that expresses the heat transfer by a moving fluid is the following:

Equation 1

$$q_{cv} = h\left(T_s - T_f\right)$$

where q_{cv} is the convective heat flux from a surface at uniform temperature T_s to the surrounding fluid at temperature T_f, while h is the convective heat transfer coefficient [46].

By the radiative mechanism, heat transfer is based the emission and absorption of electromagnetic waves. The physical laws governing the emission and thermal absorption of electromagnetic waves make use of the concept of a black body, i.e. any object capable of completely absorbing energy radiated from any direction and wavelength. According to the Planck's law, the power irradiated by a blackbody at a given absolute temperature T per unit area and wavelength, is given by the spectral exitance $M_{b,\lambda}$ that varies with the wavelength λ as:

Equation 2

$$M_{b,\lambda} = \frac{c_1}{\lambda^5\left(exp\left(\frac{c_2}{\lambda T}\right) - 1\right)}$$

where $c_1 = 2\pi hc^2 = 3.74 \times 10^{-16}$ Wm^2 and $c_2 = hc/k_B = 1.44 \times 10^{-2}$ mK, being h, k_B, c the Plank constant, the Boltzmann constant and the speed of light, respectively.

Figure 2.2 shows the emission wavelengths coming from a blackbody from 280 to 320 K in a bronze artefact inset. Here, it can be noticed that at the typical room temperature (300 K) such emission occurs mostly in the infrared wavelength range, centred at about λ=10 μm.

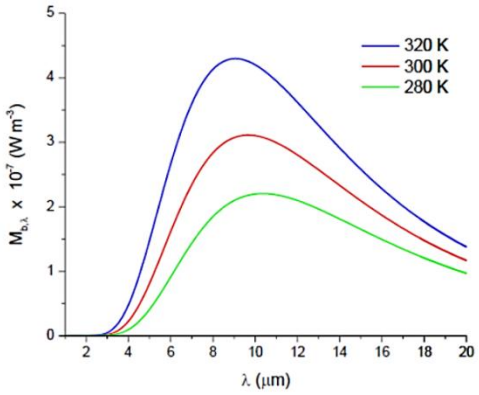

Figure 2.2 - $M_{b,\lambda}$,V_S wavelength obtained for the T values reported in a bronze inset.

Observing the curves obtained at different T values, it can be observed that each curve reaches a maximum value which decrease with T according to the Wien displacement law as [47], [48].

Equation 3

$$\lambda_{max} T = 2897.7\ \mu m\ K$$

Finally, it can be also noticed that the area under the plots shown in Figure 2.2 are larger with increasing temperatures. The values of such areas give the total power emitted per unit area of the blackbody surface which, according to the Stefan-Boltzmann law, grows with T as [49]

Equation 4

$$q_{rd,b} = \int_0^\infty M_{b,\lambda} d\lambda = \sigma T^4$$

Where σ =5.67 x 10^{-8} W/m^{2}K^4 and it is known as Stefan-Boltzmann constant.

Real objects do not behave like black bodies, as they absorb only part of the incident radiation and the remainder is reflected or transmitted. However, most objects show a spectral distribution of emitted power similar to that of the blackbody, at least for limited ranges of temperature and wavelength. For this reason, Stefan's law can also be applied to real situations by adapting Equation 3 and Equation 4 for real objects. Thus, in the grey body approximation, this can be done

by introducing a multiplicative factor ε called emissivity [50] which for a given temperature relates the spectral exitance of a real body $M(\lambda, T)$ to that maximum of a black body $M_b(\lambda, T)$ as:

Equation 5

$$\varepsilon = \frac{M(\lambda, T)}{M_b(\lambda, T)}$$

Thus, the power irradiated per unit area form a real object is obtained as:

Equation 6

$$q_{rd} = \varepsilon\, q_{rd,b} = \varepsilon\sigma T^4$$

According to the Equation 5, the emissivity ε is a unitless quantity ranging from 0 to 1 (ε =1 for a black body). Such parameter depends on several factors and properties of the material like the surface finishing or the sample temperature. Similarly, the ability of a real body to absorb electromagnetic energy is characterized by the absorbance coefficient α given by the ratio of the absorbed flux to the incident one, where $0 < \alpha \leq 1$, being α =1 for a blackbody. The relation between absorbance and emittance for a blackbody is expressed according to the Kirchhoff's law of thermal radiation as:

Equation 7

$$\alpha = \varepsilon$$

The calculations of the radiative heat transfer rate between different samples are generally complex. However, a particular frequent case can be modelled as the heat transfer between an object at temperature T_s placed in a cavity at uniform temperature T_b. The net radiative heat transfer rate, defined as the transferred power, is thus given by:

Equation 8

$$W = \varepsilon\sigma A(T_s^4 - T_b^4)$$

where A is the area of the sample surface.

From the Equation 1 and Equation 8 it can be stated that the amount of heat transferred by radiative and convective mechanisms becomes more relevant as the difference between the temperature of the sample and that of the surrounding media increases. However, in most PT experiments the induced temperature variations at sample surface are very small (< 10 K) so that radiation and

convection do not assume a primary role in the heat transfer process, which is rather governed by conduction mechanism, the contribution of which will be described below.

The conduction mechanism implies to the heat transfer resulting from the interaction between neighbouring particles of the matter at different temperature values due to their different kinetic energy. The equation which describes the generated heat flux is known as Fourier's law which, expressed in one-dimensional form as following [46], [51], [52]

Equation 9

$$q_{cd} = -k \frac{\partial T}{\partial x}$$

where q_{cd} is the heat transferred in the x-direction per unit area and time. Such flux is proportional to the component ($\partial T/\partial x$) of the temperature gradient in this direction. Here, the minus sign indicates the direction of the heat, transferred to decreasing temperature. The constant k is the thermal conductivity which is a material property that considers the conductive heat transfer mechanisms. In this respect, thermal insulators are materials characterized by low k values while at high values of k corresponds substances considered as thermal conductors.

PT measurements investigate the spatial and temporal distribution of temperature in a medium that depends, among other things, on the specific type of heating and the boundary conditions imposed by the geometry of the sample. Such a distribution can be obtained by solving the heat diffusion equation associated with the conduction mechanism, as following:

Equation 10

$$\frac{\partial^2 T(x,t)}{\partial x^2} = \frac{1}{D} \frac{\partial T(x,t)}{\partial t}$$

where t is the time and D is the thermal diffusivity of the material, namely a thermophysical quantity that considers the propagation rate of a temperature perturbation through the material. The distribution of the temperature rise, which is induced in thermographic measurements, can be obtained by solving the heat diffusion Equation 10 under appropriate boundary conditions, as described below.

Referring to Equation 6 in the previous Section, the power emitted by a sample surface related to the surrounding temperature T is calculated as follows:

Equation 11

$$W = \varepsilon A \sigma T^4$$

where A is the area of the emitting surface. When a temperature variation ΔT <<T is induced, as in active thermographic measurements, the thermal emission from the sample changes according to

Equation 12

$$\Delta W = 4\varepsilon A \sigma T^3 \Delta T$$

Equation 12 is applied in the cases where the radiation emitted in all direction is detected in the entire spectral range. In real measurements with IR detectors, their limited sensitivity in a precise spectral range (Δλ) and their geometry (Figure 2.3) are factors that influence the power emitted by a surface which is detected in thermographic measurements.

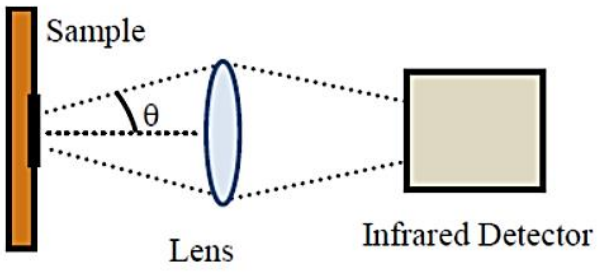

Figure 2.3. schematic representation of the geometry in the collection of thermographic signal.

Thus, a more suitable expression for defining the generation of the infrared signal *S* can be obtained as follows:

Equation 13

$$S = \varepsilon A \sigma \, sin^2(\theta) \, T(\lambda_d) R(\lambda_d) \left[\frac{\partial M_{b,\lambda}}{\partial T} \Delta\lambda \right] \Delta T$$

where θ is the angle subtended by the infrared optics, $R(\lambda_d)$ is the detector spectral sensitivity and $T(\lambda_d)$ is the spectral transmission efficiency of the optics.

Equation 13 demonstrates that, to a first order approximation, the infrared signal is proportional to the induced temperature rise ΔT. Indeed, active thermography basically relies on such a dependence to measure the induced temperature rise on a given sample surface by means of a spatially resolved detection of the IR radiation emitted at the sample surface.

2.1.2 Infrared thermography and cultural heritage

Pulsed thermography (PT) has become one of the most widely employed method for non-destructive investigations in different types of artworks, providing information on defects, inhomogeneities and subsurface features on bronzes [47], manuscripts and illuminations[53], [54], paintings on different kinds of supports [7], [55]–[57]. PT relies on the time-resolved measurement of the IR radiation locally emitted from the sample surface following the heating induced by short VIS light pulses. The detection of this emission is carried out by means of an IR camera in the form of a sequence of frames, called thermograms, recorded with increasing delay time Δt from the incident light pulse. These thermograms describe the spatial distribution of the amount of the IR radiation coming from the different parts and features of the sample, related to the temperature distribution at the sample surface and subsurface. The thermograms are often presented in the form of grayscale images, where the darkest areas correspond to the ones emitting smaller amount of IR radiation, namely the coldest ones in homogeneous samples. The sequence of IR images forms a 3D matrix (Figure 2.4), where x and y coordinates are the horizontal and vertical pixel positions, respectively, and the z coordinate corresponds to the time axis [58].

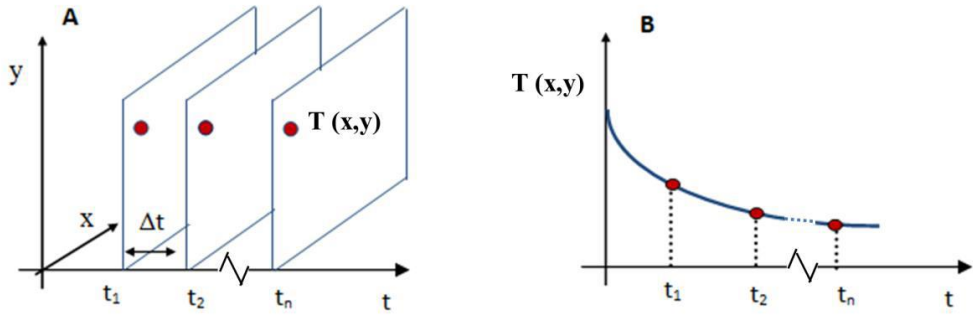

Figure 2.4 (A) Temperature 3D matrix on the time domain and (B) temperature profile for a non-defective pixel [59].

PT can be applied in two different configurations: the reflection and the transmission one (Figure 2.5) but in this thesis, the only reflection set-up was adopted. In the reflection configuration both the heating source and the detector of the emitted infrared radiation are placed at the same side of the investigated sample, while in the transmission configuration they are located on opposite sides.

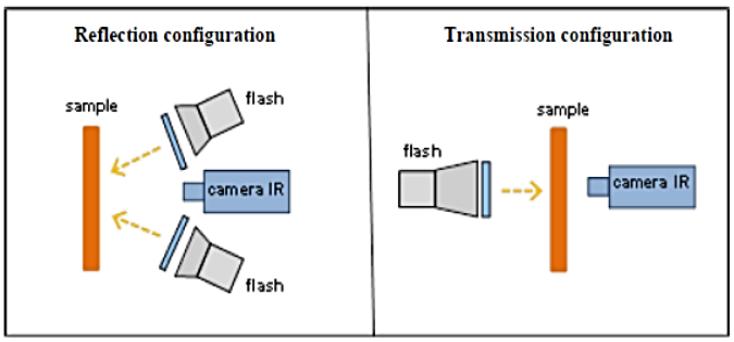

Figure 2.5 Reflection and transmission configuration scheme.

In the following, the expressions for the temperature field induced in reflection configurations will be presented to provide the basis for the description for the quantitative and qualitative PT applications carried out in this thesis.

Considering a homogeneous material slab having thickness L and homogenously heated at time $t=0$ by a short pulse that is absorbed at the surface ($x = 0, opaque\ material$), where the emitted radiation is detected as well (Figure 2.6). The subsequent heat diffusion into the sample gives rise to a local temperature change $\Delta T(x,t)$ which depends on depth x and time t.

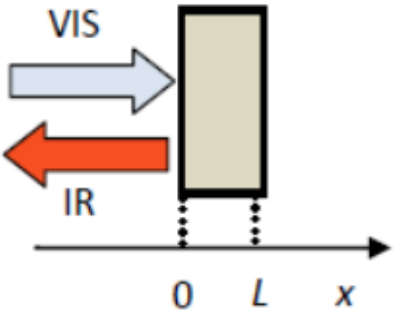

Figure 2.6 Schematic representation of the reflection configuration in the case of a homogeneous material slab.

The induced temperature variation can be calculated by solving the unidimensional heat diffusion equation (Equation 10) under the following boundary conditions:

Equation 14

$$I_0 = -k\frac{\partial T}{\partial x} \qquad x = 0$$

$$-k\frac{\partial T}{\partial x} = 0 \qquad x = L$$

The first condition states that the energy diffusing into the sample by heat conduction corresponds to the light intensity I_0 absorbed at the surface x=0. The second assumes the heat conduction from the sample to the surrounding air is negligible due to low thermal conductivity of air.

2.1.3 *Infrared thermography in opaque materials*

In the cases of opaque materials, the solution of Equation 10 obtained under the above boundary conditions provides the following equation to describe the time dependence of the temperature rise at a depth x:

Equation 15

$$\Delta T(x,t) = \frac{Q}{\sqrt{\rho c k}} \frac{\sqrt{D}}{L} \left[1 + 2 \sum_{n=1}^{\infty} cos\left(\frac{n\pi x}{L}\right) exp\left(-\frac{n^2\pi^2}{L^2} Dt\right) \right]$$

where Q is the energy density absorbed at the surface x =0; ρ, c, k are the material density, specific heat and thermal conductivity, respectively. Here, the time dependence is characterized only by the sample thickness L and thermal diffusivity D. Substituting in the expression x=0, the solution at the sample front surface can be obtained as follows:

Equation 16

$$\Delta T(0,t) = \frac{Q}{\sqrt{\rho c k}} \frac{\sqrt{D}}{L} \left[1 + 2 \sum_{n=1}^{\infty} exp\left(-\frac{n^2\pi^2}{L^2} Dt\right) \right]$$

Figure 2.7 shows the logarithmic plot of the decay of the surface temperature with time calculated for increasing L values and for D = 0.19 cm^2/s which is the typical value of thermal diffusivity for the bronze [60].

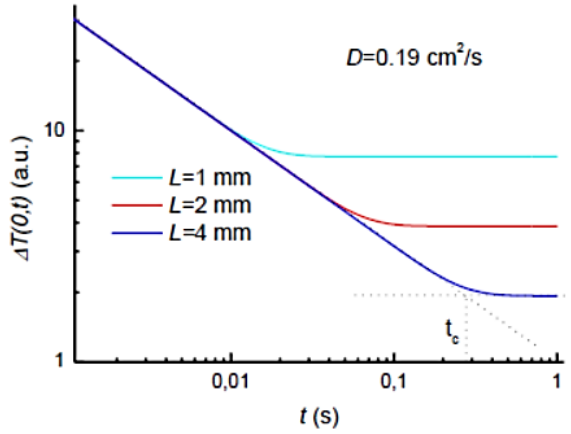

Figure 2.7 - Logarithmic plot of the decay of surface temperature calculated for the example bronze inset.

Two different behaviours can be notice from the graphs. The first, characterized by a –1/2 slope line in the logarithmic plot, is observed at short times, when the surface temperature change ΔT(0,t) evolves as $t^{-1/2}$, as expected from the theory of the heat diffusion in a semi-infinite homogeneous material according to which it can be expressed as

Equation 17

$$\Delta T(0,t)_{L=\infty} = \frac{Q}{\sqrt{\rho c k}} \frac{1}{\sqrt{\pi t}}$$

The second behaviour is observed when the heat reaches the opposite surface x=L and further diffusion is inhibited. At long times $\Delta T(0,t)$ stabilizes to the thermal equilibrium value [20, 21]

Equation 18

$$\Delta T(0,\infty) = \frac{Q}{\sqrt{\rho c k}}\frac{\sqrt{D}}{L}$$

corresponding to a horizontal plane in the graph.

The reflection configuration of PT allows the quantitative determination of the thermal diffusivity in opaque materials. From the plots shown in Figure 2.7 it is possible to derive the crossing time t_c which corresponds, in the $\Delta T(0,t)$ graphs, to the intersection point of the lines extrapolating the time dependence described by Equation 17 and Equation 18. Such parameter (when the values predicted by the two equations coincide) is therefore related to thermal diffusivity by:

Equation 19

$$D = \frac{L^2}{\pi t_c}$$

2.1.4 Infrared thermography in semi-transparent materials

In the CH field, applications on opaque artefacts are widely documented in the literature, such as those on bronzes [61]. However, there is a broad variety of artefacts (like paintings, books, handscroll) that are not opaque but semi-transparent, for which the signal generation model just outlined based on the absorption of incident light only at the sample surface cannot be applied. More complex models are therefore needed also considering the light absorption and the heat generation within the volume of the artefact.

Library materials: the readability of the hidden texts

Among other applications, pulsed thermography is often used for the study of ancient manuscripts and library heritage [54]. In particular, PT is a useful tool for the detection of sub-surface features beneath the end papers of historical book-bindings, such as hidden written parts, providing the in-depth mapping of the investigated object and also indications of reused manuscripts (see Section 1.2). In this context, the identification of hidden texts is as fundamental as the possibility of their reading, for palaeographic and codicological purposes. Indeed, recovering the legibility of texts buried under layers of paper is a very valuable element for understanding ancient texts and

reconstructing amanuensis procedures. It is therefore of paramount importance to know the conditions for obtaining a clear thermographic image of these artefacts, which are often composed of overlapping layers of materials. It is important to note that usually features located at larger depth are detected by thermograms recorded at larger delay from the light perturbation. This is due to the larger time needed by the heat, possibly absorbed by the front material, to reach the buried features and/or to travel back to the surface and be detected by the IR camera.

In the case of hidden texts, they are usually buried under layers of paper or parchment and one of the main sources of distortion of texts displayed by thermographic images is the poor sharpness of the ink edge. This distortion is usually larger the deeper the location of the features and, consequently, the larger the delay with which the thermogram was recorded. In fact, when a large time is needed for displaying the deep features also longer lateral diffusion of heat takes place, resulting in blurring of the detected elements. The loss sharpness and contrast in the text image results in a consequent loss of legibility.

In this thesis, the analysis of inked edge distortion was one of the main problems addressed and studied quantitatively. By means of paper-based samples, specially prepared to reproduce particular book structures, the evaluation of the edge distortion of sub-surface features in thermographic images was carried out as a function of the depth of the text beneath the front paper and of the time delay associated to the recorded thermograms. The mathematical model developed for this study will be presented in the following section, while the preparation of the laboratory samples, the analysis and results will be described in the following chapter Section.3.3).

Modelling of PT detection of hidden texts and edges distortion analysis

The theoretical study of the images contrast generation in fibrous semi-transparent media, such as paper and parchment, was carried out on the sample model in Figure 2.8, representing the structure of a paper sheet as support and a graphical feature buried under another paper sheet. In the sketch of the transversal section of the sample, the z-axis is considered along the sample thickness, while the $\bar{x}$ is the in-plane coordinate, Ω is the domain occupied by the paper sheet of thickness H and the ink slab, referred as Γ, is buried at the depth = d. In such configuration, the heating VIS pulse is absorbed within the volume of the specimen and a fraction of the incident light is also absorbed by the buried graphical layer. Unlike the opaque materials, in the case of semi-transparent media, the absorption of radiation is distributed within the sample, as it penetrates under the surface, so that the IR signal is generated in all the specimen volume and, in particular, also from the subsurface graphical layers.

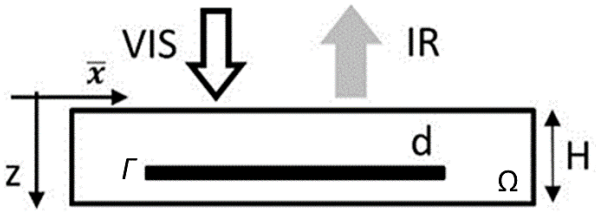

Figure 2.8 - Sketch of the test sample with its geometry and the directions of lighting/reflection.

The thermal stimulation of the sample is assumed to be produced by illuminating the sample surface at z = 0 with a VIS light pulse which, in semi-transparent media like paper, penetrates inside the sample slab and undergoes multiple reflections at its outer surface, depending on the reflection coefficient (R), which can then be neglected with respect to the VIS light absorption [48]. During its travel inside the specimen, the light beam undergoes a distributed absorption operated by the paper and a concentrated absorption operated by the ink layer each time it crosses the latter, producing a time dependent temperature distribution within the sample volume. Assuming a uniform light intensity I_0 illuminating the specimen, the VIS light time (t)-varying intensity distribution within the sample depth $I\ (\bar{x}, z)$ is given by [49] :

Equation 20

$$I(\bar{x},z) = I_0(1-R)e^{-\alpha z} + I_0(1-R)R\gamma^2 e^{-\alpha H}e^{-\alpha(H-z)} + I_0(1-R)R^2\gamma^2 e^{-2\alpha H}e^{-\alpha z} + \cdots, \qquad 0 < z < d$$

$$I(\bar{x},z) = I_0(1-R)\gamma e^{-\alpha z} + I_0(1-R)R\gamma e^{-\alpha H}e^{-\alpha(H-z)} + I_0(1-R)R^2\gamma^3 e^{-2\alpha H}e^{-\alpha z} + \cdots, \qquad d < z < H$$

where R is the reflection coefficient in the VIS range, γ is the fraction of the VIS light transmitted through the buried layer, namely the ink layer light transmission coefficient, and α is the VIS extinction coefficient of the slab taking into account both scattering and absorption effects, namely the light absorption coefficient of the paper. By analytically computing the sums of the infinite terms appearing in Equation 20, the following expressions for the VIS light distribution into the sample are obtained:

Equation 21

$$I(\bar{x},z) = \frac{I_0(1-R)}{1-e^{-2\alpha H}R^2\gamma^2}e^{-\alpha z} + \frac{I_0(1-R)R\gamma^2 e^{-2\alpha H}}{1-e^{-2\alpha H}R^2\gamma^2}e^{\alpha z} \qquad 0 < z < d$$

$$I(\bar{x},z) = \frac{I_0(1-R)\gamma}{1-e^{-2\alpha H}R^2\gamma^2}e^{-\alpha z} + \frac{I_0(1-R)R\gamma e^{-2\alpha H}}{1-e^{-2\alpha H}R^2\gamma^2}e^{\alpha z} \qquad d < z < H$$

In this model, the temperature distributions inside the slab domain (Ω) and the subsurface layer (Γ) are denoted by $T_{S(x,z,t)}$ and $T_{L(x,t)}$, respectively, both satisfying the following heat diffusion equations:

Equation 22

$$\rho c \frac{\partial T_S}{\partial t} - k_{\bar{x}} \Delta_{\bar{x}} T_S - k_z \frac{\partial^2 T_S}{\partial z^2} = f_S \qquad \text{For } \Omega \text{ domain}$$

$$h\rho_L c_L \frac{\partial T_L}{\partial t} - k_L \Delta_{\bar{x}} T_L = f_L + \bar{f} \qquad \text{For } \Gamma \text{ domain}$$

where ρ, ρ_L and c, c_L are the mass density and the specific heat of the slab and of the subsurface layer, respectively. $\Delta_{\bar{x}}$ is the Laplace operator with respect to the planar vector $\bar{x}$, while $k_{\bar{x}}$, k_z and k_L are the thermal conductivity components along the $\bar{x}$, z directions and the one referred to the subsurface layer, respectively. f_S, f_L are the heat generation terms defined as

Equation 23

$$f_S(\bar{x}, z) = \chi \frac{\partial I(\bar{x}, z)}{\partial z}$$

$$f_L = \Delta I(\bar{x}, d)$$

where f_S is the volumetric heat source due to the VIS light absorption at the slab volume and χ is the fraction of the VIS light energy converted into heat. f_L corresponds to a heat source per unit surface generated by the VIS light absorption at the buried layer, responsible for an intensity step-like decrease $\Delta I(\bar{x}, d)$ across Γ.

Once the time and spatial behaviour of the temperature inside the sample was computed, it is possible to estimate the profile of the IR radiation emitted by the sample and detected by the camera. In semi-transparent materials, such as the paper, the recorded IR signal $S(\bar{x}, t)$ is originated by the IR emission taking place not only from the sample surface but over the entire volume and, consequently, the corresponding expression is given by [48], [62], [63]:

Equation 24

$$S(\bar{x}, t) = K \int_0^H \beta T(\bar{x}, z, t) e^{-\beta z} dz$$

where K is a constant accounting for the heating light intensity and the configuration geometrical factor and β is the IR absorption coefficient of the paper.

As mentioned before, PT can be applied in two different configurations, calculating differently the signal contrast. In the configuration considered in the thesis, the reflection one, where the VIS light heating and the detection of the emitted IR radiation occur at the same sample surface, the PT signal is given by

Equation 25

$$S(\bar{x},t) = K\left[\int_0^d \beta T(\bar{x},z,t)e^{-\beta z}dz + \eta T_{\mathrm{L}}(\bar{x},t)e^{-\beta d} + \int_{\mathrm{d}}^{H}(1-\eta)\beta T_S(\bar{x},z,t)e^{-\beta z}dz\right]$$

Where η is the concentrated IR absorbance of the subsurface layer, corresponding also to its IR emissivity.

The PT signal expressions reported in Equation 24 and Equation 25 contain the physical parameters related to the thermal and optical properties of semi-transparent samples, fundamental for the application of the theoretical model to the interpretation of experimental data. Such parameters have been recently studied and quantitatively characterised for typical paper structure, summarised in Table 2.1 [49], [64], [65].

Table 2.1 – Optical and thermal parameters of ink and paper materials.

Thermal diffusivity of paper (D)	***IR extinction coefficient of paper (β)***	***VIS extinction coefficient of paper (α)***	***IR absorptance of ink (η)***
$(1.0 \pm 0.1)\ 10^{-3}\mathrm{cm}^2/\mathrm{s}$	$(2.4 \pm 0.2) \times 10^2\ \mathrm{cm}^{-1}$	$(1.30 \pm 0.15)\ 10^2\ \mathrm{cm}^{-1}$	0.9 ± 0.1

The hidden texts studied in this thesis typically correspond to texts belonging to parts of earlier library materials used in the binding of more recent books or *codex* [66]. As mentioned earlier, a part of the research carried out in this thesis concerns the analysis of contrast evolution and distortion effect in the thermographic images of inked features buried beneath paper leaves and the influence their geometric and physical parameters have on them. In order to understand the quality of the thermographic image in terms of readability of the hidden texts, the degree of the distortion was studied with the laboratory sample and compared with the typical size and spacing of text characters, the order of which typically varies between a few tenths and a millimetre. For this purpose, it is first considered the difference between the signal values at any point on the sample and that from a reference point laterally distant from the ink layer position, which can be used to denote the thermographic image contrast (C), defined as:

Equation 26

$$C_{(\bar{x},t)} = \left[S(x,y,t) - S(-\frac{A}{2},-\frac{B}{2},t)\right]$$

that is different from zero in correspondence of sample areas below which the ink layer is placed. Buried features characterized by a larger value of C can be more easily visualized in the recorded thermal images.

In order to quantitatively characterise the blurring in the images of the detected inked features, a distortion index (Δ_i) of the image is introduced according to the expression:

Equation 27

$$\Delta_i(t) = x_{\max}(t) - x_{\min}(t)$$

where $x_{\max}$ and $x_{\min}$ are the coordinates across the inked area where $C = C_{max} - \gamma C_{max}$ and $x_{\min}$ that where $C = C_{min} + \gamma C_{max}$, respectively. Here, γC_{max} (with $\gamma \sim 2\%$), corresponds to the minimum detectable contrast change. Therefore, $\Delta_i(t)$ indicates how differently from an ideal steep profile ($\Delta_i(t) = 0$) the signal contrast appears across the inked feature domain boundary.

Figure 2.9a-b shows the expected curves of change of contrast and the distortion effect with increasing delay times obtained from Equation 26 and Equation 27, respectively. In Figure 2.9a, the time dependence of the contrast is reported, calculated at the centre of the inked area with the parameter values reported in Table 2.1 at increasing delay times. Here, it is shown that the contrast reaches a maximum and then decays with time. The maximum occurs in a time t corresponding to that required by the heat generated at the ink layer position to diffuse up to the surface and it is proportional to d^2/D (where D is the thermal diffusivity of the material and d is the distance from the surface). In Figure 2.9b is reported the time dependence of the distortion parameter Δ_i which is shown to increase with time because of the lateral heat diffusion within the sample after the light pulse stimulation.

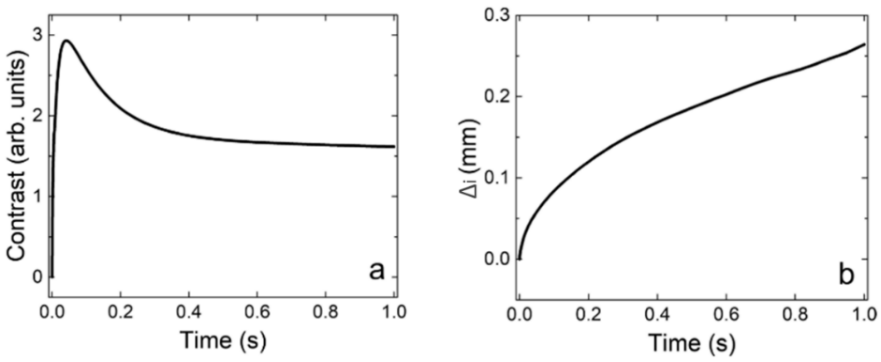

Figure 2.9 - Time dependence of the IR image contrast (a) and distortion effect (b).

Thus, for the characterisation of the distortion effect in PT images of inked features buried in semi-transparent media, experimental and theoretical approaches were followed. For the experimental, a properly-designed sample with the combination of ink and increasing thickness paper stripes was measured with PT (see Section 3.2). Then, for the theoretical evaluation, the heat diffusion equations discussed in this section were numerically solved by using the finite element model (FEM) implementation [67], [68]. To this end, the three-dimensional domains are meshed into prisms with triangular bases, whereas the two-dimensional surfaces are meshed with triangles. Linear shape functions are adopted to interpolate the nodal values of the unknown temperature inside each element. The finite element formulations were implemented in dedicated MATLAB programs used to perform the numerical simulations, shown in the next Chapter.

2.1.5 Pulsed Thermography set-up

In the PT set-up adopted in this thesis, the thermal stimulus is induced by two VIS flash lamps (Bowens Estime 3000, maximum power 650 W), employed to produce approximately 2 ms long light pulses. The lamps are usually positioned at a distance of about 0.5 m and with their axes at 45° with respect to the investigated surface. The sources were shielded with optical filters to reduce at minimum spurious infrared radiation emitted by the lamps and reaching the camera. The IR camera CEDIP Jade III MWIR was employed for the acquisition processes. Such a camera has a 320x240 Indium Antimonide (InSb) focal plane array with 30 μm pitch sensitive in the MWIR spectral range (precisely, 3.6–5.1 μm wavelength range). The adopted IR camera provides thermal images in 14 bits digital output format and is characterized by a thermal sensitivity of approximately 5 digital level (DL) units corresponding, for a black body, to a Noise Equivalent Temperature Difference (NETD) less than 25 mK at 30°C (20 mK typical). The Altair 5.50 software is used for both acquisition and post-processing phases. The software is used to process the images collected in the full frame mode with a frame rate that can be set up to 170 Hz, depending on the adopted integration time. False effects such as those associated with inhomogeneous heating, optical reflections and emissivity variations at the sample surface may result in additional contrast in the thermograms superimposing on that produced by the internal features, thus making the analysis of the recorded images more complex. To minimize these kinds of problems, several post-processing procedures were proposed, such as the so-called cold image subtraction (CIS) [44]. The latter consists in a pixel-by-pixel subtraction of the frame obtained just before the heating pulse from all the thermograms in the sequence after the pulse in order to remove static background contributions to the real contrast and increase the signal dynamics.

2.2 MWIR Reflectography

Infrared Reflectography is a well-established technique in the field of painting inspection that is especially suited for the detection of underdrawings and/or *pentimenti*. Besides the conventional NIR reflectography (NIR), more recently, MWIR reflectography (MIR) was also introduced for CH investigations with the aim of detecting features complementary to those achievable with the NIR [42], [69]. In fact, MWIR radiation is characterized by a larger penetration of the unscattered component in comparison with the NIR one, since pigments typically show different optical absorption and scattering properties in the mid-IR. For such reasons, MIR may enable the detection of elements of different compositions and also located at larger depths within the artefact in comparison to those detected by the NIR reflectography.

2.2.1 MIR operating principles

MIR reflectography basically consists in the recording of the reflected component of the IR radiation illuminating the sample. When the temperature distribution over the investigated object may be assumed almost uniform, the image contrast is mainly originated from local differences in the MWIR optical reflectivity. Thanks to the transparency in the IR range of several materials at the superficial paint layer, the incident radiation can reach the support where it can be either back-reflected or absorbed by the possibly present drawings, thus giving rise to contrasted features in the recorded reflectographic images. The degree of shielding of the paint layer is mainly due to the absorption of radiation by the pigment and the dispersion of radiation by the pigment particles.

In the MIR reflectographic measurements, the only reflected component of an incident radiation is considered. In this respect, it is worth noting that MWIR band is suitable for performing reflectographic measurements since blackbody at 293 K emits only 1.1% of its energy in the MWIR band.

2.2.2 MWIR Reflectographic set up

In the MIR setup, the sample illumination is carried out by means of carbon filament IR sources which are characterized by an emission wavelength range which includes the spectral range of sensitivity of the employed IR camera. Special care is always taken to minimize the exposure time and the power of the incident IR radiation in order to reduce the sample heating and, consequently, the mid-wave IR radiation thermally emitted by the sample, so that the sources are usually positioned at least 2m from the sample.

The same acquisition device and software used for PT are also employed for the MIR, thus ensuring the exact pixel-by-pixel correspondence of the images of the same areas recorded by the two techniques. In the case of MIR, the subtraction of the images is in general not required.

When comparing the two methods, PT was proved to be able to investigate subsurface features over a larger depth with respect to the MIR. On the other hand, MIR provides greater sensitivity to the detection of elements buried at a shallow depth or below layers with a small grain size, such as the pigments, compared to other layers made of different kinds of materials, like the fibres of a sheet of paper.

2.3 Complementary techniques

Two systems were used in this thesis for NIR reflectographic analysis on different type of artworks, exploiting two different sensors: a customised charged coupled device (CCD) camera and a laser scanner prototype.

Further non-destructive methods were employed as complementary methods for both laboratory tests and *in situ* analyses, namely colorimetry and vibro-acoustic technique.

2.3.1 NIR Reflectographic systems

CCD-based system

In CH investigations, NIR reflectography is successfully employed for revealing *pentimenti* and underdrawings thanks to the capability of the NIR radiation to propagate through the pictorial layers with respect to the visible radiation [10], [70]. In fact, this technique takes advantage of the smaller degree of scattering that affects the NIR radiation with respect to the visible one, thus providing optical access to the subsurface features of the investigated object. The transparency of a pictorial layer to the radiation, and then the visibility of the underlying features, depends on several factors, among which the optic properties of materials and, therefore, the chemical nature of the pigments, the paint layers' thickness and the radiation wavelength [65], [71]. In this thesis, NIR reflectographic measurements with the CCD-based systems were performed at the Laboratory for Non-Destructive Analyses and archaeometry (LANDA) of the "Sapienza" University of Rome. NIR reflectographs were collected with a low-noise digital CCD camera, cooled with a Peltier device and equipped with two bandpass filters (0. 9 μm and 1 μm). The CCD sensor (Kodak KAF8300) consists of a matrix of 3348 × 2574 silicon pixels (Figure 2.10). The sample was illuminated by means of two OSRAM SICCATHERM® IR lamps, with their maximum emitted intensity in the spectral range of 1.1–1.2 μm. The incident NIR radiation was diffused so as to

reduce as much as possible the reflected component from the investigated objects. The images were processed using MaxImLE acquisition software in order to subtract the CCD sensor dark noise and enhance the contrast of the displayed elements. The CCD analogue signal is converted into a 16-bit digital signal bits (65536 grey levels).

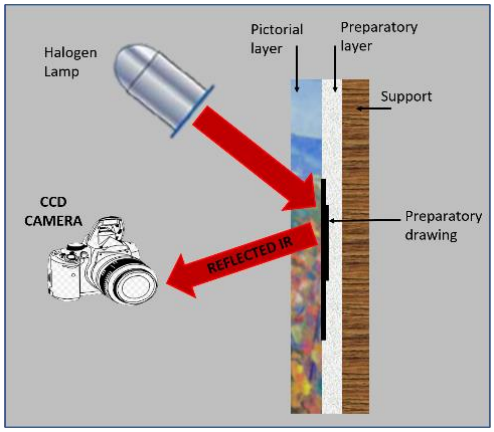

Figure 2.10 – Scheme of the NIR set up.

Laser-based system

The laser scanner employed in this thesis as complementary method for stratigraphic analysis on painted artefact is called IR-ITR (IR-Imaging Topological Radar). This is an IR laser scanner prototype entirely designed and developed at the ENEA Research Centre of Frascati (Rome, Italy), employed for the remote investigations of sub-surface features in layered objects. The scanner consists of two distinct parts (Figure 2.11): an optical head, consisting in lenses and mirrors for the focus, steering, and collection of the signals; the electronic module, for the optoelectronic signals' conversion and vectorization, the data acquisition and storage. The two modules are interconnected by a monomodal fibre, from where the laser beam is emitted, and a multimodal fibre, used for collecting the back-reflected signals from the target. The optical head includes an aspheric lens for focusing the launching laser beam on the artwork surface and a doublet lens (50 mm in diameter and 150 mm in focal length) for the detection of reflected light from a distance of up to 10 m. The laser spot has a diameter of about 2 mm and it is swept onto the target through a double-motorized MIR, which permits a TV raster-like movement of the beam on the surface.

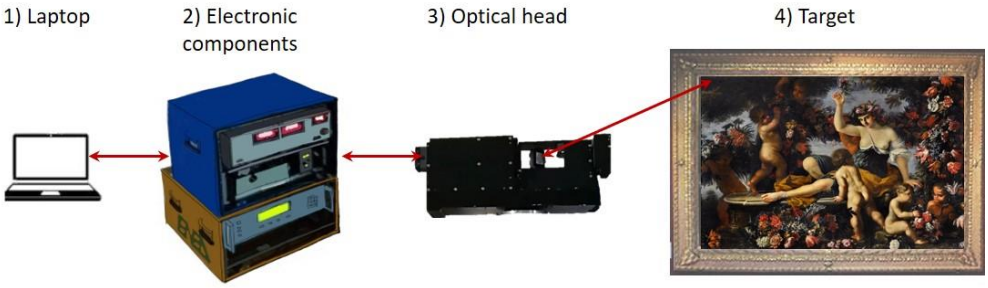

Figure 2.11. Scheme of the IR-ITR acquisition workflow.

IR-ITR prototype system is based on the amplitude modulation (AM) technique of the infrared laser source [72]. Such technique, combined with the lock-in detection, which can detect weak signals also in a noisy environment, estimates simultaneously the amplitude and the phase-shift of the signals generated by the light reflected from the target [73]. This method allows the remote probing of different types of surfaces, like the painted ones, revealing features buried beneath a few microns of the painted layer [74], [75]. The amplitude information, dependent on the laser/matter interaction characteristics at a specific optical wavelength, contributes to the grey-level intensity reconstruction of the target, while the phase-shift information can be used to estimate the distance between the scanner and the investigated surface. At present, the system is equipped with a monochromatic laser source in the NIR range (λ = 1.55 μm with a power density of less than 1 mW/mm^2)[76]. The reflected signals are detected by a low-noise photodiode detector and its amplitude and phase are measured by the lock-in amplifier unit. Due to mechanical limitations of the optical head, the rotation movement of the scanning mirror is 80° x 310°, with a maximum point-to-point precision of 0.002°, with a total resolution for a single complete acquisition of 40,000 x 155,000 pixels, equivalent to 6.2 GPixel of a commercial camera. Furthermore, the system is able to work independently from the surrounding lighting conditions, scanning the surfaces even during the night hours. The acquisition procedure and the post-processing are controlled by custom software developed in the MATLAB environment, which allow the set of the scanning parameters and the image processing algorithms to improve the mapping quality and interpretation.

2.3.2 Colorimetry

Colours are fundamental features of CH items and their characterisation and conservation are fundamental topics in CS. Nowadays, several methods and instrumentations are available for the science of measure the colour, the so-called colorimetry. The aim of colorimetry is the numerical specification of colour, which is done according to different reference systems and methods, developed throughout history for different fields of application. With the establishment in 1913 of the International Commission on Illumination, also known as the CIE from its French title, *the Commission Internationale de l´Eclairage*, the science of colour and illumination acquires the standardisation of systems and procedures [77]. For the applications presented in this thesis, two parameters belonging to the colour science were considered in pigments characterisation of artefacts:

1) reflectance spectra: for each wavelength investigated within the spectral range by the instrument, the reflectance spectrum of a studied colour is elaborated from the ratio between

the intensity of the reflected light and the incident one, measured with respect to the reflectance of a standard white reference. The reflectance spectra provide information useful for the identification of pigments because each pigment, and in general each material, has its own characteristic reflectance trend [78], [79];

2) colorimetric coordinates: in this study, the CIELAB 1976 reference system was used, represented by a three-dimensional space (Figure 2.12) in which colour is defined by L*, a*, b* coordinates. In this system, L* indicates the lightness of the measured colour and a* and b* are chromaticity coordinates translated in colour directions along the axes [79], [80].

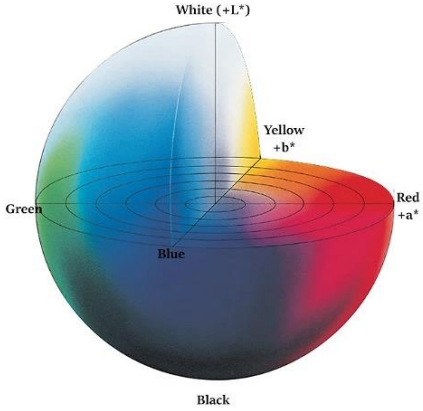

*Figure 2.12. CIELAB three-dimensional colour space with the L*a*b* coordinates [79].*

In pre- and post-restoration studies of an artefact, colorimetric measurements are carried out to assess the difference in colour and brightness following restoration and cleaning procedures. In this context, the difference between the colours (ΔE^*_{ab}) in the two different situations is given by the following expression:

Equation 28

$$\Delta E^*_{ab} = \sqrt{(L^*_1 - L^*_2)^2 + (a^*_1 - a^*_2)^2 + (b^*_1 - b^*_2)^2}$$

Such parameter, together with the difference of brightness before and after the restoration ΔL^*, are used for the evaluation of the effectiveness of cleaning and conservative practises.

Among the techniques available for colorimetric measurements, spectrophotometric instruments allow to acquire both parameters of reflectance spectra and the colorimetric coordinates. In this thesis, the fiber optics reflectance spectroscopy (FORS) was employed, which is a widely used non-destructive technique for the characterisation of the colours in painted artefact. The system employed in this thesis for colorimetric measurements consists of a cube as a probe optically coupled by means of fibres to a green-wave spectrometer, equipped with a halogen lamp as lighting

source, for measurements within the range 0.35 – 1.15 μm [81]. The cube contains an internal integrating sphere that allows the acquisition of all the backscattered light from the sample without dispersions. The collected light following the interaction with the sample is then analysed by a spectrophotometer, which is connected to a laptop providing the spectra through the software interface.

In this thesis, FORS measurements were performed on painted artefacts on paper and papier-mâché supports, as described in Chapter 4.

2.3.3 *Vibro-Acoustic imaging*

As further complementary method in laboratory tests, vibro-acoustic imaging was used, recently applied as non-destructive technique for the detection of the presence of cavities, voids and detachments areas in stratigraphic CH investigation, such as frescoes or paintings on wood. The laser doppler vibrometry (LDV) system employed in this thesis is an experimental prototypal set-up implemented Laboratory of Acoustics Research applications for Cultural Heritage (LARCH), CNR Area of Tor Vergata (Rome, Italy) for studying complex and heterogeneous layered materials by evaluating the vibration of structural inhomogeneities between adjacent elements when stimulated by acoustic waves [82]–[84]. In particular, LDV combined with acoustic excitation was used as non-invasive method for characterising the support of the laboratory sample and its induced structural defects., as described in section 3.1.2.

Such method exploits the capability of the acoustic waves to induce a vibration on the materials and on the air cavities between the delamination of multi-layers structures. Further specifications are necessary in order to better understand the principles of vibro-acoustic measurements: any material has specific vibration frequencies when it is excited by the acoustic namely, the normal modes, i.e. the fundamental mode and the high-order modes. The first one is the maximum resonance of the object. The normal modes are the vibration frequencies characteristic of the material itself, whether the presence of defects or delamination and at which an object tends to oscillate in the absence of constraints, such as ideal cases or undamaged material with regular geometrical features. Plotting these normal modes as 2D image, they will follow characteristic vibration patterns with regular geometries. Finally, the high-order modes are distinctive frequencies depending on the geometrical and physical properties of the subsurface and on the occurrence of inhomogeneities, therefore differing from the normal modes [82], [85].

The vibration frequency and the cavity depth are proportionally inverse which means that if the cavity is at a depth just beneath the surface (i.e. low *d* values), the detected frequencies will have high values.

The LDV ensures non-destructive analyses exploiting the optical interferometry: the measurement consists in the emission of two coherent beams (reference beam and measurement beam) from the optical head of vibrometer which embed an interferometer. The measurement beam is focused on the investigated surface and it is then reflected back inside the optical sensor head where it is recombined with the reference beam into the interferometer. The reflected beam is the carrier of the vibrational information from the investigated object, i.e. the vibration velocity. The difference between the reference and the reflected beams, processed by the LDV controller processor, provides the target velocities, extracted as voltage output directly proportional to the velocity of the vibrating surface.

The measurements set-up consisted in a Polytec Single Point LDV composed of the optical sensor head OFV303 and the controller processor OFV-3001-S. The Audio Spotlight commercial Parametric Acoustic Array (PAA) by Holosonics was used as contactless acoustic excitation source. A 16-bit multifunction data acquisition board and a laptop complete the system for the acoustic wave generation, vibration velocity acquisition and its processing, by using a custom software package entirely developed by the LARCH Laboratory in LabView environment for the setting of all the parameters for the measurements. Figure 2.13 shows a scheme of the experimental settings and electronics.

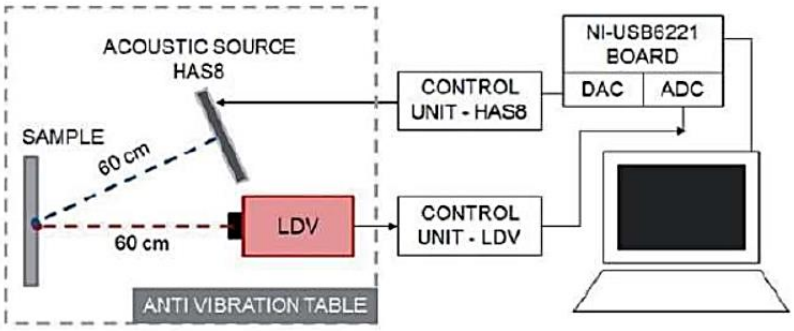

Figure 2.13 – scheme of the vibro-acoustic imaging apparatus [82].

Data processing was carried out by observing the typical frequencies of the normal modes of the sample material in order to study the behaviour of defects at the same frequencies.

The LDV optical head and the acoustic source operated in the horizontal plane fixed on an antivibration table, while the sample was mounted on a motor controlled linear guide maintaining

its central axis in the horizontal plane. The laboratory prototypal measurements set-up is shown in Figure 2.14

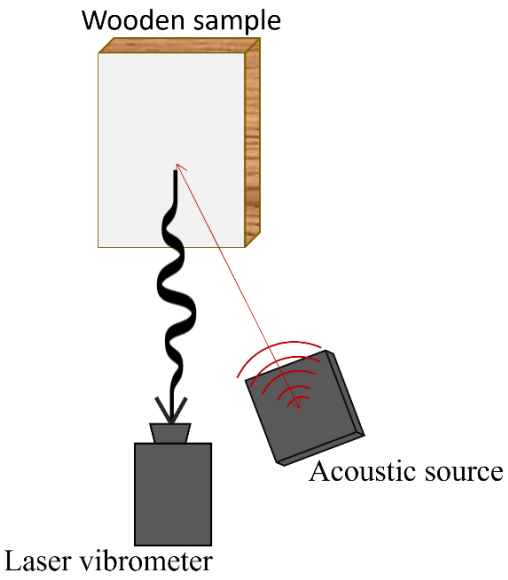

Figure 2.14 – Vibro-acoustic measurements set-up: the acoustic source and the vibrometer were positioned at 0.60m and 0.63m of distance from the sample, respectively.

3 Laboratory test samples

This chapter is divided into two parts, each including a description of the laboratory sample analysed and the relative results obtained with the techniques described in the previous chapter. The two types of samples were chosen in order to study two kinds of supports and structures representative of different real situations of artworks with layered structures and a decorative apparatus, such as those described in Chapter 4. The two types of samples have therefore been analysed with two different purposes, namely:

1) sample of painting on wood (see section 3.1) → wood panel supporting material layers with the typical layering of a panel painting and including structural defects simulating damages and inhomogeneities of a real artefact. The sample was analysed with the aims of testing the sensitivity of the imaging techniques in detecting structural features and characterizing the different materials. Moreover, the results were used for studying and comparing the spectral responses of the materials in the MWIR and NIR ranges. The techniques employed on this sample are the thermography and MWIR reflectography and complementary methods in the NIR. Furthermore, vibro-acoustic survey was carried out in order to further extend the spectral range and test the functionality of the technique on wood.
2) Sample of paper with ink elements (see section 3.2) → simulating the overlaying structure of an ancient books or manuscripts bookbinding where written paper sheets are often located under the external end-leaf. This sample was studied mainly by means of thermography, the only technique that has proven to be fully effective in the investigation of elements buried under the paper. In particular, the capability of the PT was studied to identifying hidden texts at different depths and to carrying out an experimental study for modelling the heat diffusion within semi-transparent media and quantifying the consequent distortion effect in thermal images.

3.1 Sample of painting on wood

The preparation of the laboratory sample was executed with the aim to reproduce as more as possible the materials and the mullti-layered structure of paintings on wooden supports, starting from the choice of the wooden specimen and the typical damage up to the pigments and binders. Thus, tests on the laboratory sample were performed in order to investigate the spectral response on the material in the IR range. The sample, henceforth referred to as the "wooden sample", was elaborated following the below steps:

1. Choice of the wooden specie for the support

2. Making of artificial defects
3. Ground preparation
4. Drawing of preparatory sketches
5. Application of pigments layers

The experimental analyses carried out on the sample allow to investigate the thermal and optical behaviour of the typical materials of a painting on wooden support along the IR spectral range. For these purposes, in addition to MWIR techniques, two NIR reflectographies (standard and laser-based) were used to investigate the sample. Finally, vibro-acoustic technique was employed as further NDT method.

3.1.1 *Sample preparation*

Because of the large variety of vegetal species and their characteristics, the type of the wood for the support was the first crucial choice made by an artist for the realisation of a painted artefact. In the past, the criteria followed for such a selection were based on several factors, including geographical availability, physical and mechanical characteristics and financial dispositions. Further distinction for the choice of the wooden species was made according to the type of artefact: for the supports of the paintings on wood, the species must be characterized by an excellent dimensional stability to the variations of the surrounding thermo-hygrometric conditions, while for the sculptures, fundamental are the easy workability and the aesthetic aspect. The main species employed in historical CH are summarised in Table1.2 of section 1.1.1 , which also describes the main mechanical/physical features, the principal use and their geographic areas [16], [17]. From the observation of the table, the main wooden species employed in the creation of paintings was the poplar, a very common tree in Italy and with good technological features. For these reasons, the laboratory sample chosen for this thesis is a poplar panel with a thickness of 2 cm.

In order to study the capability of the employed techniques to detect and characterise subsurface inhomogeneities, different types of damage were produced on the sample, simulating the typical defects founded in paintings on wood (detachments, cracks, galleries of woodworm) as can be seen from Figure 3.1, where also the dimensions are reported.

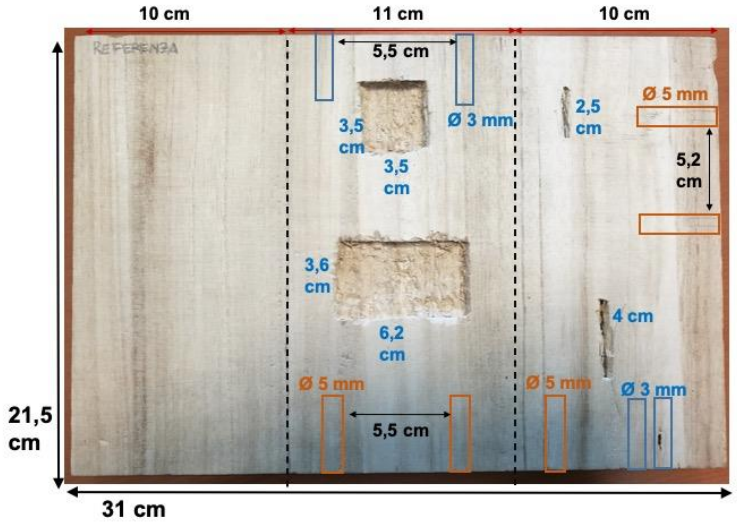

Figure 3.1 - Wooden sample with reproduced defects: the orange and cyan rectangles indicate woodworm galleries simulations. The dimensions of all the details are reported.

The repair of the defects was then simulated using plaster ready-to-use to repair the vertical cracks and two types of material to fill the bigger defects (Figure 3.2a), while the simulated woodworm galleries were left empty. Furthermore, polystyrene was inserted in one of the two rectangular defects in order to observe the thermal behaviour of the different density materials. Before the application of the painted layer, the wooden support was prepared with the typical ingredients of the ancient artistic tradition, as reported by Cennino Cennini [15]: a mixture of animal glue (rabbit glue) and gypsum was applied on the sample surface as first preparatory layer (Figure 3.2b).

Figure 3.2 - Wooden sample: (a) large defects filled with ready-to-use plaster; (b) surface of the support finished with the gypsum preparation.

The preparation and application of such mixture was carried out by the following steps:

- Melting the rabbit glue pearls in a 1:2 ratio with water;
- Adding gypsum powder to the obtained glue until the liquid is able to absorb the powder;
- Stirring the mixture until it appears homogeneous;

- Applying twice the white mixture with a middle-size brush.

After the complete drying of the above-described layer, a thing coat of plaster was applied on all the sample surface (Figure 3.3a) as simulation of the ground layer, maintaining the thickness as uniform as possible under 1 mm. Then, drawings were made differentiating the kind of materials in order to observe their different spectral behaviour by using charcoal and graphite. A simulation of underdrawings and a reference scheme was carried out directly on the plaster layer (Figure 3.3b). Although both the materials are carbon-based, they have differences in manufacturing provenance and chemical structure. Indeed, charcoal is made from burning wood, while graphite is a mineral, an allotrope of the element carbon, which occurs naturally in various types of rocks.

Charcoal is considered a popular material for drawing since the Renaissance, when it was used for preparatory purposes such as to develop initial ideas, preliminary outlines and areas of shadow. In the 19th century, artists used charcoal to make highly detailed drawings thanks to its ability to produce an interplay between light and shadow known as *chiaroscuro* [39]. Graphite was used for drawing in central Europe during the 16th century, but its use became more widespread in the late 18th century thanks to its massive fabrication and commercial spread [40]. The differences in atomic structure are shown also in the optical and thermal response to light stimulation, as is reported in the results.

Figure 3.3 – Wooden sample: a) ground layer; b) underdrawings made by charcoal (left figure) and graphite (right figure). Black stripes and squares on the left were made (from top to bottom) with one and two layers of graphite and charcoal, respectively.

As final layer, 12 bands of colour were applied over the sketches (Figure 3.4), choosing the most used mineral pigments in the pre-contemporary art in Europe, including at least 2 different pigments per colour. This choose allowed to investigate different optical and thermal responses of similar colours with different chemical composition (Table 3.1). The pigments were prepared

mixing the powders with egg tempera in a mortar and diluting with water when necessary, following the ancient recipes and artisan traditions [15], [86].

Figure 3.4 - Wooden sample: colour layer with different inorganic pigments.

Table 3.1 - pigments employed in this work [86].

Colour	***Pigment***	***Chemical formula***
Yellow	Yellow ochre	α-FeOOH
	Orpiment	As_2S_3
Green	Malachite	$CuCO_3.Cu(OH)_2$
	Green earth	$K[(Al,Fe),(Fe,Mg](AlSi_3,Si_4)O_{10}(OH)_2$
Red	Red ochre	Fe_2O_3-H_2O
	Cinnabar	HgS
	Minimum	Pb_3O_4
Blue	Lapis	$(Na,Ca)_8[(SO_4,S,Cl)_2(AlSiO_4)_6]$
	Egyptian blue	$CaCuSi_4O_{10}$
	Azurite	$Cu_3(CO_3)_2(OH)_2$
White	Lead white	$2PbCO_3$ $Pb(OH)_2$

3.1.2 Non-destructive analyses and results

The IR imaging measurements were carried out during all the preparation of the sample, using each technique at all the stage of the preparation. In this section, the results will be presented by

describing each layer and discussing the images obtained with the different techniques. The acquisition parameters are summarised in Table 3.2.

Table 3.2 - Acquisition parameters for each technique.

Technique	***System***	***Spectral range***	***Distance from the sample***	***Illumination***	***Time***
NIR reflectography	CCD sensor (Kodak KAF8300) + bandpass filters	0.9 – 1 µm	1.25 m	2 IR lamps	Integration t = 4 sec
NIR laser reflectography	IR-ITR prototype scanner	1.55 µm	5 m	No illumination	Scanning time = 25 min
MWIR reflectography	Thermal camera (CEDIP Jade)	3 ÷ 5 µm	0.50 m	Carbon filament IR sources	Instantaneous acquisition
Pulsed thermography				2 halogen flash lamps	5 sec multi-frame sequence

Preparatory layer

Imaging survey carried out with NIR CCD reflectography (Figure 3.5a) provides no evidence of features lying under the plaster. Such result was due to the high reflective power of the plaster itself, which overlays any other reflected radiation coming from the deeper layers, and to the plaster thickness (about 0.5 mm). Increasing the wavelength, indications of sub-surface features are provided by the MWIR reflectography, which is able to detect the presence of three structural defects with an evident different optical behaviour with the respect to the support (Figure 3.5b). Indeed, in the MWIR reflectogram the voids filled with plaster (upper square and bottom-right defect) and polystyrene appear darker and whiter, respectively, due to the different reflectivity of the two materials in the MWIR range. Differently, the PT image (Figure 3.5c) shows the map of all the prepared defects. Here, the heating, mainly induced by the flashlight stimulation in the front external layer, propagate to the defects interface. The defects appear darker indicating a better conduction of the heat through the fillers than the surrounding wood, the difference being less marked for the polystyrene, a worse thermal conductor with respect to the plaster. The simulated woodworm galleries are not detected by the techniques, probably because of their small dimensions and the bad thermal transport properties of the wood. It is worth noting that the reflectographic image appears grainier than the thermographic one, due to the scattering and the attenuation that affects the MWIR radiation that must travel forward and back through the front

layer. Moreover, the veining of the wood is discernible in the thermogram (Figure 3.5c), providing a further element for characterise the support.

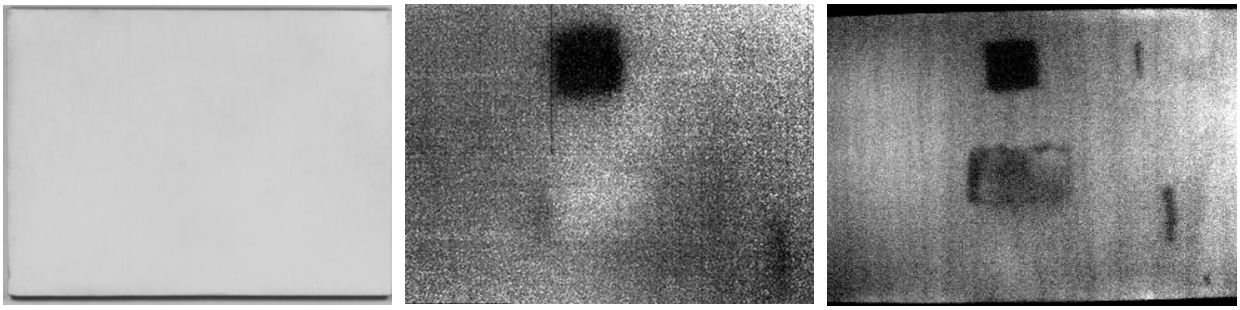

(a) (b) (c)

Figure 3.5 – Imaging results obtained at the preparatory layer: (a) NIR reflectogram at 1 µm; (b) MWIR reflectogram; (c)Thermogram recorded at large delay after the light pulse.

As complementary structural analysis on the wooden sample, vibro-acoustic measurements were carried out in correspondence of the preparatory layer, exploring the capability of the technique to detect structural defect in wooden materials covered by a plaster layer. The measurements were carried out moving the sample along the vertical and horizontal axes, in the XY plane orthogonal to the laser beam to build a 2Dmatrix composed of 31 point per 21 vertical rows. Calibration points were measured in the upper part of the sample, where no defects occurred. The measurement parameters are reported in Table 3.3.

Table 3.3 – LDV measurements parameters.

Parameter	***Values***
Spot size of the laser vibrometer	1 mm
Acoustic frequency range	1000 ÷ 16000 Hz
Measurements frequency step	200 Hz
Average measure per point	3
Measurements linear step	10 mm

Vibro-acoustic measurements on each single point per vertical row provided the values of vibration velocities as function of frequencies. Since the normal modes of the sample and the characteristic velocities of the defects were both unknown, the study of the behaviour of the two vibration modes were carried out. Figure 3.6 shows the results on several point of the sample. In particular, in Figure 3.6a the black points indicate references points where no defects were induced

on the wood, while the coloured points are in correspondence of three of the main inhomogeneities. Figure 3.6b shows the vibration velocities of a reference point and a damage (the one filled with polystyrene) acquired on the same vertical row. As can be clearly noticeable, the trends of the data are considerably different, with intensity maximum at different frequencies and narrower spikes for the reference. Similar consideration can be made by observing the Figure 3.6c, where, beside the reference, further two points were evaluated, in correspondence of the squared defect filled with plaster and a repaired crack. Also in this case, the maximum values are recorded at different frequencies and the spikes of the reference plot are more clearly discernible and narrower.

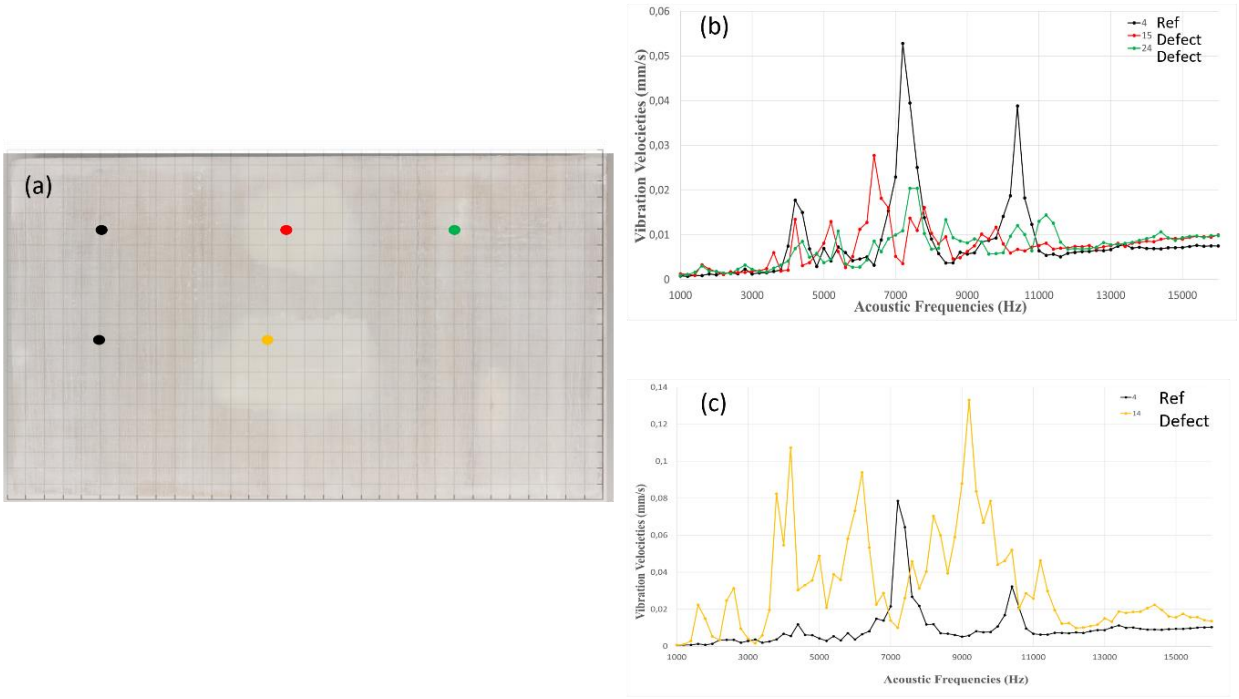

Figure 3.6 - Results of the analysis on the measured vibration velocities: a)picture of the wooden sample on which a grid was superimposed to better identify the points to be plotted; b)plots of reference and a detect data where different maximum and width of the spikes are discernible; c) plot of b)plots of reference and two detects data where the same differences can be noticed.

The difference of the velocities obtained in the different points is due to the types of measured points: the curves correspondent to the reference area show well-defined and narrower spikes, mainly in correspondence of the frequency of 7400Hz, indicating the detection of normal modes of the wooden support. On the contrary, in the case of the curved obtained from the defects area, the vibration frequencies present wider spikes and irregular profiles, stating the specific vibration velocities of the damaged multi-material areas. Common higher vibration velocities were identified at the frequency of 6200Hz in both the defects graphs.

In correspondence of the mentioned frequencies, a MATLAB post processing elaboration was performed in order to transform the frequency values into a set of matrices able to provide colour maps in the two specific frequencies, as shown in the Figure 3.7a,b, where the chosen colour scale

of the maps was selected in order to range from blue (zero vibration) to yellow (highest vibration velocity values). In Figure 3.7a, the normal modes of the sample are visible with regular geometric features, while Figure 3.7b shows the high-order modes of the central wider defect.

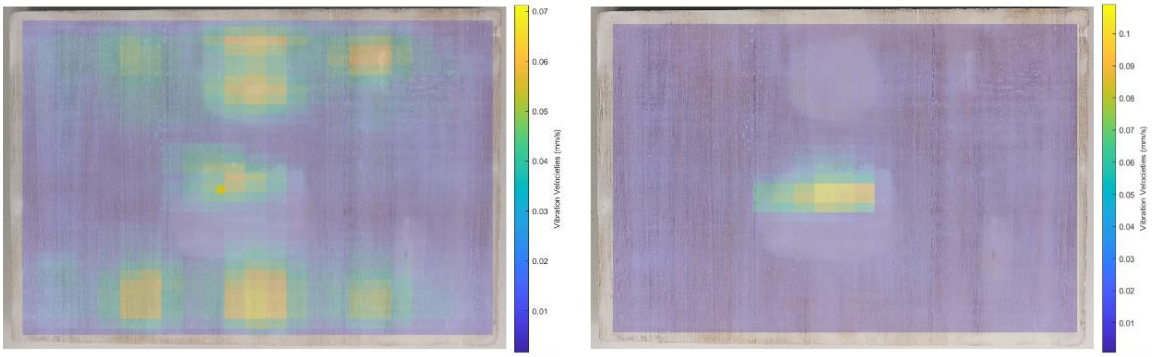

(a) (b)

Figure 3.7 - Vibro-acoustic maps: (a) normal modes visible at the frequency of 7400Hz; (b) high-order modes of the central wider defect visible at the frequency of 6200Hz.

The obtained results show the great capability of the technique to penetrate the preparatory layer made of plaster and to investigate layered and multi-materials structures by discriminating the vibration velocities of the damaged arear with the respect to the clear ones.

Sketch layer

The different spectral response of the two materials of the sketch (charcoal and graphite) is evident from all the images obtained with the different techniques. The charcoal appears darker in the NIR reflectogram acquired by the laser prototype because of its lower reflectivity than graphite (Figure 3.8a). Similar results are clearly visible from the MWIR reflectogram (Figure 3.8b), where, even in this spectral range, the charcoal traits appear more contrasted than the graphite ones whose reflectivity does not differ significantly from that of the surrounding gypsum. Concerning the PT images, the thermogram recorded immediately after the light pulse highlights the differences in light absorption and consequent emission between the two materials (the drawing is white because hotter than the wooden support)[87] (Figure 3.8c).

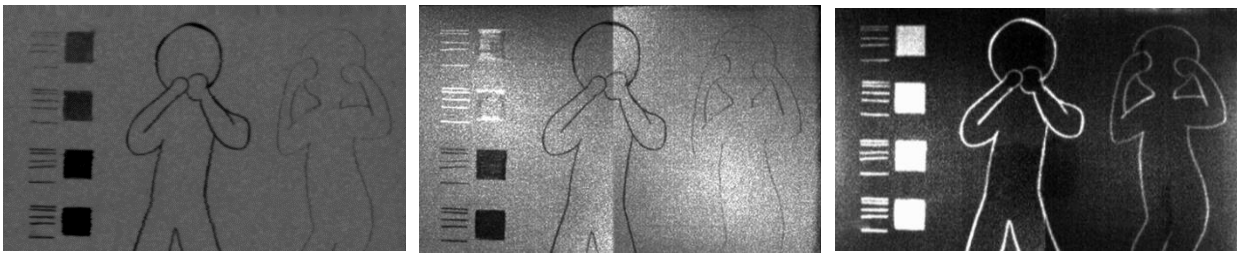

(a) (b) (c)

Figure 3.8 – Imaging results at the sketch layer: a) NIR laser reflectogram at 1.55 μm; b) MWIR reflectogram; c) thermogram recorded after the light pulse.

Pictorial level

The mapping of the optical and thermal behaviour of the used pigments and materials was obtained in the last part of the laboratory tests. From the study of the results achieved in correspondence of the pictorial layer, the different penetration capability of the used IR radiations can be observed (Figure 3.9a-f). NIR reflectograms (Figure 3.9a-c) allow the detection of the underlying drawing thanks to the different transparency of many pigments to the NIR radiation, more evident by using a larger wavelength with the laser scanner system (λ = 1.55 µm) (Figure 3.9c).

Qualitatively, the behaviour of each pigment to the incident IR radiation can be approximately addressed as transparent, reflective or absorbent. When observing the images of the pigment stripes, if the pigment is transparent, the drawings lines can be distinguished, if classified as reflective, it looks bright in the images and the lines will be hardly visible. Finally, the pigment is indicated as absorbent when the underlying lines could not be detected and the stripe will appear black. Such classification can be regarded as meaningful only if the pigments are applied over a homogeneous IR-reflecting background, such as in the case this preparatory layer. Otherwise, inhomogeneous underlying layers could play a major role in the appearance of the overlying paint layer.

Indeed, NIR at 0.9 µm is able to clearly detect the drawings under the yellow and red ochres, the orpiment, the lapis and the cinnabar while the lines are barely visible in correspondence of the green earth, the minimum and Egyptian blue but they are not-visible at all under the lead white, the malachite and the azurite pigments (Figure 3.9a). The last pigment, as well as the red ochre, the green earth and the Egyptian blue, become more transparent to the IR radiation with increasing wavelength as shown by the NIR reflectograms at 1 µm (band pass filtered CCD camera) and at 1.55 µm (IR laser scanner) (Figure 3.9b and Figure 3.9c, respectively).

Information on the reflectographic and thermographic behaviour of the pigments were obtained by the analysis of the MIR and PT images (Figure 3.9d-f). In MIR analysis, in correspondence of the brighter pigments, the reflection of the ground layer often blinded the optical reflection of the underdrawings (Figure 3.9d). However, thanks to the larger wavelength of the technique, underdrawings under the minium pigment can be investigated, unlike the possibilities of the other techniques.

By properly enhancing the PT results, the underdrawings were only partially revealed by the image recorded at short delay from the light pulse (Figure 3.9e). The features shown by this thermogram are essentially due to the selective absorption of the light that, where not absorbed by the overlying paint layer, reaches the black drawing. Black materials, being better absorbers, becomes hotter that

the surrounding and emits more radiation giving rise to a contrast image of the feature in real time. On the other hand, the thermogram recorded at larger delays (Figure 3.9f) allows the heat, wherever generated in the painting and preparatory layer, to propagate down to the support level revealing the profile of the defects under the ground layer because of their different thermal properties with respect to the surrounding wood.

Thus, by the combined use of all the employed imaging techniques, a rather complete characterisation of the layered structure of the panel painting sample was possible. Such an integrated approach can be therefore very useful in the non-destructive analysis of painted artefacts as shown in the following Chapter, where the results of applications to real artefacts are reported.

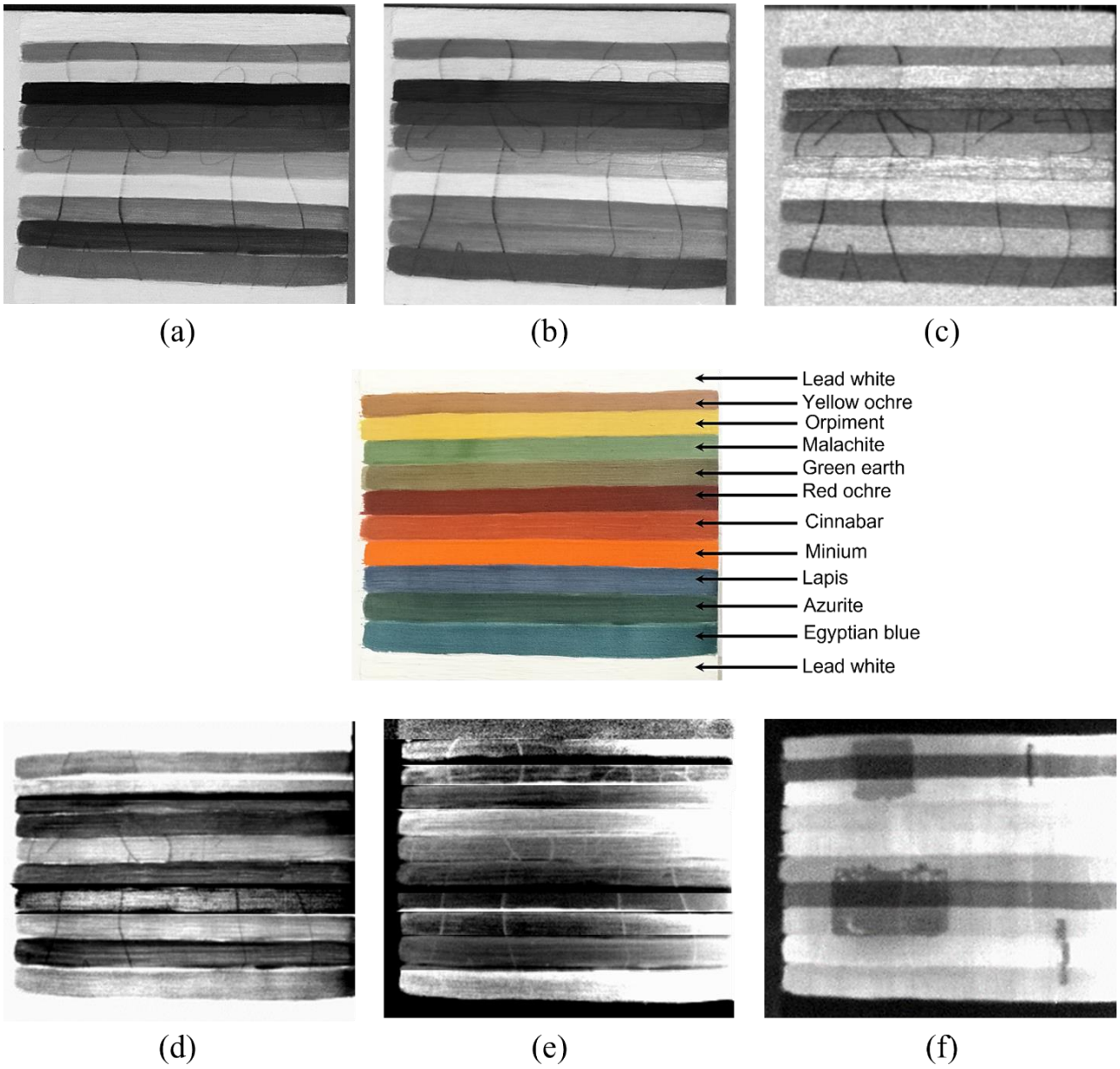

Figure 3.9 – results at the painted layer: a) NIR reflectogram at 0.9 µm; b) NIR reflectogram at 1 µm; c) NIR laser reflectogram at 1.55 µm); d) MWIR reflectogram; e) PT thermogram recorded at short delay; f) PT thermogram recorded at long delay.

3.2 Paper-based sample

In order to perform a quantitative evaluation of the distortion effect in thermal images recorded from semi-transparent materials with hidden inked features, a paper-based sample was developed and studied with PT. The latter was the only technique employed in such application because it has proving to be an efficient tool in this kind of application thanks to the MWIR detection range which allows the detection under materials such as the paper without being highly influenced by the scattering of radiation as with NIR reflectography. For this application, there are limitations also in the use of MIR mainly due to the high reflectivity of the paper in the MWIR range and to the fact that the radiation has to travel twice, forward and back, through the overlying paper thickness.

3.2.1 Sample preparation

The hidden texts studied in this thesis typically correspond to texts belonging to parts of earlier manuscripts used in the binding of more recent books and, as mentioned earlier, a main part of the research carried out in this thesis concerns the analysis of contrast and distortion in the thermographic images of inked features buried beneath paper leaves of the binding and the influence their geometric and physical parameters have on them.

The paper-based sample was designed with the aim to replicate the typical multi-layered structure of the binding of ancient books and manuscripts, in which often reused paper and parchment coming from other earlier books and documents, as described in Section1.2. Indeed, the practice of reusing parts of other books was very common in the manufacturing of manuscripts, mainly due to the high cost and low availability of paper and parchment supports that forced artists to recycle materials. Nevertheless, these elements are often not visible at naked eye and the disassembling of the manuscript and or its binding for visualise them is most of the time not possible. To overcome such issue, PT is often used as non-destructive technique for the detection of hidden texts within the layered structure of manuscripts [66], [88].

Thus, in order to simulate such a complex structure, the sample was composed by using a paper sheet as support on which an ink area was applied and covered with 4 paper stripes of different thickness from 110 µm up to 230µm, glued orthogonally with a starch adhesive to the edge of the inked area, as shown in Figure 3.10.

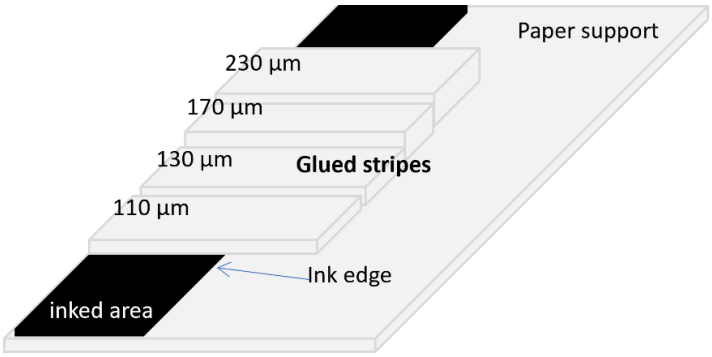

Figure 3.10 – Sketch of the paper-based test sample with the paper stripes glued on the inked area for replicating increasing depths at which the graphical features can be buried in real manuscripts.

3.2.2 PT survey and Modelling

For the thermographic measurements, standard PT set up was used: the VIS illumination was positioned at 45° with respect to the sample surface and the emitted radiation was detected by the MWIR camera placed on the same side of the illumination. The contrast in thermographic images recorded in this kind of materials is due to the local differences in the VIS absorption and the IR emission properties of the ink and the surrounding paper, as described in Section 2.2. A specific theoretical model developed for the description of the edge distortion in the thermographic images in semi-transparent artworks was presented in Section 2.1.4 and applied to the interpretation of the profiles of the thermographic signals as a function of time and ink depth.

Results

In Figure 3.11a-c the thermal images of the paper sample are shown, where the areas without ink under the paper stripes appear darker (cooler). The figures show relevant differences of contrast and blurring of the ink edge in the thermograms, that increases with time delays (Figure 3.11a-c). As can be noticed from the very firsts frame of the thermographic sequence (Figure 3.11a), the contrast appears good with a great definition in recognising each layer and also being able to distinguishing the increasing thickness of the paper stripes. On the contrary, the thermograms recorded at larger time delays look loss sharpness and the edge of the ink area appears to be less defined (Figure 3.11b, c). Such considerations can be further be confirmed by the analyses of the data obtained on the coloured lines crossing the ink edge in Figure 3.11a and then reported in Figure 3.12a-b and Figure 3.13a-b.

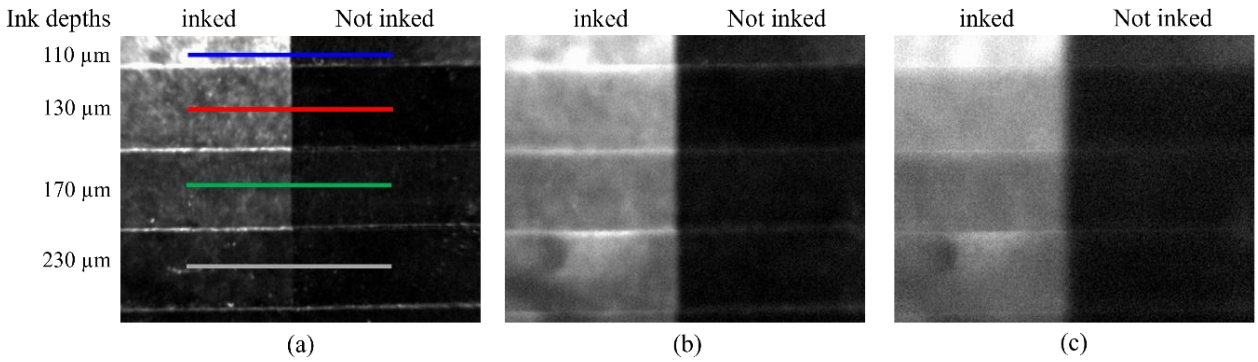

Figure 3.11 – Thermograms obtained across the edge of ink areas buried at different depths with delay times; (a) t=0.06s; (b)t=0.27s; (c) t=0.93s.

These experimental data collected from the thermograms obtained at the various delay times along the coloured lines crossing the ink edge reported in Figure 3.11 are used to perform the comparison with the theoretical simulations obtained from the application of FEM to the heat diffusion equation discussed in Chapter 2. The results corresponding to the thermograms of Figure 3.11a-c are shown in the following figures.

In Figure 3.12a-b the thermal signal profiles over the ink edges corresponding to the thermal images recorded at short delays are shown, where Figure 3.12a is referred to an early frame (0.01s delay) of the thermographic sequence and Figure 3.12b correspond to the time delay t=0.06s (Figure 3.11a). In these figures, the theoretical simulations are represented with continuous lines, while the experimental data recorded from the laboratory sample are indicated with the symbols. As can be seen, the experimental data and the theoretical simulation have a good degree of superimposition, demonstrating the validity of the adopted model. Furthermore, the grey areas marked with dotted vertical lines highlight the distortion ranges corresponding to the distortion index values, obtained from the theoretical curves and reported in the figure captions. As expected, the experimental data indicate a change in contrast trends for increasing ink layer depth: at short times (Figure 3.12a-b), the higher contrast is obtained for smaller depths because the emitted radiation from the ink feature has to pass through less paper layer and is emitted back just after the flash pulse, while the incidence light still did not reach the inked elements at larger depths and thus the contrast is lower. Moreover, at equal delay times, the contrast profile, and therefore the distortion index Δ_i, turns out to be the same for all the ink depth values.

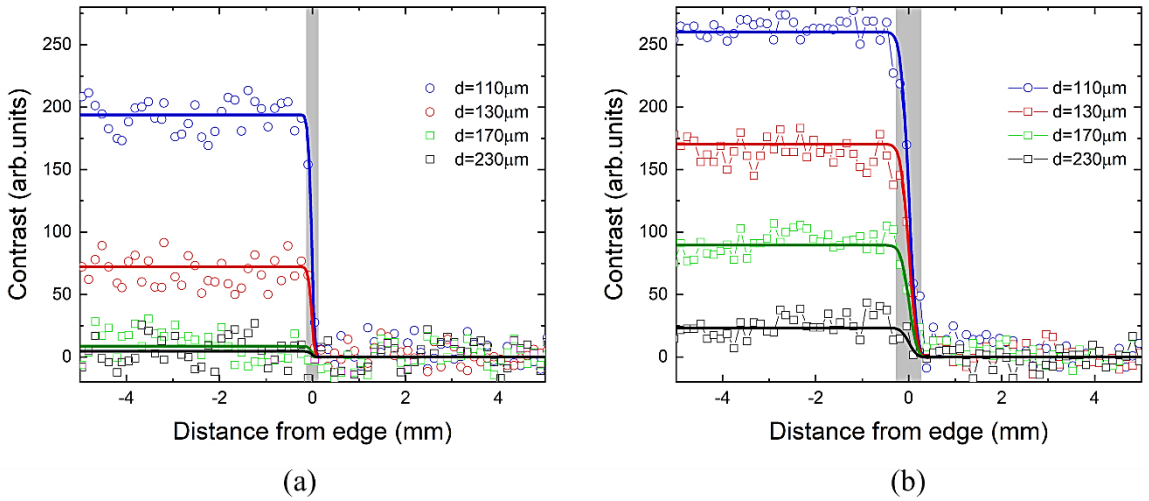

Figure 3.12 – IR image contrast across the edge of the ink area situated at different depths:(a) t = 0.01 s, Δ_i = 0.26 mm. (b) t = 0.06 s, Δ_i = 0.56 mm. Continuous lines represent the theoretical simulations. Gray range highlights the distortion extension.

In Figure 3.13a-b the thermal signal profiles corresponding to the thermal images recorded at larger delays are shown, where Figure 3.13a is referred to thermogram recorded at t=0.27s shown in Figure 3.11b and Figure 3.13b correspond to time delay t=0.93s reported Figure 3.11b. Even in these cases, the comparison between experimental data and theoretical simulations achieves a good level of overlapping. It can be noticed that, for increasing delays (Figure 3.13a-b), the contrast of ink at smaller depths is lower because all the emitted radiation is already detected by the camera, while the deeper inked appears to be more contrasted because the emission induced by the incidence radiation is still ongoing, providing an higher contrast signal at larger delays (see d = 230µm). Furthermore, Δ_i becomes broader with increasing delay time because of the more relevant role played by lateral heat diffusion, in agreement with the predictions of the theoretical simulation discussed in Chapter 2 and displayed in Figure 2.9a-b.

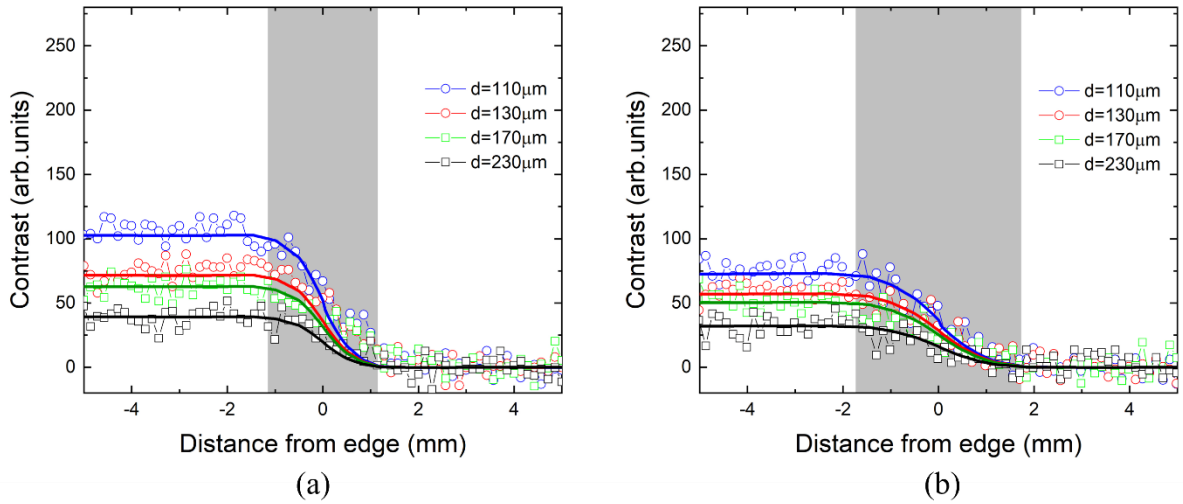

Figure 3.13 – IR image contrast across the edge of the ink area situated at different depths at: (a) t = 0.27 s. Δi = 1.24 mm; (b) t = 0.93 s. Δi = 2.30 mm. Continuous lines represent the theoretical simulations. Gray range highlights the extent of the distortion.

The values of the distortion index Δi calculated form the graphs in Figure 3.13a-b are comparable to the size of the typical graphic line (~0.5mm) and also to the spacing between adjacent elements of the written text (~2mm). The possibility of quantifying this distortion effects in thermographic images is a great step forward in optimizing the acquisition process and the images selection in layered structures, as well as an effective tool for the interpretation of specific features of the hidden texts (like its depth for instance) by analysing the behaviour of contrast and distortion as a function of time.

4 Applications

The combined approach developed for the laboratory tests was applied to original artefacts characterised by different materials and issues, such as conservative problems or underlying features. In some cases, further NDT techniques were employed as complementary method for the better achieve the aims of the particular case. In the following chapter, the results of the analyses are presented subdividing the studied artefacts into different sections according to the type of combination of support-graphic/decorative apparatus.

4.1 Paintings

Two categories of painting were investigated in this thesis, such as on wood and on canvas, respectively, with different conservative issues and artistic questions.

4.1.1 Santa Maria in Cosmedin altarpiece

The object of the study was the altarpiece preserved inside the Basilica of Santa Maria in Cosmedin of Rome which dates to the 7th century, and it is nowadays known as the Greek Melkite Catholic Church of Rome. The epithet 'Cosmedin' (from the Greek κοσμέω, to adorn) was given in the 8th century to describe the great decorations of its interiors, which are still present. The altarpiece is a representation of the Virgin Mary holding the Child Figure 4.1also identified as the iconography of the Madonna Theotókos, where the two figures wear rich and colourful garments with a background consisting of a complex black damask pattern stamped [89] on a golden substrate. The Child is represented in the characteristic Greek blessing pose holding the globus cruciger while being tenderly embraced by the Virgin's hands. The painting is in oils on a wooden support of approximately 168 × 128 cm in size, which is made by four vertically jointed panels and a thinner horizontal one in the upper side, probably added in recent times. The history of this altarpiece is documented only by a few literary sources, according to which the painting may be an ancient icon brought to Rome from the East during the iconoclastic persecutions [90]. Additional hypotheses concerning the origin were proposed over the last century: several scholars suggest it could be a medieval icon completely covered by a 'modern' [91], [92], while, the latest hypothesis is a 15th century dating due to the discovery of the inscription 'IO PIACERE' during the latest restoration, interpreted as the signature of Giovanni Piacere, an Italian artist working in central Italy during the 15th century [89].

Figure 4.1 – The Virgin with the Child altarpiece at the Basilica of Santa Maria in Cosmedin, Rome.

The aim of this work was to provide a depth-resolved non-destructive investigation of the entire layered structure for characterising both the conservation status and studying eventual hidden features. For these purposes, NIR, PT and MIR were employed allowing a comparison among the results as well as the stratigraphic investigation of the painting in order to understand the artwork's layering sequence and, therefore, its evolution over time.

Results

Several additional graphical and pictorial elements, with respect to those visible at the surface of the painting, are revealed by the IR images, thus confirming the complex structure of the altarpiece. Both the painting layer and the adhesion to the wooden support showed good conservation conditions, even though, based on the number and extension of the detected retouches, the painting areas corresponding to the panel's junctions can be considered as those most severely affected by damage.

In the analysis of the Virgin's face (Figure 4.2a), two frames of the thermographic sequence are shown revealing the in-depth extension of the defects of the wooden support. It is worth noting that, in order to make the comparison with the reflectograms more effective, in the grey scale adopted for the shown thermograms, the hot parts of the sample correspond to the dark areas. In particular, Figure 4.2b reports the thermogram recorded shortly after (20 ms) the heating light pulse. It displays two vertically oriented defects, running across both eyes (indicated by the arrows), which were repaired by a recent restoration. The damage across the right eye also runs between the nose and the mouth, in correspondence to the panel joint where the restoration is evident. The origin of such damage was associated with the mechanical stress usually involving

the surroundings of the joints. Under the left eye, a small-restored void can also be observed (marked by the circle in Figure 4.2b). The thermogram recorded with a larger delay (400 ms) reported in Figure 4.2c shows basically the same elements highlighted in Figure 4.2d, but, in correspondence to the vertical damage on the left, the thermogram also displays some aligned dark (hotter) spots (indicated by the arrow), presumably corresponding to areas where the thermal contact with the substrate is poorer. This could indicate the presence of detachments or of filled gaps below the paint layer, perhaps down to the wooden support. Similar kinds of defects, highlighted by the circle, are also revealed on the right temple. In this case, in fact, the heat generated at the most superficial level, where the VIS light can penetrate and be absorbed, has had time to propagate to a deeper level where the presence of eventual inhomogeneous features affects the heat-diffusion process. This, in turn, generates local differences in temperature inducing different amounts of emitted IR radiation. That emitted in the spectral range of 3–5 μm can travel to the IR camera through the overlying layers of the painting, maintaining a substantial unscattered component. This gives rise to the generation of the contrasted features in the thermogram displaying the buried elements. The vertical line defects and the lacuna under the left eye are also detected in the NIR and MWIR reflectograms (Figure 4.2d, e). The reflectographic images reveal an additional subsurface branched cracked area on the right-hand side of the face (framed by the rectangle in Figure 4.2d), probably corresponding to areas of restored craquelures.

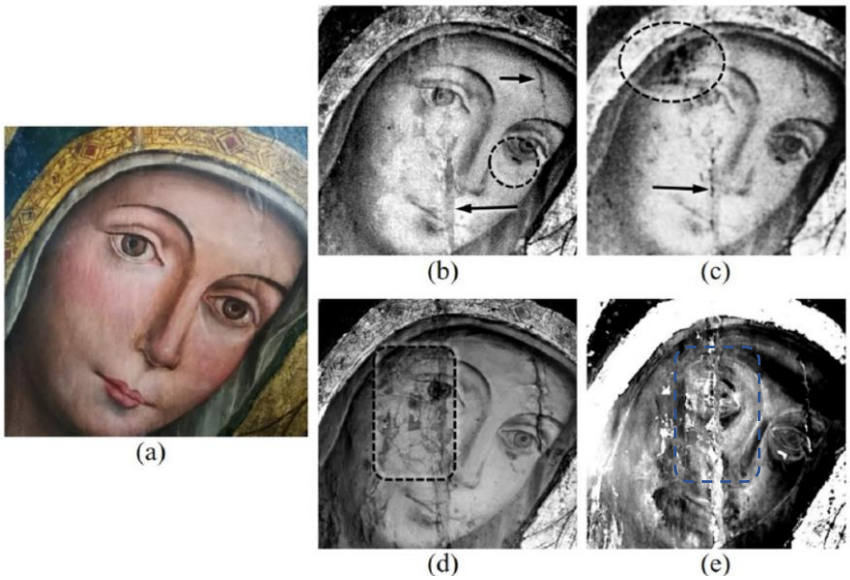

Figure 4.2 (a) Detail of the Figure 4.1; (b) PT image recorded at 20 ms after the light pulse revealing subsurface damage in the pictorial layer (arrows) and a small restored void (dashed circle); (c) PT image recorded at a larger delay (400 ms) revealing subsurface damage to the wooden support (arrows and circle); (d) NIR reflectogram highlights subsurface damage in the paint layer (dashed square); (e) MIR image reveals different details with respect to (d) and additional sub-superficial damages (rectangle).

As pointed out above, the NIR reflectogram reveals mainly features in the visible pictorial layer, such as retouches, to be ascribed to the latest restoration, while the MWIR reflectogram also

provides a map of the structural repairs beneath it, mostly corresponding to fillings of the paint voids left by detached fragments. Finally, it is very interesting to note that what appears as a vertical crack crossing the left eye in the NIR and MIR reflectograms and also in the thermogram obtained with the 20 ms delay is only barely detectable in the thermogram performed with the 400 ms delay, indicating that the in-depth extension of the defect is probably only limited to the paint layer.

The close-ups of the Virgin's face (Figure 4.3a) provide additional information about the painting layers. In particular, the thermogram obtained at 20 ms delay (Figure 4.3b) and the NIR reflectogram (Figure 4.3c) show the outlines and the shades of the nose (indicated by the arrows), while the MWIR reflectogram (Figure 4.3d) discloses pictorial features beneath the visible surface paint layer, revealing a different rendering of the Virgin's physiognomy. In particular, the facial traits highlighted by the MIR (Figure 4.3d) show a rounder-shaped eye, a narrower nose with a differently shaped tip and the eyebrows lines extending closer to the nose (arrows in Figure 4.3d).

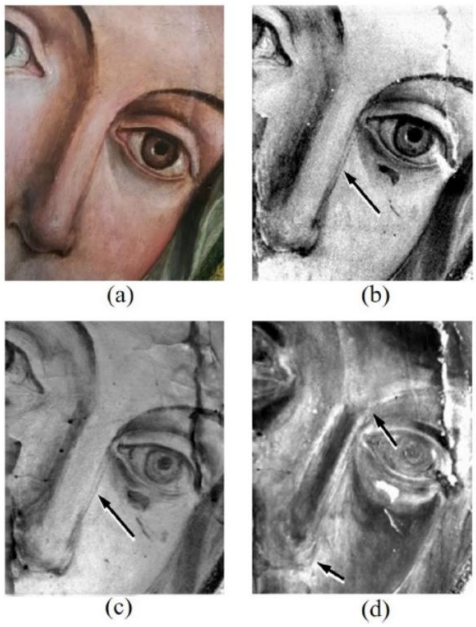

Figure 4.3 (a) Detail of Figure 4,1; (b) PT image recorded after 20 ms from the light pulse; (c)NIR reflectogram allows the better appreciate the shades and the outlines on the face (arrow);(d)MWIR reflectogram discloses the pictorial features beneath the superficial layer (a thinner nose and eyebrows extending closer to the nose).

Interesting results were also obtained by the combined analysis of the Child (Figure 4.4a), revealing differences between the visible and the subsurface layers of the painting where damaged and restored areas could be detected. In particular, in the area of the Child's hair, the PT image (Figure 4.4b, 20 ms delay) shows several inhomogeneities, such as those indicated by the arrows. The central (dark) part of the defect at the top of the head and of those on the right are not visible in the NIR (Figure 4.4d) and MIR (Figure 4.4e) reflectograms, so their contrast generation in the thermogram should be ascribed to thermal factors rather than optical ones. Therefore, they

probably correspond to detachments repaired during previous restorations. Moreover, they are barely detectable in the thermogram obtained with a delay of about 200 ms (Figure 4.4c), indicating even in this case that they do not extend much beyond the surface paint layer. Moreover, in the same area, NIR and MWIR reflectograms identify subsurface cracks beneath the restored surface paint layer similar to those observed on the Virgin's face and, even in this case, probably associated with mechanical stress effects. Finally, the MWIR reflectogram clearly reveals a variation in the Child's hair profile on the right-hand side of the image, with respect to that portrayed in the picture. More specifically, the NIR reflectogram and the thermogram obtained with the small delay display voluminous and curly hair, as indicated by the arrow in Figure 4.4c, while the hair profile detected by the MIR extends over a more restricted area (dashed rectangle in Figure 4.4e).

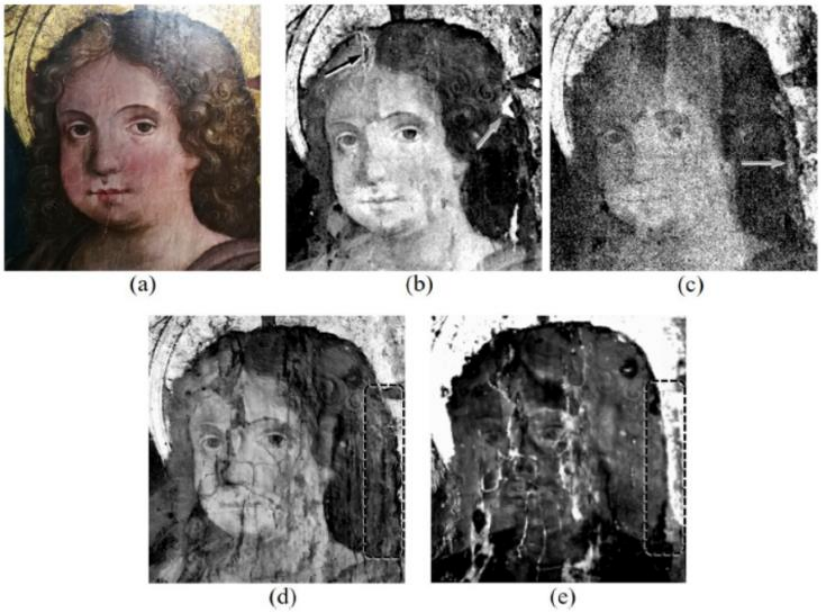

Figure 4.4 – (a) Detail of Figure 4.1; (b) PT image recorded after 20 ms from the light pulse detects structural damage and detachments indicated by the arrows; (c) PT image recorded after 400 ms from the light pulse;(d) NIR reflectogram revealing a subsurface crack);€ MWIR reflectogram reveals a different hair profile with respect to that shown in (a) and compared with (d) (dashed rectangles).

Further changes and inhomogeneity can also be observed in the other areas of the painting, such as in correspondence to the Child's hand (Figure 4.5a). Here, the PT, NIR and MIR disclose the absence of the right thumb of the Child at all investigated depths, denoting the almost complete loss of the pictorial layer in that area in the past (dashed squares in Figure 4.5b–e). In particular, Figure 4.5b, c shows the thermographic image recorded shortly after the flash pulse (20 ms) and at larger delay time (300 ms), respectively. The latter highlights some deeper cracks (indicated by the arrow) running between the restored thumb and the palm, along the boundary of the lost pictorial area.

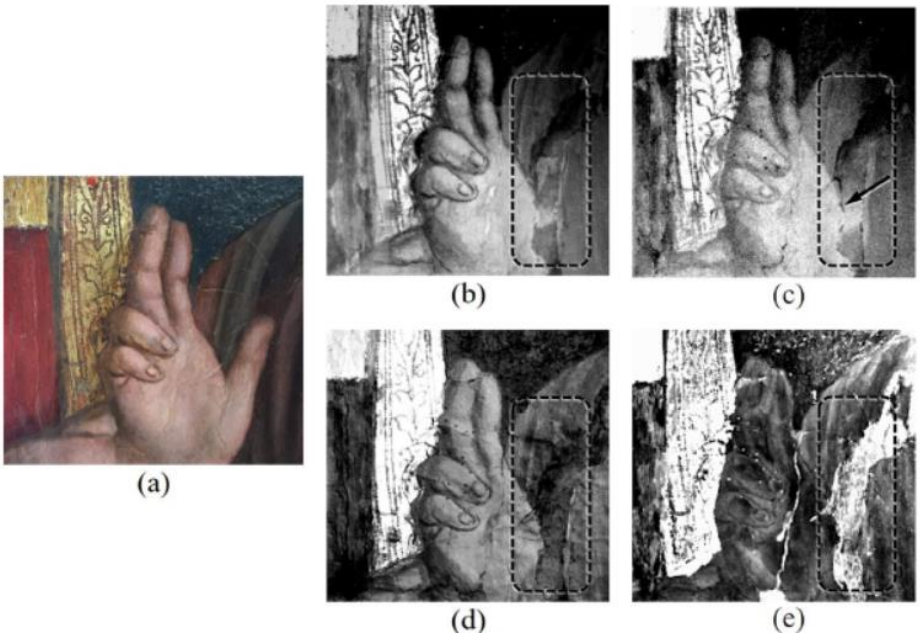

Figure 4.5 (a) Detail of Figure 4.1;(b, c) thermograms recorded with different delays (20 and 300 ms, respectively) disclose the absence of the thumb, which is also revealed in the NIR and MWIR reflectograms (d and e, respectively).

Additional defects in correspondence to the panel's junction extended down to the area of the Child's feet (Figure 4.6a), as shown in the framed areas in Figure 4.6b,d. Moreover, a defect just below the paint retouches is disclosed on the left foot by the NIR reflectogram, indicated by the arrow in Figure 4.6c. Finally, all the IR images also reveal differences in feet shape and position from those observed in the visible painting. In fact, the PT most clearly, and, to a lesser extent, also the NIR and MIR reflectographies, detect an original profile shifted with respect to that visible nowadays.

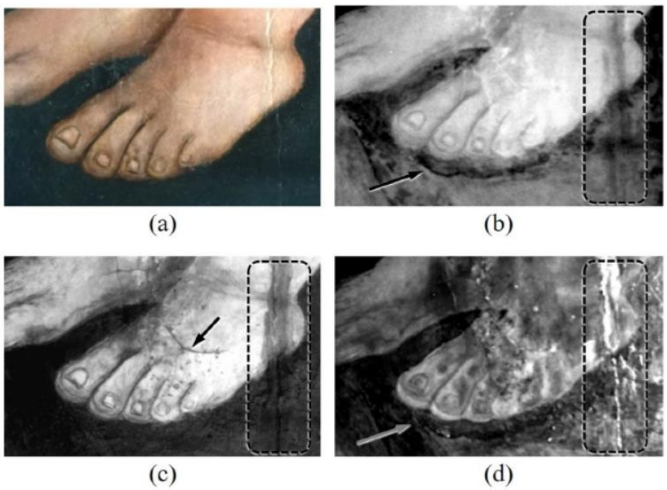

Figure 4.6 – (a) Detail of Figure 4.1; (b) PT image recorded after 20 ms from the light pulse that detects the repair in correspondence to the panels' junction (dashed rectangle) and a pentimento on the position of the feet, indicated by the arrow; (c) NIR reflectogram that reveals the same elements shown in (b); (d) MWIR reflectogram showing the pentimento (pointed out by the arrow) and the panels' junction defect (dashed rectangle).

In this case the combined use of IR imaging analysis allowed the characterisation of the relative depth of the observed subsurface features and it suggested that the presently visible painting could

be made over an earlier version of the artwork. The pictorial and graphical elements highlighted here can provide useful information for the historical and artistic placement of the artwork, which is surely composed of several overlapping layers of paint, restorations and adjustments made over the centuries. In this case, the contribution of PT combined approach is, in general, not limited only to the confirmation of the detection of the elements also revealed by other NIR and MIR imaging. On the contrary, thanks to the image generation depending on thermal as well as optical parameters, the thermograms could detect subsurface elements not revealed by the reflectographies and they could provide a useful tool for the in-depth ordering of the features detected by all the IR imaging techniques.

4.1.2 Baroque paintings on canvas of Palazzo Chigi, Ariccia

The investigated paintings are preserved at Palazzo Chigi in Ariccia (Rome, Italy), which is considered a one of the main examples of Italian Baroque architecture. The palace was originally built for a rich, local family during the second half of the 16th century, and it was restored by Gian Lorenzo Bernini for the Chigi family between 1664 and 1672 [93]. The restoration of the palace was carried out with the aim of exhibiting the splendour and the importance of the Chigi family, one of the leading families in the Italian papal lineage. In this palace, several valuable paintings are preserved, mainly dating back to the 17th century. Among these artworks, three paintings were studied: 'Ritratto di Mario Nuzzi che dipinge un vaso di fiori' by Giovanni Maria Morandi and Mario Nuzzi, 'Primavera' by Filippo Lauri and Mario Nuzzi, and 'Ebbrezza di Noè' by Andrea Sacchi.

The combined approach based on the use of MWIR techniques was used for the study of the above-mentioned paintings. The investigation was aimed at assessing the conservation status of the paintings and identifying graphic and pictorial elements beneath the surface layer.

In the following sections, after the presentation of each painting, the thermographic results will be compared with those obtained by mid-infrared reflectography. Again, for ease of comparison, the thermograms are presented with an inverted grey palette so that hotter elements appear darker.

'Ritratto di Mario Nuzzi che dipinge un vaso di fiori'

The 'Ritratto di Mario Nuzzi che dipinge un vaso di 78rit78' ('Portrait of Mario Nuzzi painting a flower vase') is one of the great masterpieces of the Roman Baroque because of its high pictorial quality and the peculiar combination of two pictorial genres (still life and portrait) made by two artists: Mario Nuzzi and Giovanni Maria Morandi, who were responsible for the floral decoration and Nuzzi's portrait, respectively (Figure 4.7). In this painting, the artist, Mario Nuzzi, called

Mario de' Fiori for his extraordinary talent for depicting flowers, is represented in his atelier, in front of his easel during the creative process, with a melancholic look towards the viewer. The canvas is composed of two identical smaller pieces, vertically stitched together. This division was created in order to make it possible for the artists to work separately on the two different parts of the painting [94]–[96].

Figure 4.7 – Giovanni Maria Morandi and Mario Nuzzi, 'Ritratto di Mario Nuzzi che dipinge un vaso di fiori', 1658–1659, oil on canvas, 195 × 265 cm, Chigi Palace, Ariccia.

A series of *pentimenti* were detected in the 'Ritratto di Mario Nuzzi che dipinge un vaso di fiori' by Giovanni Maria Morandi and Mario Nuzzi. As an example, both the thermogram (Figure 4.8b) and the MWIR reflectogram (Figure 4.8c) reveal several changes to the initial concept of the painting. The arrows in the figures indicate a different hairstyle and head contouring with respect to the current appearance of the painting (Figure 4.8a).

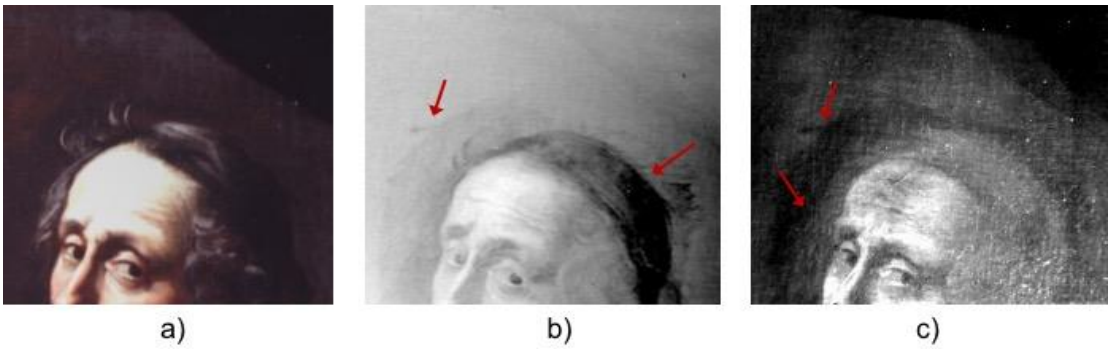

Figure 4.8 – (a) Detail of Figure 4.7, (b) thermogram recorded at short delays, (c) MWIR reflectogram. The arrows indicate the different contouring of the head.

A further element highlighted by the PT and MIR investigations is shown in Figure 4.9a-c. The thermogram (Figure 4.9b) and the MWIR reflectogram (Figure 4.9c) both detect the stitching line of the two separate pieces that form the canvas (indicated by the arrows in the figures), which was reported in the literature [97].

It is worth noting that the pentimenti was detected on only Nuzzi's head, thus evidencing the great attention shown by Giovanni Maria Morandi to the realistic representation of Nuzzi's physiognomy. With the exception of the join between the two pieces of canvas, the thermographic results do not show any defects or inhomogeneities, thus indicating the painting's good state of conservation.

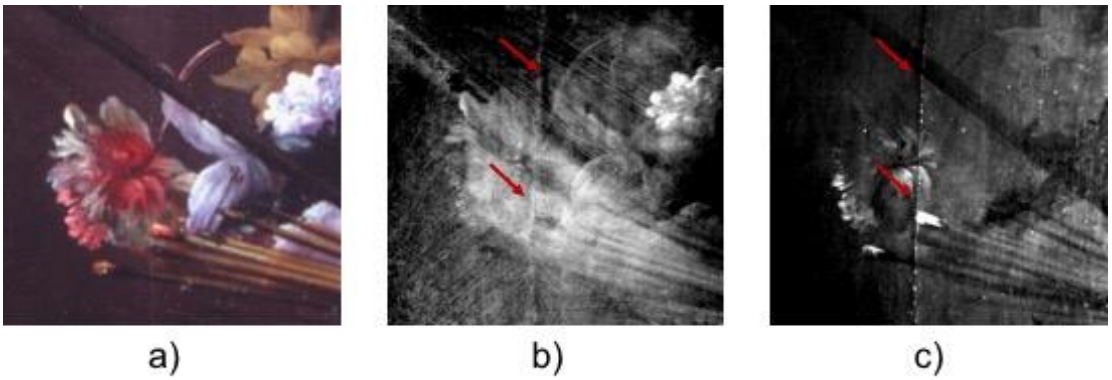

Figure 4.9 – (a) Detail of Figure 4.7, (b) thermogram recorded at short delays, (c) MWIR reflectogram. The arrows indicate the stitching line of the two parts of the canvas.

'Primavera'

The 'Primavera' ('The Spring') painting was also realised by the collaboration of two artists: Filippo Lauri painted the female figure and the cherubs, while Mario Nuzzi painted all the garlands and the floral elements. This artwork belongs to the series 'Le Quattro Stagioni' ('Four Seasons') considered one of the greatest examples of Roman Baroque painting (Figure 4.10). The entire series was commissioned by Flavio Chigi, nephew of Pope Alessandro VII, and executed between 1658 and 1659. The painting represents the allegory of spring, symbolising youth, painted as a beautiful woman surrounded by six cherubs and several types of flowers, while holding up a rose as a trophy [95], [96], [98].

Figure 4.10 – Filippo Lauri and Mario Nuzzi, 'Primavera', 1659, oil on canvas, 150 × 250 cm, Chigi Palace, Ariccia.

In the ‘Primavera’ by Filippo Lauri and Mario Nuzzi, an important *pentimento* was revealed with the MIR survey in the Flora figure. In particular, in the Flora’s hand (Figure 4.11) a change of the position of the ring finger is discernible from the thermogram (red arrow in Figure 4.11b) and especially from the MWIR reflectogram (red arrow in Figure 4.11c). In the same area, several repaired lacunas were detected (blue dashed arrows in Figure 4.11b-c), indicating a delicate painting surface and confirming the past restoration of the artwork.

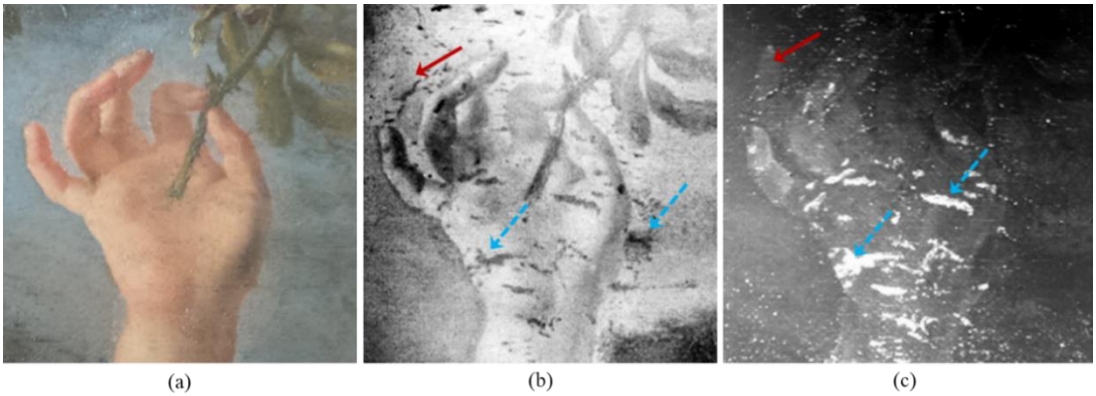

Figure 4.11 – (a) Detail of Figure 4.10, (b) thermogram recorded at short delays, (c) MWIR reflectogram. Red arrows indicate the pentimento in the ring position, blue arrows the restored lacunas.

Furthermore, interesting features came to light from the analysis of the flowers (Figure 4.12). Unlike the MIR images, which do not show any relevant features, probably because of the presence of the highly reflective varnish layer (Figure 8b), PT enabled the detection of several elements. In fact, the thermogram recorded just after the light pulse allowed the recovery of floral details (arrows in Figure 4.12c) that are not clearly visible to the naked eye, while the PT image recorded at increasing delay times revealed the canvas pattern (Figure 4.12d).

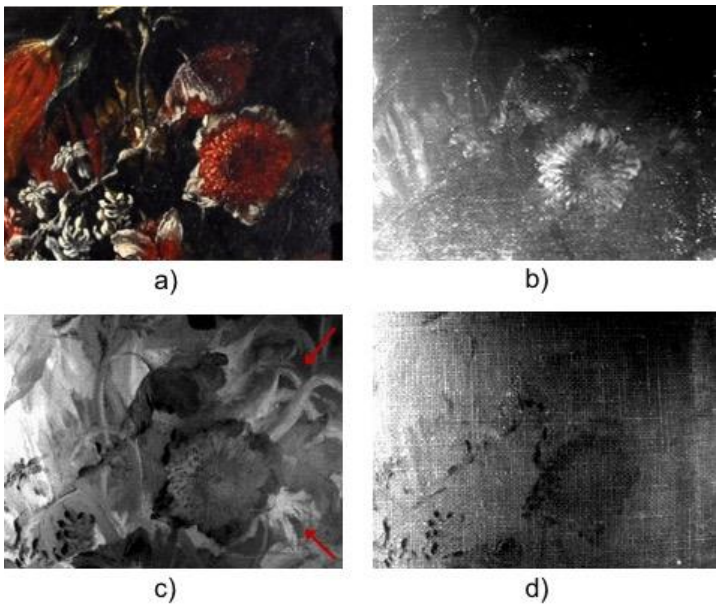

Figure 4.12 – (a) Detail of Figure 4.10, (b) MWIR reflectogram, thermograms recorded just after the light pulse (c) where the arrows indicate the recovered visibility of some flowers details, and at increasing delay times (d).

This painting was also studied by the IR-ITR laser scanner prototype described in section 2.3.1. as a complementary technique for subsurface investigations. An important feature detected by the IR survey is the *pentimento* in the Flora's face (Figure 4.13a). Here, the IR-ITR image displays another face close to the visible one (see the arrow in Figure 4.13b), possibly referring to the first appearance of the Flora character which seems to be different from the one of the final version. Such a *pentimento* is partially detected by PT at small delay times (Figure 4.13c), while it is not present in the thermogram obtained at larger delay times (Figure 4.13d), where only the structural pattern of the canvas is distinguishable. Moreover, the MWIR reflectogram did not show the *pentimento* but lighter areas corresponding to two repaired lacunas (arrows in Figure 4.13e).

Figure 4.13 – (a) Detail of Figure 4.10; (b) IR-ITR image where another face is revealed; (c) thermogram recorded after 20ms to the light pulse where the arrow indicates the second face slightly visible;(d) thermogram recorded after 300ms to the light pulse where the canvas patter can be seen;(e)MWIR reflectogram where the arrows point at repaired lacunas.

The IR investigations of the 'Primavera' painting allowed the detection of a change of mind in the representation of Flora's hand and face. This element may reflect the particular attention made by the artist to the hand pose because of the central role attributed to the gesture of Flora showing the rose as a trophy and symbol of the spring. On the contrary, the floral elements seem to be painted by the artist with less attention, as evidenced by the absence of clear *pentimenti*. Finally, the thermographic investigations enabled the detection of structural features, such as the repaired lacunas, according to the previous documented restorations of the painting [95].

'Ebbrezza di Noè'

The 'Ebbrezza di Noè' ('The Drunkenness of Noah') (Figure 4.14), preserved at the Chigi Palace, is one of the numerous replicas produced by Andrea Sacchi in the second half of the 17th century. The dating of the painting is uncertain, as is the possibility of establishing whether it is the original version or one of the many replicas [99], [100]. The large number of copies of this painting is due, among other things, to the importance of this biblical story from Genesis and the painter's constant search for perfection in its artistic production. The painting represents a famous biblical scene in which Noah is lying on a rock because of his drunkenness and, for this reason, he is being derided by Cam, while the more modest and respectful brothers, Sem and Jafet, look away. This scene was extensively represented during the Renaissance period, lasting until the 17th century, referring also to more pagan views, such as those relating to bacchanal models.

Figure 4.14. Andrea Sacchi, 'Ebbrezza di Noè', n.a., oil on canvas, 150 × 205 cm, Chigi Palace, Ariccia.

MWIR imaging investigations revealed several *pentimenti* in this painting, such as the one reported in Figure 4.15a-c. In this case, the back of the figure shows numerous modifications, which can be observed both in the thermogram (Figure 4.15b) and in the MWIR reflectogram (Figure 4.15c). In both the images, the arrows indicate the sketch of a facial profile larger than the one that is visible (Figure 4.15a). Even in this case, some restored lacunas were detected by PT (dashed circles in Figure 4.15b).

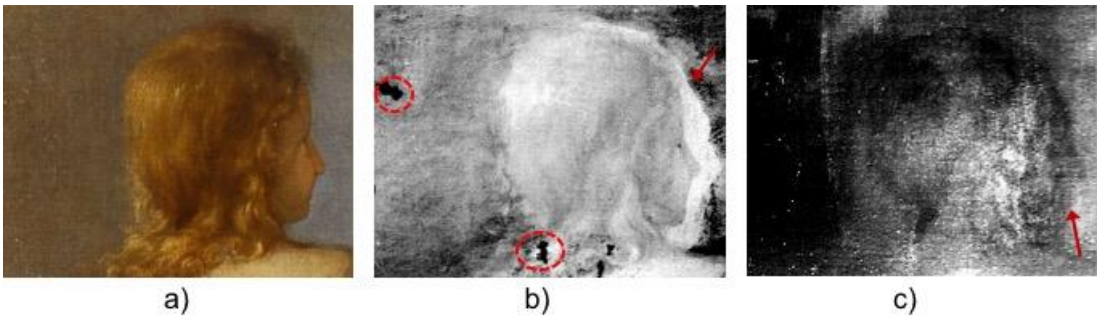

Figure 4.15- a) Detail of Figure 4.14, b) thermograms recorded just after the light pulse where repaired lacunas are marked with red circles and the pentimento indicated with the arrow; c) MWIR reflectogram where the different profile can be seen.

Another *pentimento* was observed on Noah's foot (Figure 4.16a), where a slight different contour is discernible in the thermogram (Figure 4.16b) and in the MWIR reflectogram (Figure 4.16c). Moreover, the thermogram shows a series of dark areas (the most significant is indicated by the dashed arrow in Figure 4.16b), probably corresponding to restored gaps or filled detachments, which, conversely, are barely visible in the reflectogram (Figure 4.16c).

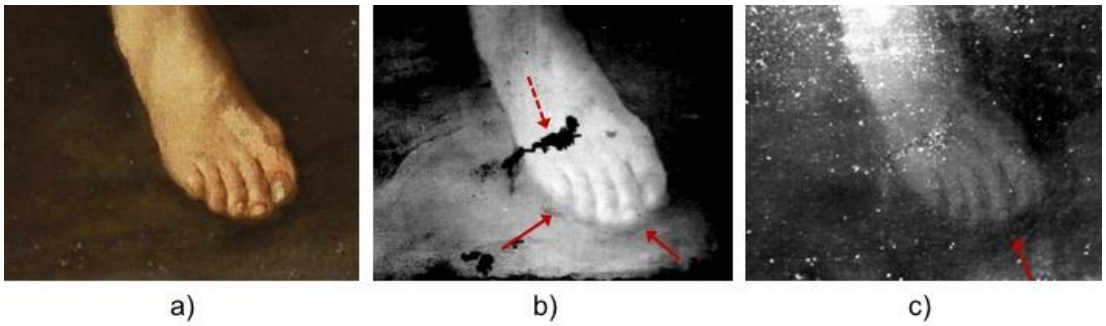

Figure 4.16 – Detail of Figure 4.14, b) thermograms recorded just after the light pulse where the repaired lacuna is indicated with the dashed arrow and the different foot contour is pointed with arrows; c) MWIR reflectogram where the different foot profile can be slightly seen (indicated with the arrow).

The *pentimenti* and small variations in the pictorial composition revealed in the painting by Andrea Sacchi by the MWIR imaging investigation could be in agreement with the continuous improvements introduced by the painter in the representation of this biblical story. Nevertheless, these variations do not indicate whether the Chigi painting is one of original versions of the numerous copies produced by the artist.

4.2 Drawings on different supports

Works created with pencils, coloured chalk or other materials, such as the sanguine, belong to the category of drawings. In this thesis, two artefacts of this category were studied, made with sanguine on different kind of supports. The first is a drawing on paper with unknown dating and authorship while the second is signed sketch made directly on wall, where the sanguine is mixed with darker material.

4.2.1 Raffaello School drawing at Istituto Nazionale della Grafica, Rome

The work studied at the Istituto Centrale della Grafica inside Palazzo Poli (Rome) was a sanguine drawing made on paper sheet glued on a canvas support, measuring 50 cm x 60 cm, assumed to belong to the school of Raphael for the style of the drawings (Figure 4.17).

One of the conservative question was to characterise the graphical material and investigate on the presence of eventual traces of additional ones. Moreover, at the moment of the analyses, the artefact presented several conservative issues, such as gaps, overlapping portions and detachments areas, so a non-destructive survey was necessary in order to mapping the most damaged areas.

Figure 4.17 – Sanguine on paper glued on canvas, preserved at the Central Institute for Graphics (Rome).

For the above-mentioned purposes, PT and MIR measures were carried out by dividing the entire surface into 36 frames. During the measurements, the IR camera and light sources were kept fixed during acquisition with the same framing of both the PT and MIR measurements, so that there was a pixel-to-pixel correspondence between the thermogram and the corresponding reflectogram. To obtain the images from all the different framing, the drawing was moved maintaining it at the focal plane of the IR camera. In this case, the image palette was inverted in order to better visualise the drawing.

Results

Thermographic survey allows to confirm the presence of sanguine as main graphical material of the artefact but both PT and MIR allow to highlight a line made of different material in correspondence of a horse leg (Figure 4.18a). Indeed, in the thermograms recorded at short and large delay (Figure 4.18c, d, respectively) such line appears much darker than the other lines of the drawing. MWIR reflectogram detected only the above-described line, while the rest of the drawing in red is not visible because its transparency to the IR range (Figure 4.18b). Such element

appears to have a different spectral behaviour with the respect to rest of the drawing made of sanguine. The provenance of this line is not clear and it is object of a debate among the conservators and the researchers.

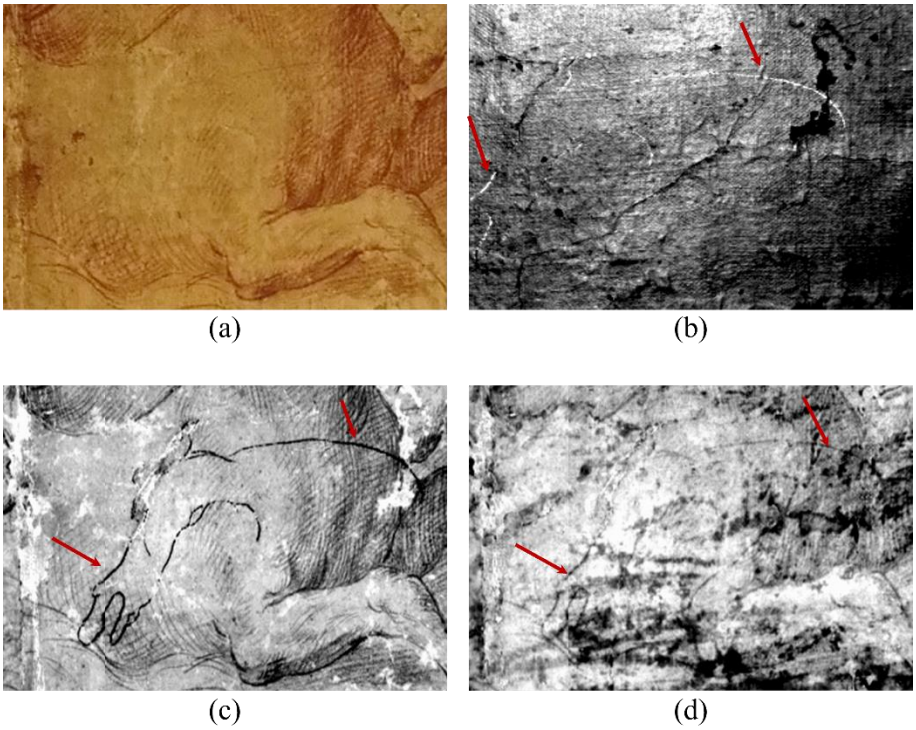

Figure 4.18 – (a) Detail of Figure 4.17; (b) MWIR reflectogram where the arrows indicate the dark line and the rest of the drawing is not visible; (c)thermogram recorded at short delay (8ms) where the darker line is indicated by arrows; (d) thermogram recorded at large delay (100ms) where the darker line is barely visible.

The thermographic mapping of the entire artwork (Figure 4.19) shows the total of the damaged areas and the overall vision of the drawing. From the image, the edges of the artwork appear to be the most critical areas, probably due to a wrong handling. Furthermore, a specific area of damage is clearly visible along the central fold line, revealing unsuitable past preservation arrangements of the artwork.

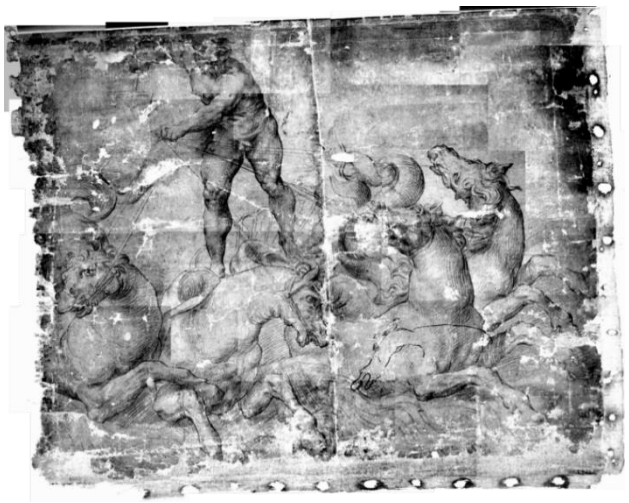

Figure 4.19. Thermographic reconstruction of the artefact obtained at 10ms of delay from the flash pulse.

4.2.2 Lorenzo Bernini drawing at Palazzo Chigi of Ariccia

The studied sanguine preserved inside the Palazzo Chigi in Ariccia (Rome, Italy) is the only signed drawing on wall made by the famous artist Lorenzo Bernini and it represents St. Joseph with the Child (Figure 4.20), completed by Bernini in 1663 for the chapel of the Palace. This is a true 'mixed work', intermediate between drawing and painting, outlined in sanguine, accompanied by gouache painting with a brush to complete some parts, obtaining the sfumato with the help of the fingers (there are still traces of fingerprints). The composition is inserted in a round painted-faux-marble stucco frame and painted directly on the curl of the irregular plaster. The inscription in capital letters establishes its dating to 1663 and confirms the authorship, unequivocally testified by the stylistic evidence: "EQVES IO LAVRENTIVS BERNINVS FAC: ANNO DÑI MDCLXIII. The sanguine is characterised by the spontaneity of the blurred and synthetic stroke, the perspective view of the Child and the expressive strength of the old man's profile. The intense emotional pathos of the saint's gesture, clasping his son as a sign of protection and turning his affectionate gaze on him, is an effective allegory of paternal love and a rarity in Josephine iconography, since the infant Jesus is most often painted in the arms of his mother. Although it was part of Bernini's practice to sketch his own extemporaneous intuitions in charcoal on the wall, the work has a complete and autonomous character. However, the use of sanguine and the rough plaster on which the composition unfolds do not make us exclude the possibility that it was a genuine sinopia or the outline for a fresco [101], [102].

Figure 4.20 – Gian Lorenzo Bernini, St. Joseph with the Child, drawing on wall, 1663, Ariccia (Rome).

Also in this case study, non-destructive MWIR investigations were performed enabling the mapping of the branched structure of superficial cracks, also highlighting deeper structural defects and previously restored areas, as can be seen in Figure 4.21a-c.

Results

PT detects a wide and long crack in correspondence of the child figure and other smaller ones and two large areas of probably past detachment of the plaster, then restored (red arrows and blue circle in Figure 4.21b, respectively). MIR highlights the superficial relief of these cracks (Figure 4.21c). For what concerns the drawing parts, while thermography is able to detect all the traits, as well as the blackish shadows under the child arm, the MIR do not display the red traits of the drawing. Such a spectral behaviour is consistent with the nature of the (iron-based) sanguine and (carbon-based) graphite that appear fully and partly transparent in the MWIR range, respectively.

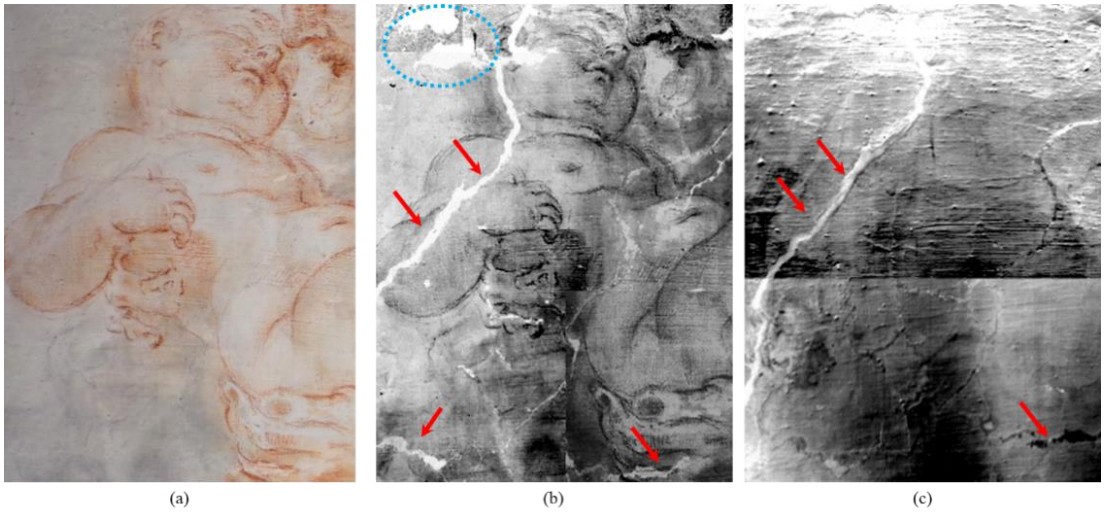

Figure 4.21 – a)Detail of Figure 4.20;b)thermogram recorded at short delays where the cracks and the repaired detachments are visible (indicated with the arrows and the blue circl, respectively); c) MWIR reflectogram shows the relief of the surface.

Similar results were obtained also in correspondence of the area of the child feet (Figure 4.22a), where the PT images detect superficial crack and small repaired detachments at short delays (red arrow and green dashed circles in Figure 4.22b) and deeper defects at larger delays (dashed arrows and green dashed circle in Figure 4.22c). MWIR reflectogram (Figure 4.22d) provides the three-dimensional extension of such defects. Even in this area, drawing traits are clearly detected only by thermography.

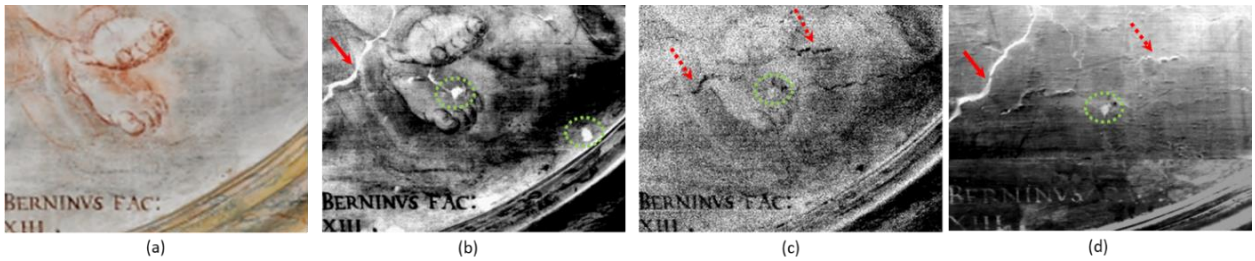

Figure 4.22 – a) Detail of Figure 4.20; b) PT images recorded at short delays detect superficial crack and small repaired lacunas (red arrow and dashed circles, respectively);c) PT images recorded at larger delays where deeper defects are visible (dashed arrows and dashed circles); d) MWIR reflectogram provides the three-dimensional extension of such defects.

4.3 Painting on parchment and paper support

In this section, the results obtained by studying three types of graphic artworks characterized by pictorial layers applied on paper and parchment will be presented. In the first case, a 14th *codex* of the Divina Commedia, a MWIR survey was carried out on the illuminations of the manuscript in order to recover the readability of the drawings where the iconographic representation appeared severely damaged. In the second case, a Japanese decorated paper handscroll was investigated by means of MWIR imaging techniques and colorimetry with the aims of characterising the conservative status of the artworks and their materials. Finally, painted papier-mâché puppets were analysed by PT to assess the preservation state of their inner structure and surface, before and after a recent restoration.

4.3.1 Illuminations of a 14th century codex of the Divina Commedia

The studied manuscript (MS. 1102) is an illuminated parchment *codex* of Dante Alighieri's Divina Commedia dated to the 14th century and preserved in the Bibliotheca Angelica in Rome. The text, arranged in two columns, was written by a single hand, which uses the Littera Textualis [103]. The manuscript also contains Jacopo Alighieri's and Bosone da Gubbio's commentaries, titled "Capitolo sulla Commedia" and, in addition, a fragment of the poem about the history of Alexander the Great 89riten by Gualterus de Castellione. However, the relevance of the *codex* is mainly as a result of artistic reasons, such as the original iconography of the 34 illuminations, which display only the canticles scenes of Dante's Inferno. In fact, the manuscript was never completed and the empty spaces meant for the insertion of the illustrations concerning the *Paradiso* and the *Purgatorio* canticles are still visible. According to several studies [103]–[105], the illuminations were ascribed to an illuminator of the Bologna workshop, where famous artists like Oderisi da Gubbio and Franco Bolognese are considered as possible authors. The manuscript appears in a good state of conservation, with few water stains and some holes due to woodworm attacks, which were restored in part in 2008.

Results

The illumination of *folio 2* verso decorates Canto III and appears to be one of the most damaged parts of the manuscript, as can be seen in Figure 4.23, where the demoniac figure appears hardly visible (rectangle in figure), probably because of the loss of the pigment layer. Here, the thermogram shows details of the water waves with greater contrast than in the picture (yellow arrow in Figure 4.23b). This indicates the high level of the finishing of the original illumination, unfortunately barely detectable in the actual deteriorated state of the illumination. The MWIR

reflectogram (Figure 4.23c) displays some further details situated even below the pictorial layers, such as possible underdrawings of tree branches (indicated by the red arrows in Figure 4.23c), which are not visible in the VIS either PT images. Moreover, the profile of the oar (yellow arrow in Figure 4.23c) seems very different from those in Figure 4.23a, b.

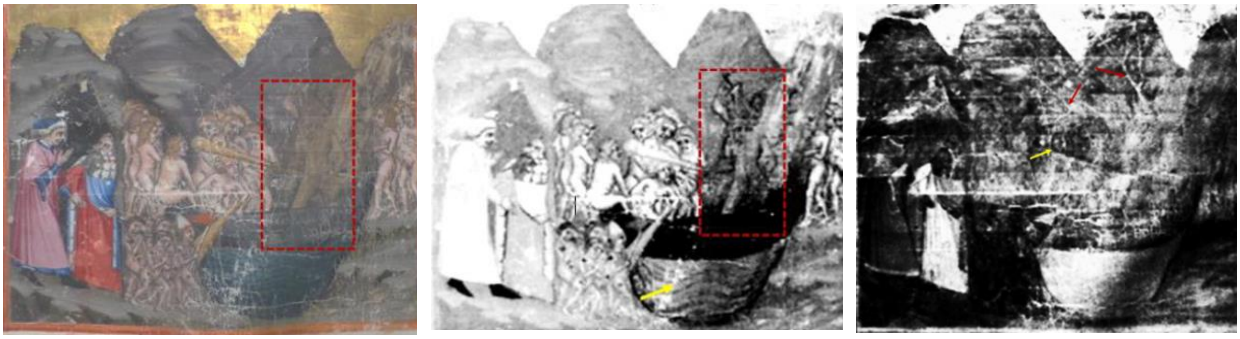

(a) (b) (c)

Figure 4.23 – Illumination of folio 2 verso: (a) picture, (b) thermogram where the dashed rectangles mark Charon and the yellow arrow indicates the waves of the river Acheron; in the MWIR reflectogram the red and the yellow arrows indicate the tree branches and the oar, respectively.

Also the demoniac figures represented in the illumination of folio 4 verso appears severely damaged (dashed rectangles in Figure 4.24a), being almost impossible to identify them through simple visual inspection. In the case of the left figure (red rectangles), the detail obtained with the thermogram (Figure 4.24b) enabled to obtain improved contrasted images of the remaining features of the figure. The arrows in Figure 4.24b indicate such features that could be described as large claws and the profile of the back end of a beast, which recall the features of the guardian Minos. This information led to the identification of the scene as the descent of Dante and Virgil into the Second Circle of the Inferno where they see the monster Minos standing in front of the endless line of sinners, ready to assign them their torments. According to the text, the sinners confess their sins to Minos, who then wraps his great tail around himself a certain number of times, thus indicating to them the number of paths the soul must cover. The detail of the MWIR reflectogram (Figure 4.24c) shows some additional elements of the decorative apparatus regarding the second demoniac figure (blue rectangle in Figure 4.24a). In particular, some somatic traits of the demon can be better distinguished, such as the nose and the open mouth, indicated by the arrows in Figure 4.24c.

(a) (b) (c)

Figure 4.24 – Illumination of folio 4 verso: (a) picture where the rectangles indicate the demoniac figures better highlighted in (b) thermogram where the red arrows indicate the large claws and the profile of the back end of a standing creature, and in (c) the MWIR reflectogram where arrows indicate the nose and the open mouth.

In the two investigated illuminations, both the thermograms and the MWIR reflectograms have enabled the recovery of images of lost details. The results allowed the identification of Charon and Minos, demoniac personifications coming from the mythological tradition and playing the role of guardians of the circles of the Inferno. This kind of information may possibly suggest that the damage could have been intentionally applied, perhaps for censoring purposes, also considering the historical and artistic period of the manufact itself.

4.3.2 Japanese handscroll

The handscroll studied in this thesis belong to the 'Vincenzo Ragusa' Fund of the *Museo Nazionale Preistorico Etnografico "L. Pigorini"* of Rome, which collects more than 4000 artefacts coming from the Japan between the 19th and 20th centuries.

The handscroll is made of Japanese *kozo* paper [106] and it has a length of more than 7 m, containing a collection of subjects painted using only black ink and a limited range of colours, generally very diluted, to achieve delicate tones and shades that enhance certain details of the subjects. The craftsmanship of the work, together with the materials and technique used, led to the hypothesis that it might be a collection of images portrayed by an apprentice who was practising painting, attempting to imitate the art of some famous masters. The evident connection with the art that flourished and spread in Japan since the 17th century has led to the hypothesis that the painted scroll no. 142 841 of the Ragusa Fund may was made and illustrated by the Japanese painter Kiyohara Tama (1861-1939), wife of Vincenzo Ragusa.

The studied artwork had come into contact with a source of moisture that had caused large and moderate-sized gore to spread from the upper margin of the sheets and the formation of larger but

less extensive gore near the lower margin. The distribution and shape of these gouges suggest that the damage was caused while the work was kept wrapped around itself. Thus, several sheet of the scroll were examined with twofold aim: on one hand, discovering the kind of inks used in the decoration; on the other hand, characterising the brightness of the paper support in order to assess the effectiveness of the interventions. For the first goal, thermographic and reflectographic survey has carried out, while colorimetric measurements have performed with FORS apparatus.

Results

MWIR analyses carried out on the *recto II folio* (Figure 4.25a) show different natures of the inked parts in the falcon representation, where shadows of black characterise the figure. From the comparison of MIWR results, it can be noticed that the grey colour was not produced by simply using a diluted mixture of black ink alone, but rather a distinct colour (perhaps obtained by mixing black with white). Such information can be obtained by observing the spectral behaviour of the different kind of inks in Figure 4.25b-c: in PT measurements, inks with a metallogenic nature absorb VIS radiation from the light sources and induces the emission of the IR radiation detected by the camera, by providing a highly contrasted image (Figure 4.25b), while in the reflectogram recorded at these wavelengths such inks are transparent. On the contrary, carbon inks maintain contrast with the background of the substrate also in MWIR reflectogram, as can be noticed by the squared areas in Figure 4.25c [107]. Furthermore, in the thermogram, the extension and shape of the gore on the supports are clearly discernible (arrow in Figure 4.25b).

(a) (b) (c)

Figure 4.25 – Japanese paper handscroll, folio II: (a) detail of the falcon, (b) thermogram recorded at short delays from the light pulse where the arrow indicates the gore; (c)MWIR reflectogram where the dashed squares indicate the different black inks.

FORS measurements have carried out on several point in the handscroll, in areas affected by different types of damage or in a good state of preservation (Figure 4.26a) in order to evaluate ΔE^*_{ab} and ΔL^* parameters for the overall assessment of the cleaning operation performed on the

occasion of a recent restoration on the supports. The results of the FORS measurements obtained before and after the dry and wet cleaning are reported in Table 4.1.

Table 4.1 – Colorimetric and brightness parameters obtained after cleaning procedures.

	P. 1	***P. 2***	***P. 3***
ΔL*	0,5	-1,5	7,0
ΔE*	3,0	5,0	10,0

The parameters show a positive performance of the cleaning procedure, indicating attenuation of the darker areas, such as the gore, and the effective general brightening of the paper support, as clearly appears from Figure 4.26b [108].

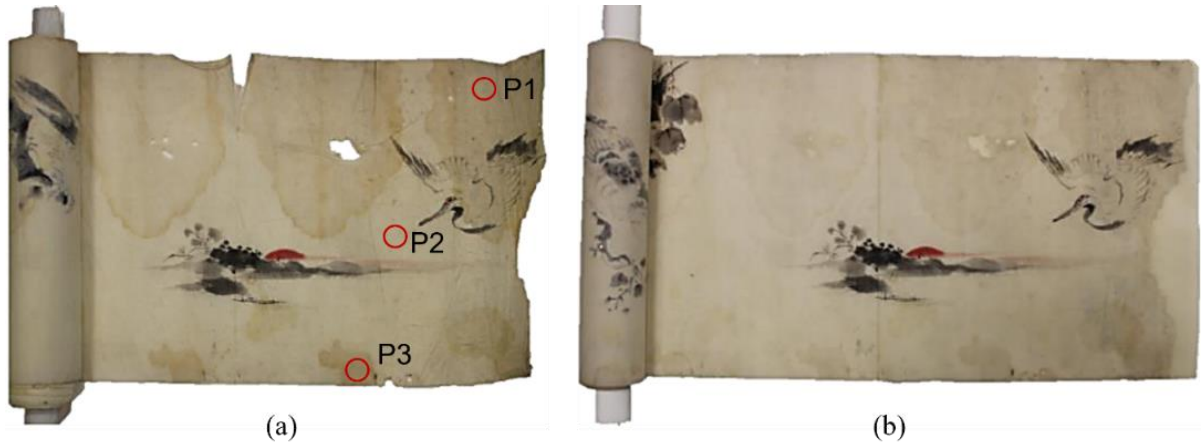

Figure 4.26 – Japanese paper handscroll: (a) FORS sampled points before cleaning; (b) artefact aspect after restoration and cleaning procedures.

4.3.3 Papier-mâché puppets

Among the several different CH forms and expressions, puppets theatre was very diffused in Italy between the 16th and 18th centuries, mainly thanks to its great versatility for themes and characters. Over the centuries, puppets were built in a multitude of materials and structures. The head can be mainly made of wood or papier-mâché, which was widely used, especially for its economic and executive advantages. The clothes are made of fabric, usually coming from recycled materials, enriched by details and accessories. Thus, the conservation of such artworks can be difficult and delicate due to the multi-materials structure. In this thesis, puppets belonging to the Lampe Minelli collection preserved at the Museum of Popular Arts and Traditions of Rome were studied. Such particular items were created by the famous Italian puppeteer Olga Lampe Minelli from which the collection takes its name and who worked during the second half of the 20th century. The structure of this particular kind of object can be summarised in 3 parts: the head, the body and any

accessories. The head of the analysed puppets are made of papier-mâché, finished with painted details of the characters, while the bodies are created by recycled clothes of the artist herself.

The puppets studied in this thesis are two male figures and one animal (Figure 4.27) with similar kinds of damage, such as abrasions and diffuse stains, papier-mâché breaks and entomological damage. Indeed, all the puppets were affected by insects' attack, as can be seen by the numerous flickering holes on the papier-mâché support. Furthermore, colour fading and detachments characterised all the painted surfaces, where the weakening of the pictorial layer caused several breakages.

(a) (b) (c)

Figure 4.27. Pictures of the puppets before the restoration: (a) n.1, the man with tie; (b) n.2, the clown; (c) n.3, the horse.

The analysed artworks were in critical conservative status thus requiring an urgent restoration also aimed to the museum display. For these purposes, a non-destructive study on the puppets was carried out by MWIR imaging, providing the mapping of the types and relevance of the defects and directing the most appropriate conservative procedure.

Results

In the puppet n.1 (Figure 4.28a), MIR images highlighted the presence of previous restorations which appear more reflective with the respect to the other parts of the puppet face (yellow arrows in Figure 4.28b). PT on the puppet n.1 detected inhomogeneities of the papier-mâché support, identifying several walkways of insects. If from the inspection of the firsts thermograms (Figure 4.28c) the defects appear superficial (red arrows), from the analysis of thermograms recorded at

larger delays (Figure 4.28d), where the same defects are still detected (red arrows), information about the depth of the damage can be obtained. Indeed, at long-delays thermograms correspond larger investigation depths, indicating a deeper inhomogeneity developed within the puppet volume, beneath the superficial level, such as the hole under the puppet eye (see the green arrows in Figure 4.28c-d).

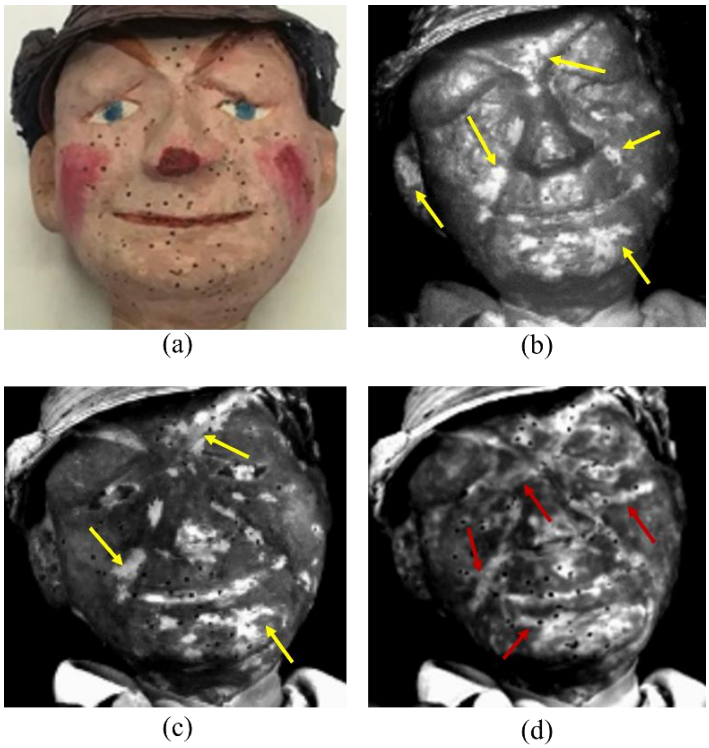

Figure 4.28. Results of analyses on the puppet n.1: (a) picture; (b) mid-IR reflectography; (c) thermogram recorded at 0,01s of delay; (d) thermogram acquires at 50 s of delay.

Also in the case of the investigations on the puppet n.2 (Figure 4.29a), MIR image detected the presence of restorations and previous adjustments shown as the more reflective elements with the respect to the background (yellow arrows in Figure 4.29b). Several detachments in correspondence of entomological holes and cracks are identified by the analysis of the thermogram recorded at short delays (red arrows Figure 4.29c). Moreover, the thermogram corresponding to larger delays (Figure 4.29d), better characterized the deeper empty areas under the surface (see red arrows). These defects are visible thanks to the contrast between dark and lighter areas: the firsts correspond to the materials through which the heat is spreading, while the seconds are the surrounding cold areas, corresponding to the cavities, in which the absence of material prevents the heat from spreading.

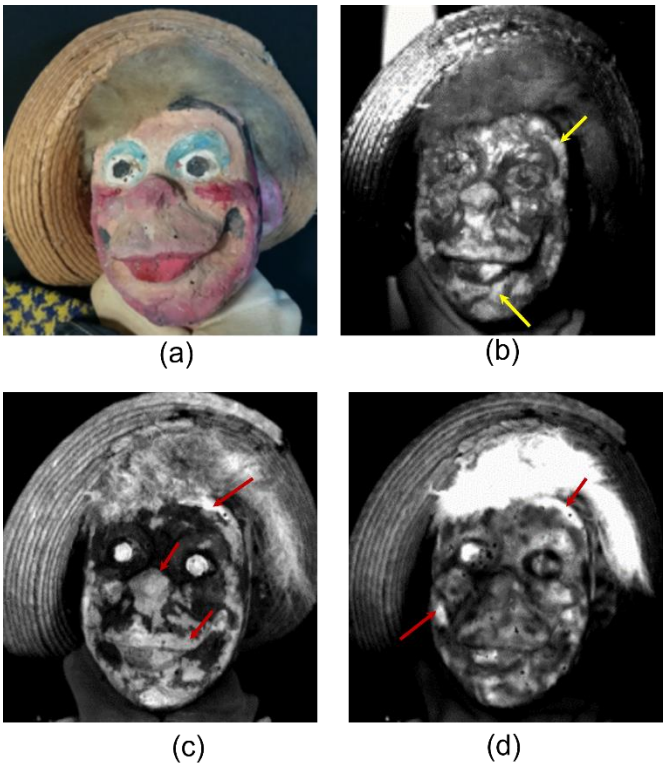

Figure 4.29. Results of analyses on the puppet n.2: (a) picture; (b) mid-IR reflectography; (c) thermogram recorded at 0,01s of delay; (d) thermogram acquires at 20 s of delay.

A similar situation occurs on the puppet n.3, such as the horse (Figure 4.30.a). The thermogram recorded at the short delay of 0.03s shows the presence of numerous flicker holes on the surface and an important inhomogeneity area (red circle and arrow, respectively, in Figure 4.30.b). Such holes appear connected to the detachment area observed in the thermogram recorded at grater delays, corresponding to larger depths (red circle in Figure 4.30.c). Thus, many of the seemingly disjointed elements on the surface are actually connected below it. Moreover, in the same thermogram, in correspondence of the neck of the animal, another detached area is visible, indicated with the red arrow.

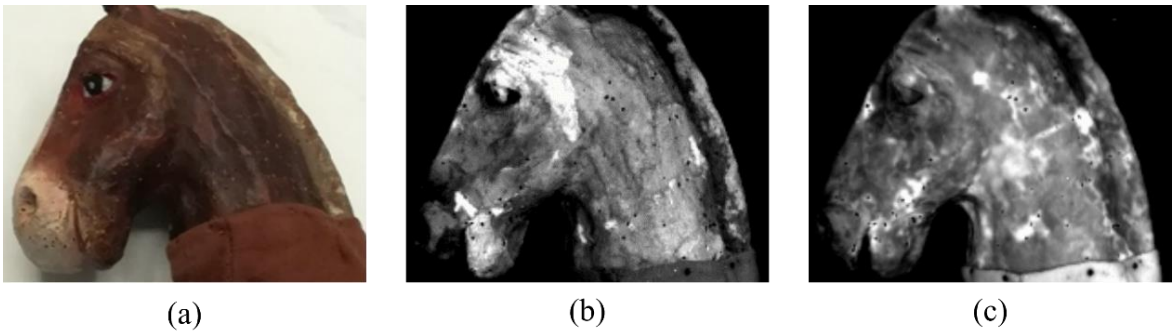

Figure 4.30. Results of analyses on the puppet n.3: (a) picture; (b) thermogram recorded at 0,01s of delay; (c) thermogram acquires at 20 s of delay.

Furthermore, colorimetric measurements were carried out on both the papier-mâché and the fabric in order to analyse the colour changes resulting from the cleaning and restoration procedures. As

can be stated by Table 4.2, colour variations and brightness increase are significant on both the papier-mâché and the fabric, demonstrating an efficient cleaning.

Table 4.2 - Colorimetric and brightness parameters obtained after cleaning procedures on the horse puppet.

	Papier-mâché head	***Cloth***
ΔL*	10,5	13,5
ΔE*	13,8	14,7

A preliminary post-processing elaboration by means of the edge detection algorithm using the MATLAB suite was performed on the PT images recorded on the puppet n.1. This algorithm was applied on numerous frames of the thermographic sequence with twofold aim: on one hand, the automatic recognition of the contours of detected elements for their analyses in geometric and depth evolution (Figure 4.31a-b); on the other, the possibility of simultaneous viewing of the comparison between PT and MIR data by overlapping the results of the edge extrapolation (Figure 4.31c). The latter was possible thanks to the use of the same detector for both PT and MIR measurements, ensuring the pixel-by-pixel correspondence of the images and, therefore, enabling the overlapping of the elements contouring obtained from the algorithm.

(a) (b) (c)

Figure 4.31. Edge detection algorithm: (a) short delays thermogram where the marked areas indicate small superficial detected features; (b) large delays thermogram where the marked areas indicate the extension in depth of the elements detected in (a); (c) edges overlapped for a simultaneous viewing of the elements detected by PT (green) and MIR (purple).

After the restoration procedures, an additional thermographic survey was carried out with the purpose of observing the condition of the puppets and verifying the effectiveness of the consolidation practices. The visual examination of the work immediately confirms the effectiveness of the restoration of the surface layer, where flicker holes and pigment detachments appear repaired (Figure 4.32b). The thermograms recorded 2 s after the perturbation before (Figure 4.32c) and after (Figure 4.32d) the restoration was compared. In the post-restoration thermogram the more contrasted areas indicate the presence of a denser material than air but less than papier-mâché, which is the filler used for the consolidation of the puppets. In fact, the filler was made with a fluidity that could be syringed inside the holes, so the contrast between consolidated and

unconsolidated areas is mainly due to the difference in the compactness between the papier-mâché and the consolidant. On the other hand, the less contrasted areas show the presence of detachments, already observable in the pre-restoration thermogram (Figure 4.32c), which could not be consolidated due to the impossibility of reaching the affected area.

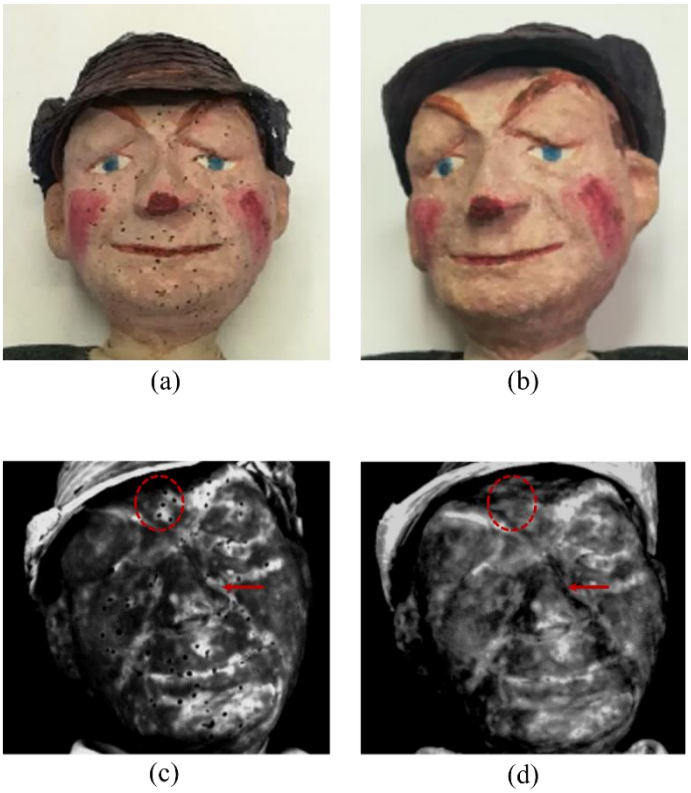

Figure 4.32 – Pre and post restoration evaluations: (a), (b) picture pre and post restoration, respectively; (c) pre-restoration thermogram recorded at 2s after the light pulse; (d) post-restoration thermogram recorded at 2s after the light pulse. The circles and the arrows indicate areas where the consolidation appeared to be efficient.

The combination of MWIR imaging techniques on papier-mâché puppets allowed the characterisation of their state of conservation, identifying superficial defects and decohesion areas within the volume. The presence of such inhomogeneities may be due to the handcrafted nature of artefact, on the contrary with the respect to industrial puppets, where the cellulosic paste of the papier-mâché mixture is usually more compact. The results were then employed for the consolidation procedures which appear to be efficient from the observation of the post-restoration diagnostic survey and the colorimetric measurements.

4.4 Structural survey on wooden bowed string instruments

As a final case not belonging to the painted artefacts category, this section will present the preliminary results of a structural study in collaboration with the Laboratory of non-Invasive Diagnostics “Arvedi” of Cremona on musical instruments using thermography and radiography. The aim of this study was to investigate the feasibility of using PT in combination with another

NDT technique for structural investigations and to assess of the state of conservation of fragments considered parts of historical bowed string instruments.

The object of the study is a fragment attributed to important violin makers Gaetano Sgarabotto (1878-1959) and his son Pietro (1903-1990), which, during the first half of the 20th century, restored several stringed instruments by replacing the most heavily damaged parts (i.e., top plates, backplates, ribs) and using them as models to reproduce their excellent aesthetic features in their modern instruments [109]. The studied fragment (F04) was selected to cover a broad range of defects generally found on an instrument and, in this case, the layered structure consists of overlapped layers of wood, glue and superficial varnishes without the pictorial/graphical components.

Results

The results of the analyses on the fragment F04 (Figure 4.33) allowed to identify several damages. The thermogram recorded at a larger delay (~150 ms) (Figure 4.33b, yellow arrows) shows the presence of several woodworm walkways in many parts of the sample and of a fracture in the left part of the image (red arrow). They are also highlighted by the radiography (Figure 4.33c). As in the previous case, the thermograms recorded just after the light pulse could not provide information about deeper galleries, confirming the effectiveness of PT to yield some helpful hints about the proximity of the defect to the surface.

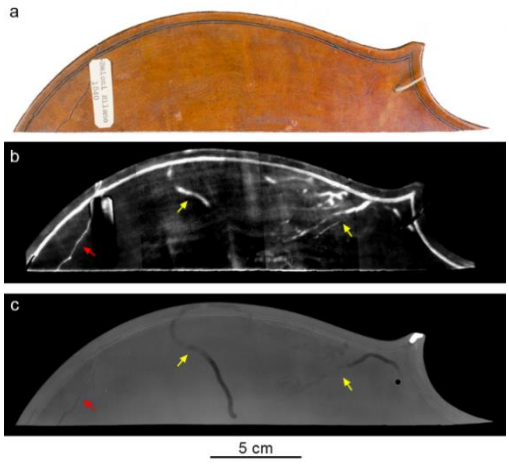

Figure 4.33 - F04 fragment: (a) Picture; (b) thermogram recorded at about 150 ms of delay; (c) radiography. Structural features described in the text are highlighted by yellow and red arrows.

In this application, for the first time the results obtained through IRT and RX were combined together, as an improvement for the commonly employed investigation strategies for bowed string instruments [110], [111]. The results allowed us to deeply document and identify a large number of defects, such as woodworm galleries and cracks, comparing the RX bidimensional images with PT stratigraphic information.

Conclusions

Imaging techniques are nowadays a widespread methodology for the investigation of Cultural Heritage. The non-destructive approach guaranteed by this type of techniques is a very valuable factor when studying fragile or damaged artworks. Furthermore, the possibility of reading and processing the data in the form of images enables a more immediate and intuitive visualisation of the results, which can also be easily shared with the scholars in the field and end-users. Among these techniques, active infrared thermography has proven to be very useful tool for the stratigraphic analysis of different categories of artworks, including those considered in this thesis, namely painted artefacts and historical books. A reflectographic approach was recently introduced as non-destructive imaging method for sub-surface examinations of CH items, based on the same spectral range of the thermography, i.e. mid-wave IR.

In this thesis, the use of these two mid-wave-IR techniques were presented by discussing its application on specifically designed laboratory samples and original artefacts, with the aim of studying their applicability on different categories of Cultural Heritage as novel combined approach. After discussing the most commonly used non-destructive testing imaging techniques in Conservation Science, focusing on pulsed thermography and mid-wave IR reflectography, an overview of the typical elements of the stratigraphic structures of the two categories considered in this thesis was provided, by describing the structures and materials. In addition, theoretical discussions on the working principles of the two techniques were included by also explaining the theory of the heat transfer and the generation of the signal for and contrast. In particular, the heat transfer principles were presented with regard to both optically-opaque samples, such as bronze artefacts, and those considered to be semi-transparent, i.e. painted artworks and library heritage, it was on the latter that the subsequent argumentation focused. A theoretical study of the images contrast generation in fibrous semi-transparent media, such as paper and parchment, was carried out for the estimation of the edge distortion of sub-surface features detected with thermography. For such quantitative evaluation, experimental and theoretical approaches were followed by analysing a laboratory sample designed with the combination of ink and increasing thickness paper stripes measured with PT and solving the heat transfer equations by using the FEM implementation. Moreover, a brief description of the complementary techniques employed in this thesis were included, such as two NIR reflectography methods using different systems: the first is based on a standard CCD sensor camera with passband filters and the other is a scanner prototype which uses IR laser sources instead of lamps. Among the complementary studies of this thesis,

colorimetric measures were performed by means of FORS technique. In addition, another prototypal system was used for vibro-acoustic imaging on the wooden laboratory sample.

Following these introductory and theoretical chapters, the description of two laboratory samples was presented. These were designed and elaborated using historically reliable materials in order to simulate and study the typical supports and structures of artworks. Concerning the sample that simulated painted artefacts, the wooden support was chosen to reproduce panel paintings, using poplar species, as the most commonly material for these kinds of artefact. Then, defects were produced in several parts with variable geometries to simulate different kinds of damage, such as detachments and woodworm galleries. To continue the simulation of a panel painting, a preparation layer made by gypsum and animal glue was applied on the sample, on which a drawing was executed with graphite and charcoal, simulating the presence of underdrawings. Likewise, mineral pigments and egg binder were employed for the pictorial part, choosing two pigments per colour in order to investigate the spectral behaviour of the same colours with different chemical composition. The results obtained from the IR survey at different wavelengths (from NIR to MWIR) on this first sample highlighted the different capabilities of the employed techniques to penetrate the layers and characterise the materials. Indeed, PT and MIR allowed the identification of the artificial defects under the preparatory layer thanks to different reflectivity and thermal conductivity of the materials used to simulate the repair of such elements with the respect to the support. Vibro-acoustic analysis allowed to characterise the structure of the sample and the artificial defects by discriminating the vibration velocities of the elements. Similarly, also the two materials used for the sketch showed different spectral responses in the NIR and MWIR ranges. Indeed, from the results obtained from the combined use of NIR and MWIR imaging techniques, charcoal appeared to be a material with a larger light-absorbing power than graphite. On the other hand, graphite had a highly reflective behaviour in the NIR-MWIR ranges. Pigments showed as well different optical and thermal behaviours, being mostly transparent to the NIR range and showing the underlying drawing in correspondence of yellow and red ochres, the orpiment, the lapis and the cinnabar while the lines are barely visible under the green earth, the minimum and the Egyptian blue. In all the obtained images the lead white shielded all radiations, as well as the malachite. In correspondence of the brighter pigments, the MWIR reflectogram is saturated because of the reflection of the ground layer which often blinded the optical reflection of the underdrawings up to the detector. However, thanks to the larger wavelength of the technique, the sketches under the minium pigment can be investigated, unlike in the other analyses. Regarding PT results, the underdrawings were only partially revealed by the image recorded at short delay from the light pulse while the profiles of the defects under the ground layer were detected by the

thermogram recorded at larger delays. Thus, by the combined use of NIR-MWIR imaging techniques, an overall description of the layers composing the panel painting sample was possible, demonstrating the great value of using an integrated and complementary approach in different spectral ranges.

As regards the mock-up of an historical book, this was realised simulating the complex structure of codices or books containing the so-called waste bindings, i.e. parts of historical books reused as reinforcement of the binding of newer books. Such elements were often written pages and their use in the construction of new *codex* provide a complex overlying configuration where further written parts were hidden under layers of paper and/or parchment. Thus, the laboratory sample was realised on a paper sheet support by drawing an ink area covered by paper stripes with increasing thickness. These stipes were glued on an inked area with a starch adhesive, simulating the reliable materials in the realisation of historical books. In this case, the thermography was used as the technique proven to be effective in the investigation of elements buried under the paper materials without being highly influenced by the scattering of radiation, as in the case of NIR reflectography. In particular, the aim of the employment of PT on this sample was twofold: on one hand studying the capability of the PT to identifying hidden texts at different depths and, on the other, carrying out an experimental study for modelling the heat diffusion within semi-transparent media and quantifying the consequent distortion effect in thermal images. Indeed, the distortion effect the distorting effect noticeable in thermographic images, especially in those recorded at larger delays, leads to a loss of legibility of the texts detected by thermography, decreasing the great value of using this technique in the identification of hidden texts. For the mentioned purposes, the experimental data collected from the laboratory sample with PT were used to perform the comparison with the theoretical simulations obtained from the application of FEM to the heat diffusion equation. The obtained results indicated a decrease in the contrast signal as a function of the depth of the ink element, correlated with an increase in the edge distortion effect. Thus, at short delays the thermographic image is well-contrasted with sharp edges while, at increasing delays, the detected contrast and sharpness decrease due to the larger depth of the elements whose emitted radiation have to pass through more layers, being also dispersed between them. Nevertheless, the experimental data and the theoretical simulations showed a good degree of superimposition, demonstrating the validity of the adopted model and enabling the characterisation of the distortion effect. Thus, the quantification of such distortion appears to be very useful for a subsequent correction of image blurring in post-processing.

As last chapter, applications of the adopted methods for the laboratory wooden sample were presented by illustrating the results of the investigations on a series of selected artefacts belonging to various CH categories. The studied items were divided on the basis of the support and the graphical/decorative apparatus, namely, paintings, drawings on different supports, wooden artefacts, painting on paper support, painted artefacts on miscellaneous support. The artefacts were studied by using of the MWIR techniques as main approach with complementary further methods, such as NIR imaging and FORS. In every study, the combined use of PT and MIR allowed the investigation of both the subsurface elements and the volume by using the same framing and just switching the illumination source. In several cases, the MWIR analyses provided information about elements not detected by other techniques, such as in the case of the study of the Santa Maria in Cosmedin altarpiece, where MWIR results showed a different iconography of the Virgin. The combination of thermographic and reflectographic images in the MWIR range adopted in the study of Palazzo Chigi paintings allowed the identification of several pentimenti and structural features at different depths under the visible layer. These techniques were also useful for the discrimination of the material used in several drawings, such as the one preserved at Palazzo Poli which appeared to be in sanguigna, like the Lorenzo Bernini drawing at Palazzo Chigi. Here, the mapping of the plaster cracks was also provided by the two MWIR techniques by showing different spread and depth. Similar results were obtained in the analyses of a Japanese handscroll and of an illumination of a 14th *codex*, where the techniques allowed the recognition of the used inks in the first case and the recovery of the painted figures in the second. As final application, an innovative use of the two techniques was applied in the study of painted puppets made of papier-mâché. In this case, the complete characterisation of the conservative status of the artefacts was possible, providing precious indication for the proper restoration procedure.

The combination of MWIR imaging technique on the study of laboratory samples highlighted the capability of the proposed method to investigate multi-layered structures composed of semi-transparent media, detecting hidden elements within the structures. Such effectiveness combined use of PT and MIR was then confirmed in several applications on original artefacts, being able to characterise complex structured in a totally non-destructive approach. In this thesis, the described novel approach, the experimental modelling simulations and the complementary measurements involved the collaboration of several external research institutions and the consequent networking between the researchers, establishing the importance of the multidisciplinary of the sciences applied to the study of Cultural Heritage items.

References

[1] D. A. Bradley and D. C. Creagh, *Physical techniques in the study of art, archaeology and cultural heritage (Vol. 1)*. Amsterdam: Elsevier, 2006.

[2] J. J. Chen, A. Shugar, and A. Jehle, "X-radiography of cultural heritage materials using handheld XRF spectrometers," *X-Ray Spectrom.*, vol. 48, no. 4, pp. 311–318, Jul. 2019, doi: https://doi.org/10.1002/xrs.2947.

[3] M. Schreiner, B. Frühmann, D. Jembrih-Simbürger, and R. Linke, "X-rays in art and archaeology: An overview," *Powder Diffr.*, vol. 19, no. 1, pp. 3–11, 2004, doi: 10.1154/1.1649963.

[4] G. Poldi, G. C. Villa, and L. Bonizzoni, *Dalla conservazione alla storia dell'arte: Riflettografia e analisi non invasive per lo studio dei dipinti*. Pisa: dizioni della Normale, 2006.

[5] A. Casini, F. Lotti, M. Picollo, L. Stefani, and E. Buzzegoli, "Image Spectroscopy Mapping Technique for Non-Invasive Analysis of Paintings," *Stud. Conserv.*, vol. 44, no. 1, pp. 39–48, 1999, doi: https://www.jstor.org/stable/1506694.

[6] F. Mercuri, U. Zammit, N. Orazi, S. Paoloni, M. Marinelli, and F. Scudieri, "Active infrared thermography applied to the investigation of art and historic artefacts," *Journal of Thermal Analysis and Calorimetry*, vol. 104, no. 2. pp. 475–485, May 2011, doi: 10.1007/s10973-011-1450-8.

[7] G. Cadelano *et al.*, "Monitoring of historical frescoes by timed infrared imaging analysis," *Opto-electronics Rev.*, vol. 23, no. 1, pp. 100–106, 2015, doi: 10.1515/oere-2015-0012.

[8] J. K. Delaney, M. Thoury, J. G. Zeibel, P. Ricciardi, K. M. Morales, and K. A. Dooley, "Visible and infrared imaging spectroscopy of paintings and improved reflectography," *Herit. Sci.*, vol. 4, p. 6, 2016, doi: 10.1186/s40494-016-0075-4.

[9] P. Dondi, L. Lombardi, M. Malagodi, and M. Licchelli, "Automatic identification of varnish wear on historical instruments: The case of Antonio Stradivari violins," *J. Cult. Herit.*, vol. 22, pp. 968–973, 2016, doi: https://doi.org/10.1016/j.culher.2016.05.010.

[10] M. Gargano *et al.*, "Multi-analytical investigation of panel, pigments and varnish of The Martyirdom of St. Catherine by Gaudenzio Ferrari (16th century)," *J. Cult. Herit.*, vol. 46, pp. 289–297, Nov. 2020, doi: 10.1016/J.CULHER.2020.06.014.

[11] G. Artioli, *Scientific Methods and Cultural Heritage*. Oxford: Oxford University Press, 2010.

[12] "ISO 20473:2007 Optics and photonics — Spectral bands," 2007. [Online]. Available: https://www.iso.org/standard/39482.html.

[13] International Commission on Illumination (CIE), "CIE S 017/E:2020." 2020, [Online]. Available: https://www.techstreet.com/cie/standards/cie-s-017-e-2020?product_id=2200946#jumps.

[14] R. Paschotta, "Infrared Radiation." https://www.rp-photonics.com/infrared_light.html (accessed Apr. 28, 2022).

[15] C. Cennini, *Il libro dell'arte*. Neri Pozza, 1400.

[16] M. Follieri and L. Sadori, "Legni Archeologici," in *La biologia vegetale per i beni culturali vol.II*, G. Caneva, Ed. Firenze: Nardini Editore, 2005, pp. 19–30.

[17] M. L. Abbate Edlmann, L. De Luca, and S. Lazzeri, *Atlante anatomico degli alberi ed arbusti della macchia mediterranea*. Firenze: Istituto Agronomico per l'Oltremare, 1994.

[18] L. UZIELLI and M. FIORAVANTI, "Physical and mechanical behavior of wood used for panel paintings," in *Panel painting – Technique and Conservation of Wood Supports*, M. Ciatti, C. Castelli, and A. Santacesaria, Eds. Edifir, 2006, pp. 59–80.

[19] S. V. Glass and S. L. Zelinka, "Wood Handbook - wood as an engineering material." doi:

10.1161/01.RES.39.4.523.

[20] J. Hill Stoner and R. Rushfield, “A history of Western easel painting material from early Renaissance to 2020,” in *Conservation of easel paintings*, Second edi., Taylor&Francis, 2021, pp. 49–243.

[21] R. R. Bresee, “General effects of ageing on textiles,” *J. Am. Inst. Conserv.*, vol. 25, no. 1, pp. 39–48, 1986, [Online]. Available: https://cool.culturalheritage.org/jaic/articles/jaic25-01-004_indx.html#.

[22] R. Marini Bettolo, L. M. Migneco, and M. Plossi Zappalà, “La carta,” in *La chimica per l’arte*, 2007, pp. 411–484.

[23] H. M. Szczepanowska, “Materials and conservation practice - Paper,” in *Conservation of Cultural Heritage: Key Principles and Approaches*, Routledge, 2013, pp. 127–143.

[24] A. Basanoff, *Itinerario della carta - Dall’oriente all’occidente e la sua diffusione in Europa*. Milano, 1965.

[25] R. Casciaro, *La scultura in cartapesta - Sansovino, Bernini e i Maestri leccesi tra tecnica e artificio*. Milano: Editore, Silvana, 2008.

[26] E. Flammia, *Storia dell’arte della cartapesta*. 2017.

[27] R. Casciaro, *Cartapesta e scultura polimaterica*. 2012.

[28] E. Cao, “Quattro burattini in cerca di un restauratore. Studio e analisi della cartapesta.,” UNIVERSITA’ DEGLI STUDI DI ROMA “TOR VERGATA,” 2019.

[29] J. F. Gleeson, “Intonaco.” http://www.palazzospinelli.org/plaster/glossary/scheda.asp?Id=4179 (accessed Jun. 01, 2022).

[30] M. F. La Russa and S. A. Ruffolo, “Mortars and plasters - How to characterize mortar and plaster degradation,” *Archaeol. Anthropol. Sci.*, vol. 13, no. 10, pp. 1–11, 2021, doi: 10.1007/s12520-021-01405-1.

[31] A. Weyer *et al.*, *EwaGlos - European Illustrated Glossary Of Conservation Terms For Wall Paintings And Architectural Surfaces*. .

[32] J. Hill Stoner and R. Rushfield, *Conservation of Easel Paintings*. 2013.

[33] D. Davies and J. Green, “Methods and materials of Nothern European paintings in the National Gallery, 1500-1550,” *Natl. Gall. Tech. Bull.*, vol. 18, pp. 6–55, 1997.

[34] L. Adrover Gracia, Imma Borgioli and N. Bevilacqua, *I Pigmenti nell’Arte dalla Preistoria alla Rivoluzione Industriale*. Padova, 2010.

[35] E. Reinkowski-Häfner, “Tempera: narratives on a technical term in art and conservation,” in *Tempera Painting 1800–1950 Experiment and Innovation from the Nazarene Movement to Abstract Art*, P. Dietemann, W. Neugebauer, E. Ortner, R. Poggendorf, E. Reinkowski-Häfner, and H. Stege, Eds. 2019, pp. 21–32.

[36] J. Schlesinger, “Ueber Tempera-Bilder und deren Restauration,” in *Ueber Restauration alter Oelgemälde*, 1828, pp. 35–47.

[37] W. S. J. Taft and J. W. Mayer, *The Science of Paintings*, vol. 53, no. 9. Springer, 2000.

[38] J. P. Filedt Kok, “Underdrawing and other technical aspects in the paintings of Lucas van Leyden,” *Netherlands Yearb. Hist. Art / Ned. Kunsthist. Jaarb.*, vol. 29, no. 1, pp. 1–184, 2013, doi: 10.1163/22145966-90000496.

[39] The Metropolitan Museum of Art (MET), “The Materials and Techniques of Drawings: charcoal.” https://www.metmuseum.org/about-the-met/collection-areas/drawings-and-prints/materials-and-

techniques/drawing/charcoal (accessed Nov. 24, 2021).

[40] The Metropolitan Museum of Art (MET), “The Materials and Techniques of Drawings: graphite.” https://www.metmuseum.org/about-the-met/collection-areas/drawings-and-prints/materials-and-techniques/drawing/graphite (accessed Nov. 24, 2021).

[41] M. L. Agati, *The Manuscript Book. A Compendium of Codicology*. L’Erma di Bretschneider, 2017.

[42] N. Orazi, “Mid-wave Infrared Reflectography and Thermography for the Study of Ancient Books: A Review,” *Stud. Conserv.*, vol. 65, no. 8, pp. 437–449, 2020, doi: 10.1080/00393630.2020.1734383.

[43] W. H. Langwell, *The Conservation of books and documents*. Sm. ISAAC PITMAN & SONS, 1967.

[44] B. Liu, H. Zhang, H. Fernandes, and X. Maldague, “Quantitative Evaluation of Pulsed Thermography, Lock-in Thermography and Vibrothermography on Foreign Object Defect (FOD) in CFRP,” doi: 10.3390/s16050743.

[45] A. O. Chulkov *et al.*, “Evaluating quality of marquetries by applying active IR thermography and advanced signal processing,” *J. Therm. Anal. Calorim.*, vol. 143, no. 5, pp. 3835–3848, 2021, doi: 10.1007/s10973-020-09326-2.

[46] D. P. Almond and P. M. Patel, *Photothermal science and techniques*. London, 1996.

[47] N. Orazi *et al.*, “Thermographic analysis of bronze sculptures,” *Stud. Conserv.*, vol. 61, no. 4, pp. 236–244, Jul. 2016, doi: 10.1179/2047058415Y.0000000025.

[48] R. D. Tom, E. P. O’Hara, and D. Benin, “A generalized model of photothermal radiometry,” *J. Appl. Phys.*, vol. 53, no. 8, pp. 5392–5400, 1982, doi: 10.1063/1.331468.

[49] G. Caruso, S. Paoloni, N. Orazi, C. Cicero, U. Zammit, and F. Mercuri, “Quantitative evaluations by infrared thermography in optically semi-transparent paper-based artefacts,” *Meas. J. Int. Meas. Confed.*, vol. 143, pp. 258–266, Sep. 2019, doi: 10.1016/j.measurement.2019.04.086.

[50] W. R. Mccluney, “Introduction to Radiometry and Photometry,” *Sens. Rev.*, vol. 18, no. 4, pp. 159–163, 1998, doi: 10.1108/sr.1998.08718dae.002.

[51] X. Maldague, *Theory and practice of infrared technology for nondestructive testing*. New York: Wiley, 2001.

[52] A. V. Luikov, “Physical Fundamentals of Heat Transfer,” in *Analytical Heat Diffusion Theory*, J. P. Hartnett and A. V. B. T.-A. H. D. T. LUIKOV, Eds. Academic Press, 1968, pp. 1–34.

[53] C. Cucci *et al.*, “The illuminated manuscript Corale 43 and its attribution to Beato Angelico: Non-invasive analysis by FORS, XRF and hyperspectral imaging techniques,” *Microchem. J.*, vol. 138, pp. 45–57, 2018, doi: 10.1016/j.microc.2017.12.021.

[54] G. Doni *et al.*, “Thermographic study of the illuminations of a 15th century antiphonary,” *J. Cult. Herit.*, vol. 15, no. 6, pp. 692–697, 2014, doi: 10.1016/j.culher.2013.12.001.

[55] S. Ceccarelli, N. Orazi, F. Mercuri, S. Paoloni, U. Zammit, and F. Petrucci, “Thermographic and reflectographic imaging investigations on Baroque paintings preserved at the Chigi Palace in Ariccia,” *Acta IMEKO*, vol. 10, no. 1, pp. 187–192, 2021, doi: 10.21014/ACTA_IMEKO.V10I1.828.

[56] J. Peeters *et al.*, “IR Reflectography and Active Thermography on Artworks: The Added Value of the 1.5–3 μm Band,” *Appl. Sci.*, vol. 8, no. 1, p. 50, 2018, doi: 10.3390/app8010050.

[57] K. Blessley, C. Young, J. Nunn, J. Coddington, and S. Shepard, “The feasibility of flash thermography for the examination and conservation of works of Art,” *Stud. Conserv.*, vol. 55, no. 2, pp. 107–120, 2010, doi: 10.1179/sic.2010.55.2.107.

[58] C. Ibarra-Castanedo, M. Genest, J.-M. Piau, S. Guibert, A. Bendada, and X. P. V Maldague, "ACTIVE INFRARED THERMOGRAPHY TECHNIQUES FOR THE NONDESTRUCTIVE TESTING OF MATERIALS," in *Ultrasonic and Advanced Methods for Nondestructive Testing and Material Characterization*, WORLD SCIENTIFIC, 2007, pp. 325–348.

[59] C. Ibarra-Castanedo, J. R. Tarpani, and X. P. V Maldague, "Nondestructive testing with thermography," *Eur. J. Phys.*, vol. 34, no. 6, pp. S91–S109, 2013, doi: 10.1088/0143-0807/34/6/s91.

[60] F. Scudieri, F. Mercuri, and R. Volterri, "Non-invasive Analysis of Artistic Heritage and Archaeological Findings by Time Resolved IR Thermography," *J. Therm. Anal. Calorim.*, vol. 66, no. 1, pp. 307–314, 2001, doi: 10.1023/A:1012420622561.

[61] N. Orazi *et al.*, "The Boxer at Rest and the Hellenistic Prince: A comparative thermographic study," *J. Archaeol. Sci. Reports*, vol. 24, pp. 115–121, Apr. 2019, doi: 10.1016/j.jasrep.2018.12.016.

[62] H. G. Walther, U. Seidel, W. Karpen, and G. Busse, "Application of modulated photothermal radiometry to infrared transparent samples," *Rev. Sci. Instrum.*, vol. 63, no. 11, pp. 5479–5480, 1992, doi: 10.1063/1.1143372.

[63] R. E. Imhof, A. D. McKendrick, and P. Xiao, "Thermal emission decay Fourier transform infrared spectroscopy," *Rev. Sci. Instrum.*, vol. 66, no. 11, pp. 5203–5213, 1995, doi: 10.1063/1.1146151.

[64] S. A. Lavrykov and B. V. Ramarao, "Thermal Properties of Copy Paper Sheets," *Dry. Technol.*, vol. 30, no. 3, pp. 297–311, 2012, doi: 10.1080/07373937.2011.638148.

[65] M. Missori *et al.*, "Optical response of strongly absorbing inhomogeneous materials: Application to paper degradation," *Phys. Rev. B - Condens. Matter Mater. Phys.*, vol. 89, no. 5, pp. 16–19, 2014, doi: 10.1103/PhysRevB.89.054201.

[66] F. Mercuri *et al.*, "Hidden text detection by infrared thermography," *Restaurator*, vol. 34, no. 3, pp. 195–211, 2013, doi: 10.1515/res-2013-0011.

[67] O. C. Zienkiewicz, R. L. Taylor, and J. Z. Zhu, *The finite element method: its basis and fundamentals*. Elsevier, 2005.

[68] T. J. R. Hughes, *The finite element method: linear static and dynamic finite element analysis*. Courier Corporation, 2012.

[69] C. Daffara, D. Ambrosini, L. Pezzati, and D. Paoletti, "Thermal quasi-reflectography: a new imaging tool in art conservation," *Opt. Express*, vol. 20, no. 13, p. 14746, 2012, doi: 10.1364/oe.20.014746.

[70] J. R. J. van Asperen de Boer, "Infrared Reflectography: a Method for the Examination of Paintings," *Appl. Opt.*, vol. 7, no. 9, p. 1711, 1968, doi: 10.1364/ao.7.001711.

[71] P. Kubelka and F. Munk, "An article on optics of paint layers," *Z. Tech. Phys.*, vol. 12, no. 1930, pp. 593–601, 1931.

[72] L. Mullen, A. Laux, B. Concannon, E. P. Zege, I. L. Katsev, and A. S. Prikhach, "Amplitude-modulated laser imager," *Appl. Opt.*, vol. 43, no. 19, p. 3874, 2004, doi: 10.1364/AO.43.003874.

[73] M. Guarneri *et al.*, "Imaging topological radar technology as a general purpose instrument for remote colorimetric assessment, structural security, cataloguing, and dissemination," *Stud. Conserv.*, vol. 60, no. sup1, pp. S134–S142, 2015, doi: 10.1179/0039363015Z.000000000218.

[74] S. Ceccarelli, M. Guarneri, M. F. De Collibus, M. Francucci, M. Ciaffi, and A. Danielis, "Laser scanners for high-quality 3D and IR imaging in cultural heritage monitoring and documentation," *J. Imaging*, vol. 4, no. 11, 2018, doi: 10.3390/jimaging4110130.

[75] S. Ceccarelli *et al.*, "Remote and contactless infrared imaging techniques for stratigraphical investigations in paintings on canvas," *Appl. Phys. B Lasers Opt.*, vol. 127, no. 8, 2021, doi: 10.1007/s00340-021-07654-1.

[76] S. Ceccarelli, M. Guarneri, M. Ferri de Collibus, M. Francucci, M. Ciaffi, and A. Danielis, “Laser Scanners for High-Quality 3D and IR Imaging in Cultural Heritage Monitoring and Documentation,” *J. Imaging*, vol. 4, no. 11, Nov. 2018, doi: 10.3390/jimaging4110130.

[77] “CIE - International Commission on Illumination,” 2022. https://cie.co.at/ (accessed May 10, 2022).

[78] M. Bacci, S. Baronti, A. Casini, F. Lotti, M. Picollo, and O. Casazza, “Non-Destructive Spectroscopic Investigations on Paintings Using Optical Fibers,” *MRS Proc.*, vol. 267, no. c, pp. 265–283, 1992, doi: 10.1557/proc-267-265.

[79] C. Oleari, *Misurare il colore*. 2008.

[80] “Konika Minola - CIELAB Colour Space,” 2022. https://sensing.konicaminolta.asia/what-is-cie-1976-lab-color-space/ (accessed Apr. 08, 2022).

[81] “StellarNet FORS systems,” 2021. https://www.stellarnet.us/systems/color-measurement-systems/.

[82] P. Calicchia, S. De Simone, and S. Privitera, “Validation of contactless vibro-acoustic imaging for the detection of glaze delamination in glaze ceramic tiles,” in *International Conference Glaze Ceramics in Cultural Heritage*, 2018, pp. 208–226.

[83] E. Esposito, “Laser Doppler Vibrometry,” in *Handbook on the use of lasers in conservation and conservation science*, M. Schreiner, M. Strlič, and R. Salimbeni., Eds. Brussels: COST Office, 2008.

[84] P. Castellini, E. Esposito, B. Marchetti, N. Paone, and E. P. Tomasini, “New applications of Scanning Laser Doppler Vibrometry (SLDV) to non-destructive diagnostics of artworks: mosaics, ceramics, inlaid wood and easel painting,” in *Lacona iv*, 2001, pp. 203–206.

[85] L. E. Kinsler, *Fundamental of Acoustics*. John Wiley & Sons, Inc., 2000.

[86] K. Pigmente, “Kremer Pigments,” 2020. https://www.kremer-pigmente.com/it/shop/pigmenti/.

[87] M. Attas *et al.*, “Near-infrared spectroscopic imaging in art conservation: investigation of drawing constituents,” *J. Cult. Herit.*, vol. 4, no. 2, pp. 127–136, Apr. 2003, doi: 10.1016/S1296-2074(03)00024-4.

[88] F. Mercuri, S. Paoloni, C. Cicero, U. Zammit, and N. Orazi, “Infrared emission contrast for the visualization of subsurface graphical features in artworks,” *Infrared Phys. Technol.*, vol. 89, pp. 223–230, 2018, doi: 10.1016/j.infrared.2018.01.012.

[89] M. Nuzzo, “La Theotókos di Santa Maria in Cosmedin: Un contributo per la figura del pittore romano Giovanni Piacere,” in *“Domus sapienter staurata”. Scritti di storia dell’arte per Marina Righetti*, Cinisello Balsamo: Silvana Editoriale, 2021, pp. 398–407.

[90] M. Crescimbeni, *L’istoria della basilica di S.Maria in Cosmedin di Roma*. Ordine Generale Adunanza degli Arcadi, 1715.

[91] A. Cavallaro, *Antoniazzo Romano e gli antoniazzeschi*. Udine: Campanotto, 1992.

[92] G. Russo, “Antoniazzo Romano,” Università degli Studi di Napoli ‘Federico II,’ 2013.

[93] D. Petrucci and F. Petrucci, *The Chigi Palace in Ariccia*. Ariccia: Arti Grafiche Ariccia, 2019.

[94] F. Petrucci, “Sull’attività ritrattistica di Giovanni M. Morandi,” *Labyrinthos 33/34*, pp. 131–174, 1998.

[95] F. Petrucci, “Mario Nuzzi, detto Mario de’ Fiori / La Primavera, L’Estate, L’Autunno, L’Inverno,” in *Fiori. Natura e simbolo dal Seicento a Van Gogh*, D. Benati, F. Mazzocca, and A. Morandotti, Eds. Forlì, 2010, pp. 136–145.

[96] V. Golzio, *Mario de’ Fiori e la natura morta*. L’Urbe, 1965.

[97] F. Petrucci, *Pittura di Ritratto a Roma. Il Seicento*. Roma, 2008.

[98] L. Laureati, “Mario dei Fiori,” in *The Dictionary of Art*, London, 1996.

[99] G. P. Bellori, “Vita di Andrea Sacchi,” in *Le vite de’ Pittori, Scultori e Architetti Moderni*, 1976.

[100] L. Arcangeli, “Andrea Sacchi, Ebbrezza di Noè,” *Quaderni del Barocco – Dipinti inediti del Barocco Italiano*, Ariccia, 2010.

[101] F. Petrucci, *Bernini pittore : dal disegno al maraviglioso composto*. Roma, 2006.

[102] P. F. De Chantelou, *Viaggio del Cavalier Bernini in Francia*. 1988.

[103] F. Terlizzi, M. Medica, and C. Illuminati, *LA DIVINA COMMEDIA Manoscritto 1102 della Biblioteca Angelica di Roma*. Rimini, 2017.

[104] M. Salmi, *La miniatura italiana*. Milano: Electa, 1956.

[105] M. G. Ciardi Duprè Dal Poggetto, *Fioritura Tardogotica Nelle Marche*. Milano: Electa, 1998.

[106] G. F. Priori and M. V. Quattrini, “La caratterizzazione delle carte orientali,” in *Bollettino ICR Nuova Serie*, 2005, pp. 134–150.

[107] L. Burgio, “Pigments, dyes and inks: their analysis on manuscripts, scrolls and papyri,” *Archaeol. Anthropol. Sci.*, vol. 13, no. 11, 2021, doi: 10.1007/s12520-021-01403-3.

[108] M. Redi, “Tra le spire della carta . Il restauro dei 4 rotoli della Collezione Ragusa,” Università di Roma Tor Vergata, 2019.

[109] A. Zanrè, *I Segreti di Sgarabotto*, Edizioni S. Parma, 2019.

[110] C. Invernizzi *et al.*, “Non-invasive mobile technology to study the stratigraphy of ancient Cremonese violins: OCT, NMR-MOUSE, XRF and reflection FT-IR spectroscopy,” *Microchem. J.*, vol. 155, no. August 2019, p. 104754, 2020, doi: 10.1016/j.microc.2020.104754.

[111] G. Valentina Fichera *et al.*, “Innovative Monitoring Plan for the Preventive Conservation of Historical Musical Instruments,” *Stud. Conserv.*, vol. 63, no. sup1, pp. 351–354, 2018, doi: 10.1080/00393630.2018.1499853.

List of publications

1. Guarneri, M., Ceccarelli, S., Ferri De Collibus, M., Francucci, M., and Ciaffi, M., *Multi-wavelengths 3D laser scanning for pigment and structural studies on the frescoed ceiling "the Triumph of Divine Providence*, Int. Arch. Photogramm. Remote Sens. Spatial Inf. Sci., XLII-2/W15, 549–554, https://doi.org/10.5194/isprs-archives-XLII-2-W15-549-2019;

2. Ceccarelli S., Orazi N., Mercuri F., Paoloni S., Zammit U., Petrucci F., *Middle-wave infrared imaging analysis of the XVII century canvas paintings of the Ariccia*, Proceedings of IMEKO TC-4 International Conference on Metrology for Archaeology and Cultural Heritage, Florence, Italy, December 4-6, 2019, pp. 160-165, ISBN: 978-92-990084-5-4;

3. Ceccarelli S., Orazi N., Cicero C., Mercuri F., Zammit U., Paoloni S., Felici A.C., Matera F., Nuzzo M., *Multi-band infrared imaging for the characterization of underlying elements in the Santa Maria in Cosmedin altarpiece*, Proceedings of IMEKO TC-4 International Conference on Metrology for Archaeology and Cultural Heritage, Florence, Italy, December 4-6, 2019, pp. 439-443, ISBN: 978-92-990084-5-4;

4. Mercuri F., Caruso G., Orazi N., Zammit U., Ceccarelli S., Cicero C., Vadrucci M., Paoloni S., " Depth-Resolved Analysis of Double-Layered Cultural Heritage Artifacts by Pulsed Thermography ", *Int J Thermophys* **41,** 6 (2020), https://doi.org/10.1007/s10765-019-2587-0;

5. Ceccarelli S., Guarneri M., Romani M., Giacopini L., Francucci M., Ciaffi M., Ferri De Collibus M., Puiu A., Verona-Rinati G., Colao F., Fantoni R., *Are the blue daemons really blue? Multidisciplinary study for the colours characterization of the mural paintings inside the Blue Daemons Etruscan tomb*, Journal of Cultural Heritage, 2020, https://doi.org/10.1016/j.culher.2020.09.002*;*

6. Uueni A., Bertacchi S., Ceccarelli S., Apollonio F. I, Hiiop H., Valge C., Tiidor T., Randla A., *Colour measurement and documentation in historical painted interiors restoration: the good practice at the workshop of Estonian Academy of Arts in Tallinn*, XVI Color Conference, Bergamo 2020, Colour and Colorimetry. Multidisciplinary Contributions. Vol. XVIB, ISBN 978-88-99513-13-9, pp.127-134;

7. Mercuri F., Ceccarelli S., Orazi N., Cicero C., Paoloni S., Felici A.C., Matera F., Nuzzo., Zammit U., *Combined use of infrared imaging techniques for the study of underlying features in the Santa Maria in Cosmedin altarpiece*, Archaeometry, 2021, https://doi.org/10.1111/arcm.12653;

8. Ceccarelli S., Orazi N., Mercuri F., Paoloni S., Zammit U., Petrucci F., *Thermographic and reflectographic imaging investigations on Baroque paintings preserved at the Chigi Palace in Ariccia*, March 2021, ACTA IMEKO 10(1):187, http://dx.doi.org/10.21014/acta_imeko.v10i1.828;

9. Ceccarelli, S., Guarneri, M., Orazi, N. et al. Remote and contactless infrared imaging techniques for stratigraphical investigations in paintings on canvas. Applied Physics B 127, 106 (2021). https://doi.org/10.1007/s00340-021-07654-1;

10. Redi M., Ceccarelli S., Terrei A., Orazi N., Guglielmotti V., Hampai D., Dabagov S., Mercuri F. 2021. *Diagnostic analysis for colour restoration of a painted Japanese emakimono*. In: Proceedings of the International Colour Association (AIC) Conference 2021. Milan, Italy, ISBN: 978-0-6484724-3-8, 615-620;

11. Caruso G., Mercuri F., Zammit U., Paoloni S., Ceccarelli S., Orazi N., *3D heat flow effects in the imaging of subsurface graphical features in semi-transparent media by pulsed thermography*, Measurement, Vol. 185, 2021, 110111, https://doi.org/10.1016/j.measurement.2021.110111;

12. Ceccarelli S., Caruso G., Mercuri F., Paoloni S., Zammit U., Orazi N., *Study of the edge distortion effect in thermographic detection in semi-transparent Cultural Heritage*, Proceedings of IMEKO TC-4 International Conference on Metrology for Archaeology and Cultural Heritage, Milan, Italy, October 20-22, 2021;

13. Fiocco G., Ceccarelli S., Albano M., Rovetta T., Malagodi M., Orazi N., Paoloni S., *Structural feature investigation of wooden artifacts through imaging techniques: a step forward in the preservation of historical musical instruments,* Proceedings of IMEKO TC-4 International Conference on Metrology for Archaeology and Cultural Heritage, Milan, Italy, October 20-22, 2021;

14. Valge C., Ceccarelli S., Bertacchi S., Uueni A., Hiiop H., Randla A., Apollonio F. I, *Colour measurement and documentation in historical buildings: the case study of the Kirna Manor House in Estonia,* Color Culture and Science Journal Vol. 14 (1), pp. 123-130, https://doi.org/10.23738/CCSJ.140115;

15. Orazi, N.; Mercuri, F.; Cicero, C.; Caruso, G.; Zammit, U.; Ceccarelli, S.; Paoloni, S. The "Lost Guardians" of Dante's Inferno: Medium Wave Infrared Imaging Investigations of a XIV Century Illuminated Manuscript. Heritage 2022, 5, 991-1002. https://doi.org/10.3390/heritage5020054;

16. G. Fiocco, S. Ceccarelli, M. Albano, T. Rovetta, M. Malagodi, N. Orazi, S. Paoloni, *Structural feature investigation of wooden artifacts through imaging techniques: a step forward in the preservation of historical musical instruments,* J. Phys.: Conf. Ser. 2204(1), 012033;

17. Ceccarelli, S.; Cao, E.; Orazi, N.; Cicero, C.; Mercuri, F.; Zammit, U.; Terrei, A.; Paoloni, S. Papier-Mâché Puppets' Characterization by Infrared Imaging Techniques. Heritage 2022, 5, 1419-1432. https://doi.org/10.3390/heritage5030074;

18. S. Ceccarelli, M. Redi, A.Terrei, N. Orazi, V. Guglielmotti, D. Hampai, S. Dabagov, F. Mercuri, 2021, *Diagnostic analysis for colour restoration of a painted Japanese emakimono,* SCIRES (under review)